WROCŁAW UNIVERSITY OF SCIENCE AND TECHNOLOGY
FACULTY OF CHEMISTRY

AND

UNIVERSITY OF FLORENCE
DEPARTMENT OF CHEMISTRY "UGO SCHIFF"

Constrained secondary structures to develop bioactive peptides and peptidomimetics

Doctoral dissertation

mgr Agnieszka Natalia Staśkiewicz

Supervisors:

Prof. Dr hab. Rafał Latajka (Department of Bioorganic Chemistry, Faculty of Chemistry, Wrocław University of Science and Technology, Poland)

Prof. Dr. Anna Maria Papini (Interdepartmental Research Unit of Peptide and Protein Chemistry and Biology, Department of Chemistry "Ugo Schiff", University of Florence, Italy)

WROCŁAW 2024

I would like to express thanks to both my supervisors
Prof. Dr hab. Rafał Latajka *and* **Prof. Dr. Anna Maria Papini**
for their motivation and support during the research.

I would like to thank
Dr. Francesca Nuti
for the help with the synthesis
and for supporting me during the work performed during the lockdown in Italy.

I would like to acknowledge
Dr. Michał Jewgiński
for the help with molecular modelling, NMR studies,
and a friendly atmosphere at work.

I would like to thank
Dr. Patrycja Ledwoń
for her patience and wonderful friendship.

TABLE OF CONTENTS

mgr Agnieszka Natalia Staśkiewicz

CONSTRAINED SECONDARY STRUCTURES TO DEVELOP BIOACTIVE PEPTIDES AND PEPTIDOMIMETICS

Abstract

Oxytocin (OT) is a peptide hormone and neurotransmitter involved in various biological functions through interacting with its cognate G protein-coupled receptors. In humans and other mammals, one oxytocin and three closely related vasopressin receptors such as V_{1a}, V_{1b}, and V_2. Oxytocin is a cyclic nonapeptide with a disulphide bond between Cys^1 and Cys^6. The biomedical use of oxytocin is limited by its short half-life *in vivo* and by the low receptor selectivity. However, the design and synthesis of OT-derived analogues can be interesting for imaging applications and targeting various diseases. The presented studies aim to increase the stability of oxytocin by replacing the disulphide bridge with the stable and more rigid 1*H*-[1,2,3]triazol-1-yl moiety. In this context, the Cu(I)-catalysed side chain-to-side chain azide-alkyne 1,3-cycloaddition (CuAAC) macrocyclisation strategy was employed to stabilise β-turns secondary structures. This doctoral dissertation reports the design, synthesis, conformational analysis, and *in vitro* pharmacological activity of a series of $C\alpha^1$-to-$C\alpha^6$ side chain-to-side chain 1*H*-[1,2,3]triazol-1-yl-containing oxytocin analogues differing in the length of the bridge and the orientation and location of the linking moieties. By developing this macrocyclisation method, it was possible to produce a series of compounds that provided attractive insight into the structure-conformation-function relationship.

Moreover, the secondary structure of peptides or proteins plays a crucial function in their bioactivity. In this sense, Myelin Basic Protein (MBP) peptides have been synthesised and played a significant role in effectively recognising IgM antibodies in Multiple Sclerosis (MuSc). MuSc is a demyelinating, neuroinflammatory, autoimmune disease that attacks the central nervous system (CNS). Genetic and environmental aspects, *e.g.*, viral and bacterial infections, participate in this process. The MBP is an intrinsically disordered protein demonstrating an interesting α-helix motif, which can be considered a conformational epitope. This PhD thesis investigated the role of the sequences and structures of synthetic MBP peptides that have been used to identify specific antibodies in Multiple Sclerosis patient sera. Therefore, the studies of the relationship between the secondary structure and the bioactivity of the series of MBP peptides are discussed.

mgr Agnieszka Natalia Staśkiewicz

CONSTRAINED SECONDARY STRUCTURES TO DEVELOP BIOACTIVE PEPTIDES AND PEPTIDOMIMETICS

Streszczenie

Oksytocyna (OT) jest hormonem peptydowym i neuroprzekaźnikiem zaangażowanym w różnorodne funkcje biologiczne poprzez interakcję z pokrewnymi receptorami sprzężonymi z białkiem G. U ludzi i innych ssaków występuje jeden receptor oksytocyny i trzy blisko spokrewnione receptory wazopresyny, takie jak V_{1a}, V_{1b} i V_2. Oksytocyna jest cyklicznym nonapeptydem z wiązaniem disulfidowym pomiędzy Cys^1 i Cys^6. Biomedyczne zastosowanie oksytocyny jest ograniczone przez jej krótki okres półtrwania *in vivo* oraz niską selektywność receptorową. Jednak projektowanie i synteza analogów wywodzących się z OT może być interesująca między innymi do obrazowania oraz zwalczaniu różnorakich chorób. Przedstawione w niniejszej rozprawie doktorskiej badania mają na celu zwiększenie stabilności oksytocyny poprzez zastąpienie mostka disulfidowego stabilnym i sztywniejszym ugrupowaniem 1*H*-[1,2,3]triazol-1-ilowym. W tym kontekście zastosowano strategię makrocyklizacji łańcuchów bocznych azydka, katalizowanych przez jony Cu(I), do łańcuchów bocznych alkinu w 1,3-cykloaddycji (CuAAC) w celu ustabilizowania struktur drugorzędowych β-kartek. W tejże pracy doktorskiej przedstawiono projektowanie, syntezę, analizę preferencji konformacyjnych oraz aktywność farmakologiczną *in vitro* analogów oksytocyny różniących się długością, orientacją oraz rozmiarem mostka triazolowego. Dzięki opracowaniu odpowiedniej metody makrocyklizacji możliwe było utworzenie serii związków, które dostarczyły ciekawych informacji na temat zależności struktura chemiczna, a funkcja biologiczna.

Ponadto, drugorzędowa struktura peptydów lub białek odgrywa kluczową rolę w ich bioaktywności. W tym celu zsyntetyzowano peptydy zasadowego białka mieliny (MBP), które odgrywają znaczącą funkcję w skutecznym rozpoznawaniu przeciwciał IgM w stwardnieniu rozsianym (MuSc). MuSc jest chorobą demielinizacyjną, która atakuje ośrodkowy układ nerwowy. W tym procesie biorą udział aspekty genetyczne jak i środowiskowe, np. infekcje wirusowe i bakteryjne. MBP jest wewnętrznie nieuporządkowanym białkiem wykazującym interesujący motyw α-helisy, który można uznać za epitop konformacyjny. W niniejszej pracy doktorskiej zbadano rolę sekwencji i struktur drugorzędowych serii syntetycznych peptydów MBP, które zostały użyte do identyfikacji swoistych przeciwciał w surowicach pacjentów ze stwardnieniem rozsianym. Wobec powyższego omówiono badania zależności między strukturą drugorzędową, a bioaktywnością serii peptydów MBP.

Riassunto

L'ossitocina (OT) è un ormone peptidico e un neurotrasmettitore coinvolto in varie funzioni biologiche attraverso l'interazione con i suoi recettori accoppiati a proteine G. Nell'uomo e in altri mammiferi, l'ossitocina e tre recettori della vasopressina sono strettamente correlati come V_{1a}, V_{1b} e V_2. L'ossitocina è un nonapeptide ciclico con un legame disolfuro tra Cys^1 e Cys^6. L'uso biomedico dell'ossitocina è limitato dalla sua breve emivita *in vivo* e dalla bassa selettività recettoriale. Tuttavia, la progettazione e la sintesi di analoghi derivati da OT potrebbero essere interessanti per applicazioni di imaging e mirare a varie malattie. Gli studi presentati mirano ad aumentare la stabilità dell'ossitocina sostituendo il ponte disolfuro con la funzione $1H$-[1,2,3]triazol-1-ile stabile e più rigida. In questo contesto, la strategia di macrociclizzazione catalizzata da Cu(I) mediante la reazione azide-alchino 1,3-cicloaddizione (CuAAC) è stata impiegata per stabilizzare le strutture secondarie β-turn. In questa tesi di dottorato, è stato riportato il disegno, la sintesi, l'analisi conformazionale e l'attività farmacologica *in vitro* di una serie di analoghi $C\alpha^1$-to-$C\alpha^6$ $1H$-[1,2,3]triazol-1-yl dell'ossitocina che differiscono per la lunghezza del ponte e l'orientamento e la posizione delle funzioni di collegamento. Sviluppando questo metodo di macrociclizzazione, è stato possibile ottenere una serie di composti che hanno fornito interessanti informazioni sulla correlazione tra struttura e funzione.

Inoltre, la struttura secondaria dei peptidi o delle proteine svolge una funzione cruciale nella loro bioattività. In questo senso, sono stati sintetizzati i peptidi della proteina basica della mielina (MBP) che svolgono un ruolo significativo nel riconoscimento efficace degli anticorpi IgM nella sclerosi multipla (MuSc). MuSc è una malattia demielinizzante, neuroinfiammatoria, autoimmune che attacca il sistema nervoso centrale. A questo processo contribuiscono fattori genetici e ambientali, ad esempio infezioni virali e batteriche. MBP è una proteina intrinsecamente disordinata che dimostra un interessante motivo ad α-elica, che può essere considerato un epitopo conformazionale. Questa tesi di dottorato ha indagato il ruolo delle sequenze e delle strutture di una serie di peptidi sintetici di MBP che sono stati utilizzati per identificare anticorpi specifici nei sieri dei pazienti affetti da sclerosi multipla. Pertanto, vengono discussi gli studi sulla relazione tra la struttura secondaria e la bioattività della serie di peptidi di MBP.

List of abbreviations

1D	One-Dimensional
2D	Two-Dimensional
3D	Three-Dimensional
Abs	Antibodies
ACN	Acetonitrile
AgAAC	Silver(I)-catalysed Azide-Alkyne Cycloaddition
Ags	Antigens
AMP	Antimicrobial Peptide
APCs	Antigen-Presenting Cells
AT	Adoptive-Transfer
AVP	Vasopressin
B3LYP	Becke, 3-parameter, Lee-Yang-Parr
BCA assay	Bicinchoninic Acid Assay
BSA	Bovine Serum Albumin
CD	Circular Dichroism
Cit	Citrulline
CNS	Central Nervous System
COSY	Correlation Spectroscopy
cryo-EM	Cryo-Electron Microscopy
CSD	Chemical Shift Deviation
CSF	Cerebrospinal Fluid
CuAAC	Copper(I)-catalysed Alkyne-Azide Cycloaddition
DFT	Density Functional Theory
DIC	N,N'-diisopropylcarbodiimide
DIPEA	N,N'-diisopropylethylamine
DMF	Dimethylformamide
DMSO	Dimethyl Sulfoxide
DPC-d$_{38}$	Dodecylphosphocholine-d$_{38}$
DQF-COSY	Double Quantum Filtered Correlation Spectroscopy
DSS	Sodium 4,4-dimethyl-4-silapentane-1-sulphonate-d$_6$
E	Energy
EAE	Experimental Autoimmune Encephalomyelitis
EBV	Epstein-Barr Virus
EC$_{50}$	Half Maximal Effective Concentration
ECL2	Extracellular Loop 2
ECL3	Extracellular Loop 3
ELISA	Enzyme-Linked Immunosorbent Assay
EPR	Electron Paramagnetic Resonance
ESI-MS	Electrospray Ionization Mass Spectrometry
FBS	Fetal Bovine Serum

GFP	Green Fluorescent Protein
GOAT	Ghrelin *O*-acyltransferase
Golli	Genes of Oligodendrocyte Lineage
GPCR	G Protein-Coupled Receptor
GSK	Glycogen Synthase Kinase
HBTU	(2-(1*H*-benzotriazol-1-yl)-1,1,3,3-tetramethyluronium Hexafluorophosphate
HEK293	Human Embryonic Kidney 293 cells
HIV	Human Immunodeficiency Virus
HIV-1	Human Immunodeficiency Virus Type 1
HSP1	Hylaseptin-P1
HSQC	Heteronuclear Single Quantum Correlation
HTRF	Homogeneous Time-Resolved Fluorescence
IC$_{50}$	Half Maximal Inhibitory Concentration
IgG	Immunoglobulin G
IgM	Immunoglobulin M
IL-10	Interleukin 10
IP-1	Inositol-1-phosphate
IP-3	D-*myo*-inositol 1,4,5-trisphosphate
***i*Pr$_2$O**	Diisopropyl Ether
K$_D$	Dissociation Constant
K$_i$	Inhibition Constant
LP	Lumbar Punctures
MAPK	Mitogen-Activated Protein Kinase
MBP	Myelin Basic Protein
MIC	Minimal Inhibitory Concentration
MRI	Magnetic Resonance Imaging
MuSc	Multiple Sclerosis
MW	Microwave
MW-SPPS	Microwave-Assisted Solid-Phase Peptide Synthesis
n.d.	No Data
NA	No Antimicrobial Activity
NMR	Nuclear Magnetic Resonance
NOESY	Nuclear Overhauser Effect Spectroscopy
OL	Oligodendrocyte
OT	Oxytocin
OT(PDB)	Oxytocin downloaded from Protein Data Bank
OTR	Oxytocin Receptor
PAD4	Protein Arginine Deaminase 4
PBS	Phosphate Buffered Saline
PCM	Polarisable Continuum Model
PDB	Protein Data Bank
PLP	Proteolipid Protein

pNPP	*p*-nitrophenyl Phosphate
PPI	Protein-Protein Interactions
PPMuSc	Primary Progressive Multiple Sclerosis
PRMuSc	Progressive Relapsing Multiple Sclerosis
RCM	Ring-Closing Metathesis
rmC1	Recombinant Murine 18.5-kDa C1
RMS	Root Mean Square
RMSD	Root Mean Square Deviation
ROE	Rotating-Frame Overhauser Effect
ROESY	Rotating Frame Nuclear Overhauser Effect Spectroscopy
RP-FLC	Reverse-Phase Flash Liquid Chromatography
RP-HPLC	Reversed-Phase High-Performance Liquid Chromatography
RP-HPLC ESI-MS	Reversed-Phase High-Performance Liquid Chromatography Electrospray Mass Spectrometry
RRMuSc	Relapsing-Remitting Multiple Sclerosis
RT	Room Temperature
RuAAC	Ruthenium(II)-catalysed Azide-Alkyne Cycloaddition
SAR	Structure-Activity Relationship
SAS	Substrate Activity Screening
SDS	Sodium Dodecyl Sulphate
SEM	Standard Error
SFTI-1	Sunflower Trypsin Inhibitor-1
SP-ELISA	Solid-Phase Enzyme-Linked Immunosorbent Assay
SPMuSc	Secondary Progressive Multiple Sclerosis
SPPS	Solid-Phase Peptide Synthesis
TFA	Trifluoroacetic Acid
TFE	2,2,2-trifluoroethanol
TGF-β	Transforming Growth Factor-Beta
Th	T Helper Cells
TIS	Triisopropylsilane
TMs	Transmembrane Helices
TNF-α	Tumour Necrosis Factor-Alpha
TOCSY	Total Correlation Spectroscopy
TRIS	Tris(hydroxymethyl)aminomethane
TSP	Trimethylsilylpropanoic Acid

1   INTRODUCTION

Peptides play a significant role in several biological functions and a great interest in chemical, pharmaceutical, and biochemical studies [1]. Treatments based on synthetic peptides are relevant in the drug market due to their abundant properties. Peptides can penetrate tissues and organs because of their small size. Moreover, this group of chemical compounds has limited immunogenic activity, and their synthesis is becoming more and more inexpensive and effortless [2].

Furthermore, the usage of peptides as drugs is reduced by susceptibility to proteases, liability under unusual acid-base and oxidation-reduction conditions, and their exceeding conformational flexibility. In general, peptides are flexible molecules that adopt various dynamically equilibrating forms, although they can only assume a single specific one when bound to their related target [1].

The unique folding and conformation management triggers bioactivity. This essential subject in pharmacology is named the structure-activity relationship (SAR) study. Determining the connection with the activity of biologically relevant peptides, *e.g.*, hormones and the conformation, is of interest in designing selective and effective antagonists or agonists that can be applied as pharmacological investigations or drug candidates [2].

Likewise, the development of chemically modified peptides, generally named peptidomimetics, achieved rising value in recent years [3]. Peptidomimetics are molecules that can mimic natural peptides and proteins. Structures of peptidomimetics can maintain the capability for interactions with the biological targets and demonstrate identical *in vivo* effects of the corresponding unmodified peptides [4].

The other significant issue of peptides or proteins is their conformational preferences. It is known that there exist four types of structures. This doctoral thesis highlights the leading role of secondary structure, especially α-helix or β-turn conformation, in peptides and peptidomimetics.

Moreover, intramolecular side chain-to-side chain cyclisation is a popular approach to increase resistance toward proteolytic degradation, stabilise the bioactive conformations, improve metabolic stability *in vivo* and *in vitro* and develop additional vital properties such as bioavailability, pharmacodynamics, and pharmacokinetics [2,5]. Intramolecular side chain-to-side chain cyclisation through bridges also consists of those formed by the Red-Ox susceptible and hydrophobic disulphide bonds between cysteine residues, the polar lactams,

and all the hydrophobic stable rings. Cyclopeptides possess protein-like epitopes with controlled conformational flexibility, which can directly mimic the bioactive conformation and reduce the entropic effect of binding to its biological target [2].

The cyclisation of bioactive linear peptides has been effectively proven, for instance, to increase antagonist or agonist potency, prolong biological activity, develop pharmacokinetics, and increase receptor specificity. These characteristics enhance the unique component, presenting as ensembles of conformers in dynamic steady-state equilibrium [6].

In this sense, the "click chemistry" reaction, especially the Cu^I-catalysed azide-alkyne 1,3-dipolar cycloaddition, well-known as a copper-catalysed Huisgen cycloaddition (CuAAC), shows an attractive opportunity to generate a novel concept for producing cyclopeptides *via* an intramolecular side chain-to-side chain cyclisation [7].

Numerous studies led to the suggestion that the 1,4- and 4,1-disubstituted [1,2,3]-triazolyl moieties can be used as a surrogate for amide bonds and for substitution of peptide bonds for forming isosteric and heterodetic pseudo peptide bonds. The attractive disulphide and peptide bond mimetic, presented by the 1,4- or 4,1-disubstituted [1,2,3]-triazolyl moieties, require improved chemical and metabolic stability compared to the disulphide bonds.

With this idea in mind, the presented study aims to define secondary structural motifs essential for the biological activity of a series of peptides, such as synthetic Myelin Basic Protein (MBP) peptides that have been used to identify specific antibodies in Multiple Sclerosis patient sera, and peptidomimetics such as analogues of oxytocin in which the disulphide bridges have been replaced by the [1,2,3]-triazolyl moieties to improve selectivity and stability.

2   LITERATURE REVIEW

2.1   Characterisation of oxytocin

2.1.1   Oxytocin in organism

Oxytocin is an endogenous cyclo-nonapeptide hormone produced in the hypothalamus and secreted into the bloodstream by the posterior pituitary gland [8]. This peptide is recognised for its hormonal role in parturition and lactation. OT is present in the hypothalamic neurohypophyseal system and in other regions of the central nervous system (CNS) [9]. It displays diverse biological effects on contractile and membrane-transport phenomena [1,8]. The fact that OT is found in corresponding concentrations in the plasma and neurohypophysis of both sexes indicates that OT possesses numerous physiological functions [10]. The morphological, electrophysiological, neurochemical, and behavioural studies show that OT plays a significant role in several central functions such as maternal and sexual behaviour, memory and learning procedures, yawning, feeding, grooming, thermoregulation, cardiovascular regulation, or stress-related disorders [9]. It is able to regulate various physiological functions, such as milk ejection or uterine contractions. OT can interfere with salt and water balance. Furthermore, OT is clinically managed to control postpartum haemorrhage and stimulate labour. It retains a short half-life *in vivo*, approximately 2-5 minutes, and is administered to patients intravenously [11,12].

It is worth mentioning that OT is not only selective for the oxytocin receptor (OTR). It also interacts with related vasopressin (AVP) receptors such as V_{1a}, V_{1b}, and V_2 [13].

The design and synthesis of analogues of OT, their agonists or antagonists, could be fascinating for targeting a wide array of pathologies, for instance, cancer, pain, autism, premature parturition, or anxiety-related disorders [1,8].

2.1.2 Chemical structure of oxytocin

The peptide chain of OT consists of nine amino acid residues: S^1,S^6-cyclo(C-Y-I-Q-N-C)-P-L-G-NH$_2$ (**Figure 1**). The chemical structure of OT is comparable to a different nonapeptide, vasopressin. AVP differs from OT by two amino acid residues - isoleucine in OT, phenylalanine in AVP at the third position, and leucine in OT, arginine in AVP at the eighth position [14]. The sequence of OT is characterised by a disulphide bridge between Cys^1 and Cys^6, forming a 20-membered ring, which is essential for functional activity and binding to OTR [15].
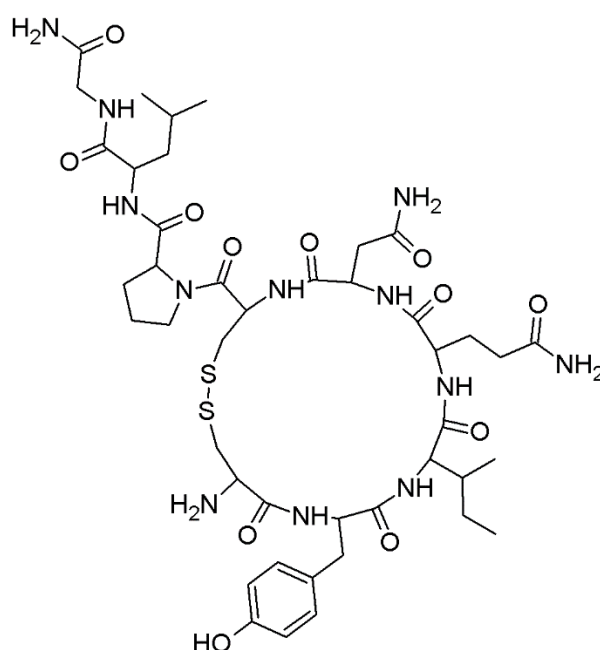
Figure 1 The chemical structure of oxytocin [14].

Oxytocin preferentially adopts a type I β-turn conformation in water, centred on Ile^3-Gln^4 residues. In contrast, the predominant conformations presented both in crystal structure and DMSO solution are type II β-turn stabilised by a hydrogen bond between C=O of Tyr^2 and N-H of Asn^5, and type III β-turn, which is stabilised by a hydrogen bond between C=O of Cys^6, and N-H of Gly^9. Another hydrogen bond between C=O of the Asn^5 side chain and N-H of Leu^8 is observed in DMSO [16–20].

2.1.3 Receptor of oxytocin

The human oxytocin receptor has particular interest for its role as a potential therapeutic target in a wide array of behavioural and physiological disorders [21]. It is expressed in the uterus, ovary, brain, heart, mammary gland, kidney, bones, and endothelial cells. OTR mediates uterine contractions and the oxytocic effect of OT in the uterus [10]. The significant impacts of OT remain the focus of scrutiny in animals [22–26] and humans [27–33] as a potential therapeutic agent for the treatment of autism and other anxiety disorders [34].

The OTR can bind endogenous ligands, *i.e.*, oxytocin, with an affinity of approximately 1-10 nM [35] and AVP, with an affinity of about 100 nM-1 μM [35]. Apart from OT, other molecules, such as AVP and oxytocin antagonists or agonists, are able to bind to the OTR because of their similarities in peptide chains [36].

The gene of the OTR is located in a single copy on chromosome 3p25 and contains four exons and three introns [36]. OTR belongs to the rhodopsin-type (class I) G protein-coupled receptor (GPCR) family and is coupled to phospholipase C [10].

The seven transmembrane α-helices are most conserved among the GPCR family representatives. Preserved amino acid residues among the GPCRs may be involved in a standard method for transducing signals and activating the G protein [10]. In the first class of the GPCR family, the aspartic acid in transmembrane domain two (Asp[85] in human OTR), a tripeptide part (E/D RY) at the interface of transmembrane two, and the initial intracellular loop is supposed to be essential for activation of the receptor [37]. In respect of Asp[85], this theory was developed for the human OTR. When Asp[85] can be replaced by other amino acid residues, *e.g.*, asparagine, glutamine, or alanine, the receptors signal transduction, and agonist binding reduces [38,39].

Modification at the tripeptide motif DRY (DRC in case of the OTR) effect in either inactive or a constitutively active OTR [38]. In the first and second extracellular loops, the cysteine residues are connected by a disulphide bridge and protected within the GPCR family. The other two well-conserved cysteine residues belong to the COOH-terminal domain [10].

Furthermore, the OTR has two (in mice and rats) or three (in humans, rhesus monkeys, bovines, sheep, and pigs) potential N-glycosylation sites (N-X-S/T consensus motif) in its extracellular H_2N-terminal domain [10]. Therefore, OTR is generally used as a target for the development of tocolytics, and the only drugs established in particular for the management of preterm labour are the OTR antagonists [40].

2.1.4   Oxytocin receptor agonists

Agonists of oxytocin receptors have been studied as pharmacological agents or prospective treatments for the management of neuropsychiatric diseases, for instance, anxiety-related disorders, autism, or schizophrenia. In the literature, there are many examples of OTR agonists, which may be peptides such as [Thr^4]OT, [HO^1][Thr^4]OT, [Thr^4,Gly^7]OT, [HO^1][Thr^4,Gly^7]OT or non-peptides, *i.e.*, WAY-267464 [41–44].

Synthetic OT is applied to accelerate labour and treat postpartum haemorrhage. Demoxytocin is an oxytocin analogue used for inducing labour, though it is less effective than prostaglandins [45]. Another synthetic peptide analogue of oxytocin, Carbetocin, is specified for the inhibition of atony of the uterus after caesarean section with epidural or spinal anaesthesia. This molecule possesses a longer half-life than natural OT and can be administered in a single dose, intravenously or intramuscularly [46].

2.1.5   Oxytocin antagonists as tocolytic agents

The therapeutic target in treating preterm labour is the pharmacological inhibition of uterine contractions using numerous tocolytic factors. They are applied to support pregnancy for 24 to 48 hours to enable corticosteroid administration to act and to allow the transfer of the mother to a centre with a neonatal intensive care unit. Ritodrine, nitric oxide, calcium-channel blocker donors such as glyceryl trinitrate, and COX-2 inhibitors, *i.e.*, Indomethacin, are some available tocolytics [47].

2.1.5.1   Peptide antagonists of oxytocin receptor

Selective human oxytocin receptor antagonists have been synthesised as tocolytic agents for managing preterm labour [36].

Due to their increased specificity to the uterus, OTR antagonists such as Atosiban (deamino-[D-Tyr^2-(*O*-ethyl)-Thr^4-Orn^8]vasotocin) can behave as a suppressant of contractions with advanced safety profiles [48]. Atosiban is an AVP V_{1a} receptor antagonist with a lower affinity for the OTR. Its action system is *via* dose-dependent inhibition of OT-mediated increase

in intracellular calcium levels, which requires the closing of voltage-gated channels to inhibit calcium influx [49]. Atosiban has been accepted for treatment in Europe of premature labour. However, it is administered through a bolus injection followed by an infusion and is not indicated for dosing beyond 48 hours [48]. Atosiban is safer than β-receptor agonists and is comparable in clinical efficacy to conventional β-agonist therapy such as Ritodrine, Terbutaline, or Salbutamol. However, it is better tolerated and is related to fewer maternal cardiovascular side effects [36].

On the other hand, Atosiban presents some disadvantages when applied as a tocolytic. It requires parenteral administration and hospitalisation, possessing limited bioavailability and low affinity of the OTR. Moreover, it is an antagonist for the V_{1a} receptors that cause side effects. Demonstrated limitations have led to efforts for the discovery of innovative peptide and non-peptide antagonists of OT for managing preterm labour [41].

Several highly selective OT peptide antagonists have been designed and synthesised, for instance, $d(CH_2)_5[Tyr(Me)^2]OVT$, $desGly-NH_2,d(CH_2)_5[Tyr(Me)^2,Thr^4]OVT$, $desGly-NH_2,d(CH_2)_5[D-Tyr^2,Thr^4]OVT$, $d(CH_2)_5,[D-Thi^2,Thr^4,Tyr-NH_2^9]OVT$, and $desGly-NH_2,d(CH_2)_5[D-Trp^2,Thr^4,Dap^5]OVT$. These compounds are both AVP and OT receptor antagonists. Nevertheless, they are more potent as OT antagonists than V_{1a} antagonists [50].

Furthermore, some peptide OT or AVP antagonists have a higher affinity for the human receptor than the Atosiban. For instance, $desGly-NH_2,d(CH_2)_5[D-2-Nal^2,Thr^4]OVT$, $desGly-NH_2,d(CH_2)_5[2-Nal^2,Thr^4]OVT$, $d(CH_2)_5[D-2-Nal^2,Thr^4,Tyr-NH_2^9]OVT$ and $d(CH_2)_5[2-Nal^2,Thr^4,Tyr-NH_2^9]OVT$ may be candidates as possible tocolytic agents [41].

Another selective peptide OT antagonist with a high affinity for the human OTR and low for the V_{1a} receptor is Barusiban. It possesses a higher potency and a longer duration of action than Atosiban. In contractility experiments with isolated human myometrium, Barusiban inhibits OT-induced myometrial contractions of both preterm and term myometrium, and this action was at least as potent as the action of Atosiban [51].

2.1.5.2   Non-peptide antagonists of oxytocin receptor

Non-peptide OTR antagonists are also under development. Since peptide antagonists lack oral bioavailability, pharmaceutical companies have investigated efficient non-peptide OT antagonists. Retosiban, 2'-methyl-1',3'-oxazol-4'-yl morpholine amide derivative, is a non-peptide OT antagonist more than 15-fold more potent than Atosiban for the OTR [52].

Another nonpeptide OT antagonist is L-368,899 (1-(((7,7-dimethyl-2(S)-(2(S)-amino-4-(methylsulphonyl)butyramido)bicyclo[2.2.1]-heptan-1(S)-yl)methyl)sulphonyl)4-(2-methylphenyl) piperazine). L-368,899 was a potent OT antagonist inhibiting spontaneous uterine contractions in pregnant rhesus monkeys. The organism of a pregnant woman can block OT-stimulated uterine postpartum activity with an effectiveness comparable to that of the pregnant rhesus monkey [36].

Additionally, the non-peptide OTR antagonist is Nolasiban. It is a selective, orally administered, and potent antagonist of OTR with a low affinity towards the AVP V_{1a} and V_2 receptors [53].

2.2   Replacement of the disulphide bridge

The disulphide bonds establish a crucial structural element in the stabilisation, folding, and structuring of peptides and proteins [8,54,55]. The S-S bridge is essential for binding to the OTR. However, it represents the peptide susceptible to endogenous degradation [56].

The three-dimensional (3D) structures of peptides and proteins can be rigidified or stabilised by forming macrocycles. For peptides, the biological activity of these compounds is related to precise structure folding. The S-S bridges are labile in peptides or proteins despite their stabilising effect. The disulphide isomerases, reducing agents, and thiols can affect this covalent bond and lead to structural rearrangement with complete activity loss. The replacement of this component by hydrolytically, reductively, and stable substitutes is of great interest to scientists [8].

Substitution of an unstable bridge with a more Red-Ox-stable linker is an attractive approach to improve the metabolic integrity of OT. Unfortunately, it is not trivial because its biological activity is sensitive to structural modifications within the cyclic framework.

Even minor distortions such as increasing the 20-membered ring by group, penicillamine, one methylene replacement of cysteine residue by amide, or substitute of the disulphide bond by a lanthionine or dicarba bond lead to the significant decrease in the activity of agonists [56]. The replacement of the S-S bridge has been reported to be more stable covalent linkers, for instance, thioethers (R_1-S-R_2), diselenides (Se-Se), or carbon-based bridges [8,57].

The reactivity of the disulphide bond is not required for bioactivity and is proven by the biological functions possessed by analogues of OT in which the 20-membered rings have been preserved. Nevertheless, the methylene group can replace one or both sulphur atoms with an ethylene group (**Figure 2**) [58].
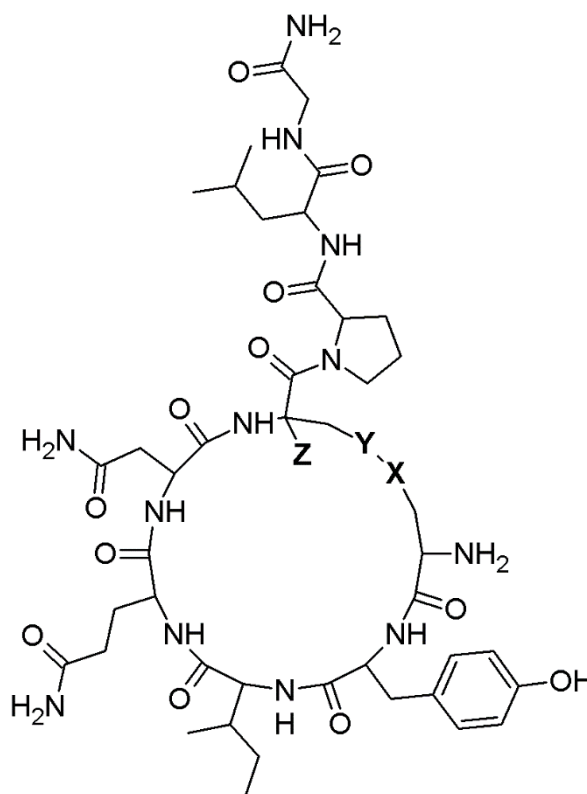
Figure 2 Structure of oxytocin lactam analogues, [*cyclo*-(1-L-aspartic acid,6-α,β-diaminopropionic acid)]oxytocin (**X** = CO; **Y** = NH; **Z** = NH_2) and [*cyclo*-(1-β-alanine,6-aspartic acid)]oxytocin (**X** = NH; **Y** = CO; **Z** = H) [58].

It is shown that substituting the S-S bridge with an amide of two isomeric forms results in analogues that retain enough conformational integrity to interact with receptors responsive to neurohypophyseal hormone [58].

Moreover, the synthesis of diamino acids and cyclic peptide derivatives using ring-closing metathesis (RCM) affords the chance to substitute a metabolically less stable disulphide bond with two methylene groups, a structural modification that results in the replacement of LL-cystine with LL-diaminosuberic acid (**Figure 3**) [59].
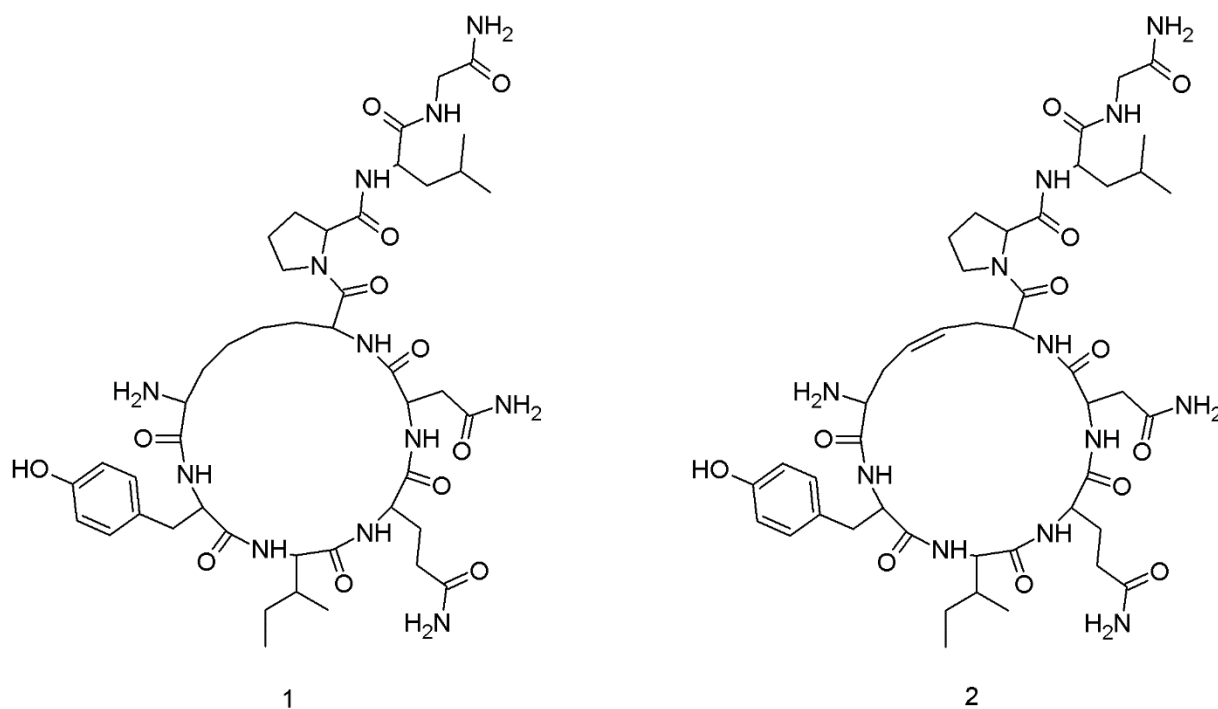
Figure 3 The structures of analogues of oxytocin in which the disulphide bridges are replaced by (**1**) saturated and (**2**) unsaturated hydrocarbon moieties [59].

It is presented that the substitution of the cysteines with L-allylglycine residue allows RCM for the facile generation of more rigid olefinic analogues and provides access to the saturated dicarba derivative. The ability of RCM to introduce more rigid ethylene bridges in place of metabolically less stable disulphide moieties may help generate analogues of a host of biologically active peptides or proteins [59].

In contrast, OT bioactivity is maintained when the S-S bridge of OT is replaced by chalcogen linkages such as cystathionine (CH_2-S), diselenide (Se-Se), selenylsulphide (Se-S) and ditelluride (Te-Te) bonds, where the 20-membered ring framework is conserved. For instance, substituting the disulphide bonds with the isosteric Se-Se bonds can improve

stability and peptide folding. It is envisaged that the replacement of the disulphide bridge by a non-reducible selenocystathionine bond might enhance the metabolic stability of cyclic peptides with minimal structural perturbation [56].

2.3   "Click chemistry"

The concept of "click chemistry" was introduced by Sharpless in 1999. He defined the rules of "click chemistry" as a set of chemical reactions that *"must be modular, wide in scope, give very high yields, generate only inoffensive by-products that can be removed by nonchromatographic methods, and be stereospecific (but not necessarily enantioselective). The required process characteristics include simple reaction conditions (ideally, the process should be insensitive to oxygen and water), readily available starting materials and reagents, no solvent or a benign solvent (such as water) or easily removed, and simple product isolation. Purification, if required, must be by nonchromatographic methods, such as crystallisation or distillation, and the product must be stable under physiological conditions"*.

The idea of "click chemistry" includes feasible and uncomplicated linking reactions to perform, present high yields, require minimal purification steps, and are versatile in joining diverse structures without the prerequisite of protection steps.

The classification of "click reactions" is identified below:

- cycloadditions – primarily refer to 1,3-dipolar cycloadditions. However, involving hetero-Diels-Alder cycloadditions,
- nucleophilic ring-openings – indicate the openings of strained heterocyclic electrophiles, such as epoxides, aziridines, cyclic sulphates, aziridinium or episulphonium ions,
- carbonyl chemistry of the non-aldol type – examples include the formations of ureas, thioureas, hydrazones, oxime ethers, amides, and aromatic heterocycles,
- additions to carbon-carbon multiple bonds – consist of epoxidations, aziridinations, dihydroxylations, sulphenyl halide, nitrosyl halide, and certain Michael additions.

Among the four major classifications, CuAAC is the most widely applied [60].

2.3.1 The Cu^{I}-catalysed Huisgen 1,3-dipolar cycloaddition

The Cu^{I}-catalysed Huisgen 1,3-dipolar cycloaddition of azides and terminal alkynes to form [1,2,3]-triazolyl moiety is the model example of a "click reaction" (**Figure 4**) [60].
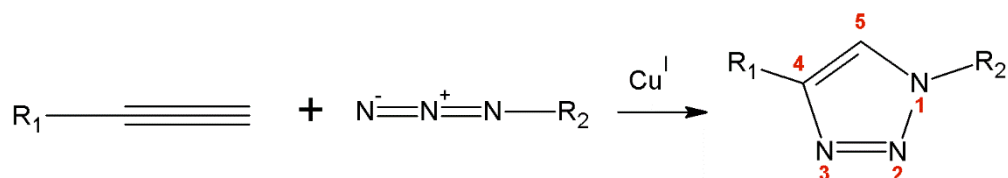
Figure 4 The scheme of the Cu^{I}-catalysed Huisgen 1,3-dipolar cycloaddition [60].

The success of CuAAC is established because it is a quantitative solid, standard, and orthogonal ligation reaction, suitable for even biomolecular ligation and *in vivo* tagging or as a polymerisation reaction for synthesising long linear polymers. This reaction is not sensitive to conditions if Cu(I) ions are present and may be performed in an aqueous or organic environment or solution and on solid support [61]. In **Figure 5**, there is the proposed mechanism of CuAAC.
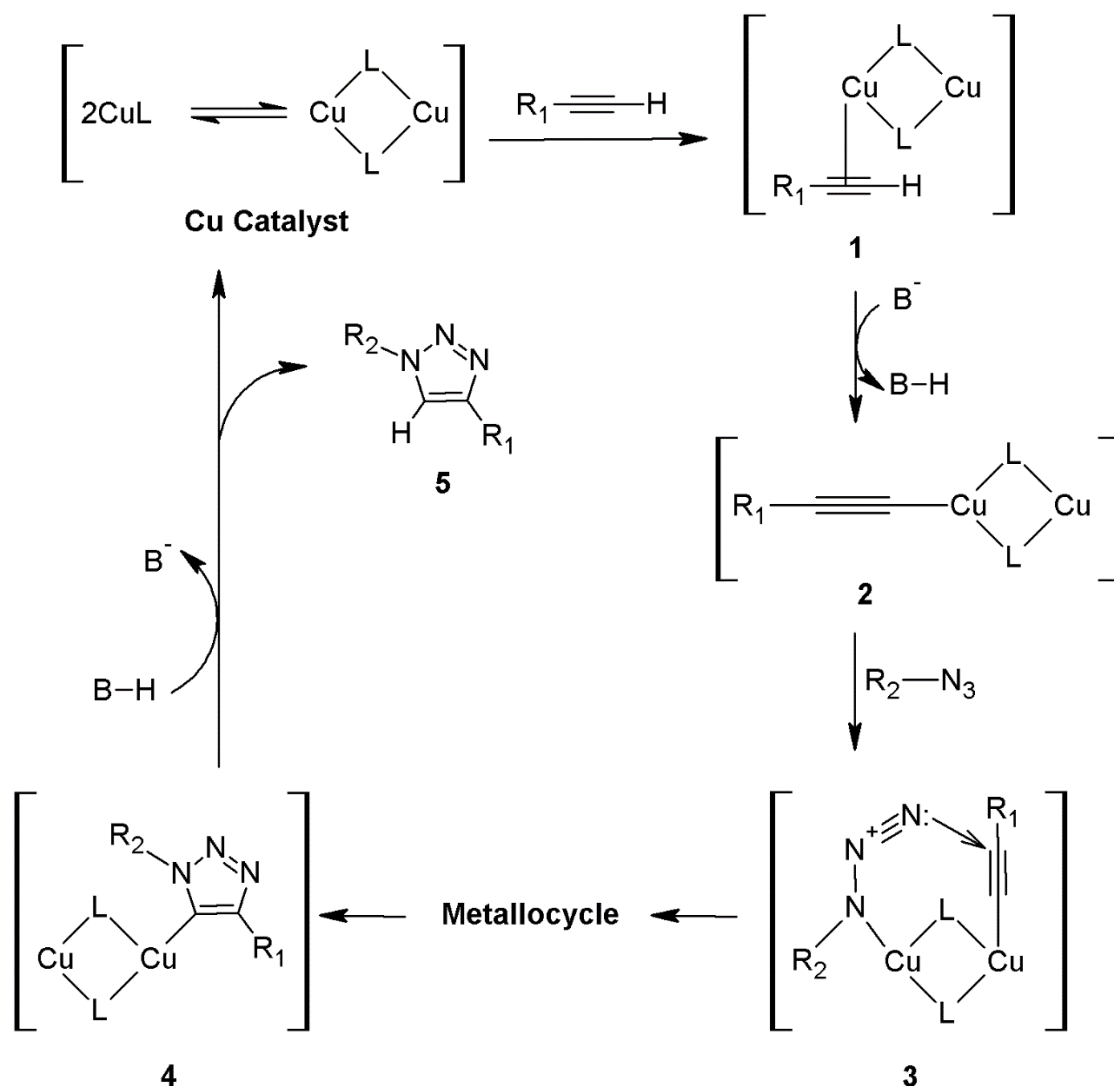
Figure 5 Proposed mechanism for the CuAAC reaction [60].

For the reason that Cu^I can readily insert itself into terminal alkynes, it is envisioned that the first step of the reaction involves the π-complexation of a Cu^I dimer to the alkyne (structure **1** in **Figure 5**). After that, deprotonation of the terminal hydrogen occurs to form a Cu-acetylide. The π-complexation of Cu^I decreases the pKa value of the terminal alkyne, allowing deprotonation to appear in an aqueous solvent without adding a base. If a non-basic solvent such as acetonitrile (ACN) was to be used, then the base, such as 2,6-lutidine or N, N'-diisopropylethylamine (DIPEA), would have to be beaded. In the following step, the nitrogen atom displaces one of the ligands from the second copper in the Cu-acetylide

complex to form structure **3**. This action brings the azide for nucleophilic attack. Due to proximity and electronic factors, the nitrogen atom can attack the carbon atom of alkyne, leading to a metallocycle. Then, the metallocycle contracts when the lone pair of electrons of the nitrogen atom attacks the carbon atom to form the triazole (**4**). Once structure **4** forms, the attached copper dimer immediately complex to a second terminal alkyne. However, this second alkyne cannot undergo a cycloaddition owing to the unfavourable structure of the complex, and it dissociates upon protonation to reform **4**. One final protonation releases the Cu^I catalyst from the 1,2,3-triazole product (**5**) to undergo a second catalytic cycle with different substrates. Each protonation results from interactions with a protonated external base and/or solvent [61].

More procedures exist to generate the active catalyst for the CuAAC. One standard method is reducing Cu(II) salts, such as $CuSO_4 \cdot 5H_2O$, *in situ* to form Cu(I) ions. The advantages of this strategy are low cost, the possibility to perform in the water, and deoxygenated conditions. Nevertheless, the main disadvantage of the mentioned technique is the possibility of reducing Cu^{II} to Cu^0 form [60].

2.3.2   The [1,2,3]-triazolyl moiety as a surrogate for unstable bond

The application of the triazolyl ring as the substitute of the disulphide bridge in peptide chemistry was first reported by Meldal and co-workers. The chemical orthogonality of the azide and alkyne, the robust synthetic scheme using "click chemistry" *via* either a copper-catalysed cycloaddition, the hydrogen bonding capabilities, and the increased water solubility causes the triazole motif the attractive pattern for designing novel bioactive analogues [62].

Moreover, the triazole-containing compounds have previously exhibited improved metabolic stability through increased stability to isomerases or proteases. The triazoles were selected for replacing the disulphide bridge due to their conformational stability, high dipole moment, chemical orthogonality, and uncomplicated method of synthesis using the Cu^I-catalysed Huisgen 1,3-dipolar cycloaddition [62].

Triazoles are five-membered aromatic heterocyclic molecules. Their structure possesses two carbon and three nitrogen atoms [63]. The triazolyl moieties can occur in two tautomeric forms: the 1,2,3-triazole or the 1,2,4-triazole (**Figure 6**), depending on the position of the NH group in the ring [64].
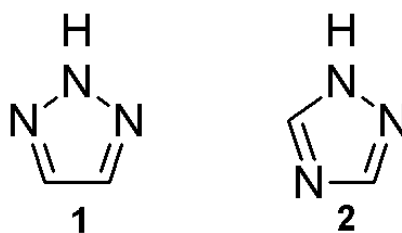
Figure 6 Structures of the two isomeric forms of triazoles: (**1**) 1,2,3-triazole; (**2**) 1,2,4-triazole [64].

The 1,2,3-triazole ring can be a weak hydrogen-bond acceptor with a large dipole that could align with the other amides in the peptide secondary structure. Overall, the 1,2,3-triazoles may be potential surrogates of amide bonds for numerous peptide modifications [65].

Guan *et al.* have developed an effective convergent strategy for constructing the β-turn mimicking unit through Cu(I)-catalysed alkyne-azide cycloaddition between the termini of two peptide chains. The prepared molecular modelling showed that a 1,4-connected 1,2,3-triazole ring might provide a geometry similar to the β-turn. This led to the proposal that cycloaddition between peptide chains, derivatised with the azides and terminal alkynes, may provide a means to synthesise β-turn units. They found that the tendency of β-turn formation for the triazole core strongly depends on the length of the linker. It was evidenced that a three-carbon linker is optimal for stabilising β-turn [65].

According to the literature, the molecules with triazolyl moieties maintain a variety of biological functions. They can be active against cancer or microorganisms, including fungi, bacteria, and viruses, *e.g.*, human immunodeficiency virus (HIV) [5].

2.3.3 The synthetic approach of triazole-modified compounds

The substituted triazoles are widespread structural changes in many organic and bioactive compounds. Following the literature, various methods have been developed to synthesise triazolyl moieties [5,66].

An intramolecular 1,5-electrocyclisation of β-substituted α-diazocarbonyl compounds is a studied technique for designing the triazole motifs. Unfortunately, the conditions

of this method are limited because they require mostly commercially available starting materials.

Jordão *et al.* have characterised this method by two pathways. Pathway **I** starts from β-amino-α,β-unsaturated esters or ketones, followed by a diazo transfer reaction. Conversely, pathway **II** starts from α-diazocarbonyl compounds, followed by α-diazoimino formation (**Figure 7**). The diazo-donor reagents can be sulphonyl azides, for example, methanesulphonyl azide, tosyl azide, 3-diazo-1,3-dihydro-2*H*-indol-2-one or *p*-carboxylbenzenesulphonyl azide [67].

R = Bn and R_1 = OEt

R = Bn and R_1 = Me

R = *n*-Bu and R_1 = OEt

R_2 = H and R_3 = 4-FC$_6$H$_5$
R_2 = Thiophene-2-yl and R_3 = BrCH$_2$CH$_2$
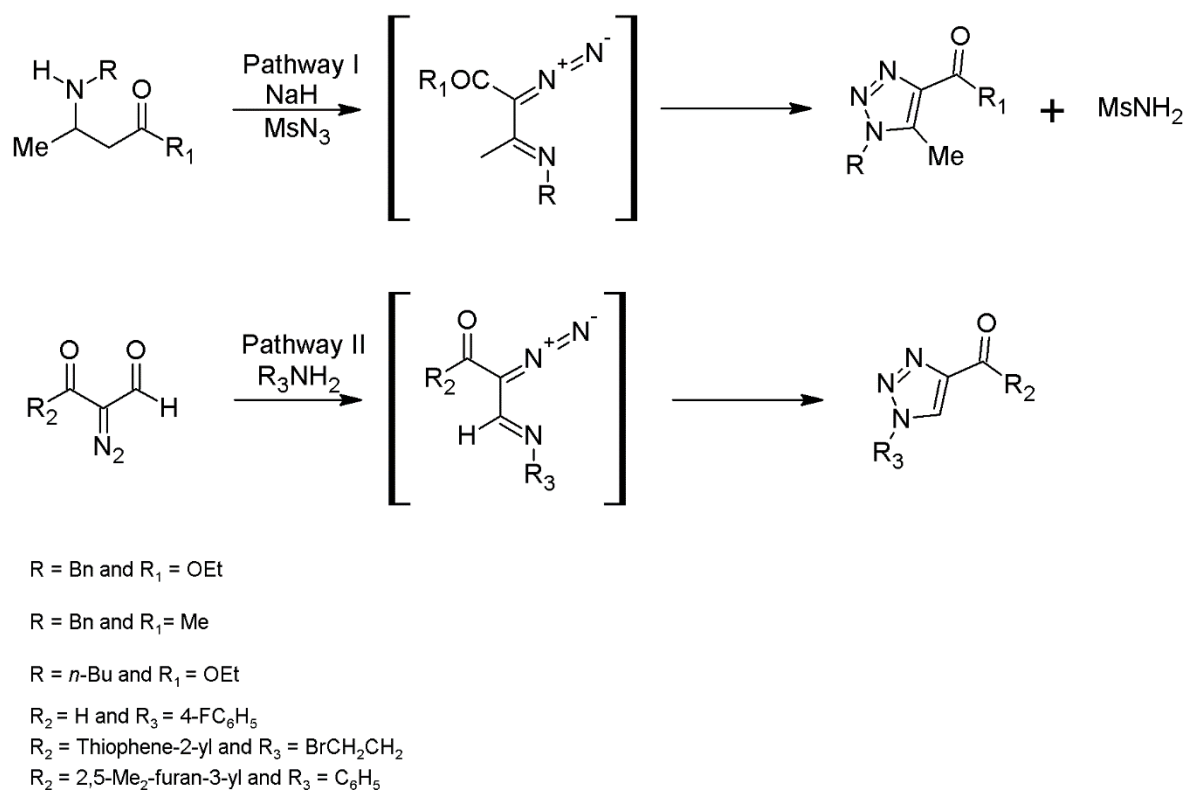R_2 = 2,5-Me$_2$-furan-3-yl and R_3 = C$_6$H$_5$

Figure 7 Techniques of preparation of the triazoles starting from α-diazoimines [67].

Nagasawa and colleagues developed the method for the transition metal-catalysed preparation of 1,2,4-triazoles. They used the coupling nitriles with amidines to obtain the 1,2,4-triazole analogues by efficient copper-catalysed synthesis [68].

Furthermore, Beifuss *et al.* developed an innovative and effective copper-catalysed reaction between ammonium carbonate and imidates to synthesise symmetrically substituted 3,5-diaryl-1,2,4-triazoles [69]. This procedure was efficient, but most considered the substrates, such as amidines or imidates synthesised from nitriles [70].

Moreover, Zhang and co-workers characterised the catalytic transformation of azides and alkynes mediated by ruthenium(II) ions (RuAAC) that give selective admission to 1,5-disubstituted 1,2,3-triazoles [71].

The most widespread "click reaction", CuAAC, was carried out to generate the five-membered heterocyclic compounds containing the triazole moiety without complicated reagents. The azide-alkyne cycloaddition was identified as the most helpful approach to conjugate two or more structural motifs [72]. Huisgen described the principal method for the synthesis of triazolyl moiety in 1963 [73]. The cycloaddition between azides and alkynes is a particularly atom-economical reaction, leading to the design of the 1,2,3-triazoles. However, this method is not regioselective. The result is the development of both forms: 1,4- and 1,5-disubstituted 1,2,3-triazoles [74]. The reaction was performed between azide and acetylene under reflux conditions in toluene, leading to a combination of 1,4- and 1,5-regioisomers of 1,2,3-triazoles [64].

2002 was disruptive because Meldal and Sharpless and their co-workers separately described the most significantly used "click chemistry" method [75,76]. The cycloaddition catalysed by copper(I) ions conduces to 1,4-disubstituted 1,2,3-triazoles under mild conditions (**Figure 8**) [77].

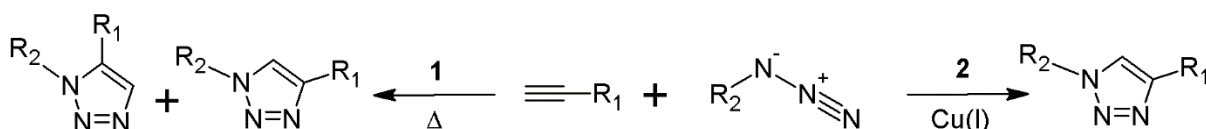
Figure 8 The Huisgen cycloaddition: (**1**) under thermal conditions and (**2**) catalysed by copper(I) ions [77].

Additionally, the copper-catalysed azide-alkyne cycloaddition is selective, efficient, and can be performed in a gentle reaction condition. This procedure may be performed in water and organic solvents with complete selectivity and conversion [77]. The reaction involves Cu(I)

or Cu(II) salts in organic solvents or a mixture of *tert*-butyl alcohol and water at room temperature (RT) [78]. The mentioned method is one of the instances of "click reaction" proceeding with high purity, yield, regioselectivity, and comprehensive chemical transformation [79].

Furthermore, the 1,2,3-triazoles are recognised as valuable peptidomimetic moieties [80]. Kuang and colleagues have designed the reaction in non-reductive conditions between $Cu(OAc)_2$ and N-containing additional ligands in which the azide chelation significantly improves the reaction rate [81].

McNulty *et al.* studied homogeneous silver(I) catalysed azide-alkyne cycloaddition (AgAAC) due to the toxicity of redox-active copper(I) ions for many biological aspects. The reaction was carried out at RT, including a silver acetate and a thermally stable phosphane ligand. Nevertheless, heating up to 90°C was required to enhance the yield of the reaction [82].

Smith and co-workers described a zinc-mediated azide-alkyne cycloaddition, which can form 1,5- and 1,4,5-substituted 1,2,3-triazoles at RT. The reported reaction was performed with a catalytic amount of N-methylimidazole, which is obligatory to generate the zinc acetylide [83].

Fokin *et al.* have described the first transition metal-free catalytic azide-alkyne cycloaddition for synthesising 1,5-diaryl-1,2,3-triazoles. The triazolyl ring was generated between aryl azides and terminal alkynes in the presence of a catalytic amount of hydroxide at RT. This reaction is insensitive to atmospheric oxygen or moisture [84].

Furthermore, the methods including ultrasounds have the advantage of allowing to perform the reactions in both heterogeneous and homogeneous systems [78]. Cintas and colleagues described the synthesis of 1,4-disubstituted 1,2,3-triazole analogues under ultrasounds without adding any ligand *via* metallic copper [85].

The triazole motif is applied as a popular peptidomimetic moiety and can adjust the secondary structure of the peptide. The synthesis of triazole amide substitutes by a peptidomimetic ligation method involves N- and C-terminally modified peptides with α-azido acids and α-amino alkynes, independently. Chiral α-amino alkynes can be synthesised in a few phases, beginning with the protected parent amino acids. The inclusion of 1,4-disubstituted triazoles into the backbone of a peptide chain was achieved by traditional solid-phase peptide synthetic (SPPS) strategies, including triazole-containing pseudo-dipeptides as building blocks [80].

The synthesis of low molecular weight triazolyl cyclopeptidomimetics is performed by peptide synthesis in solution *via* the precursor followed by CuAAC (**Figure 9A**). In the case of extended amino acid sequences, the triazolyl core can be included in the peptide chain during peptide elongation by standard SPPS coupling technique (**Figure 9B**). Otherwise, the heterocyclic structures may be connected to the solid support by the copper-catalysed azide-alkyne cycloaddition between the alkyne precursor and azide (**Figure 9C**). The conjugation of the peptide fragments after CuAAC, a practical approach for proteins, can be carried out from azide and alkyne in the solution (**Figure 9D**) [86].
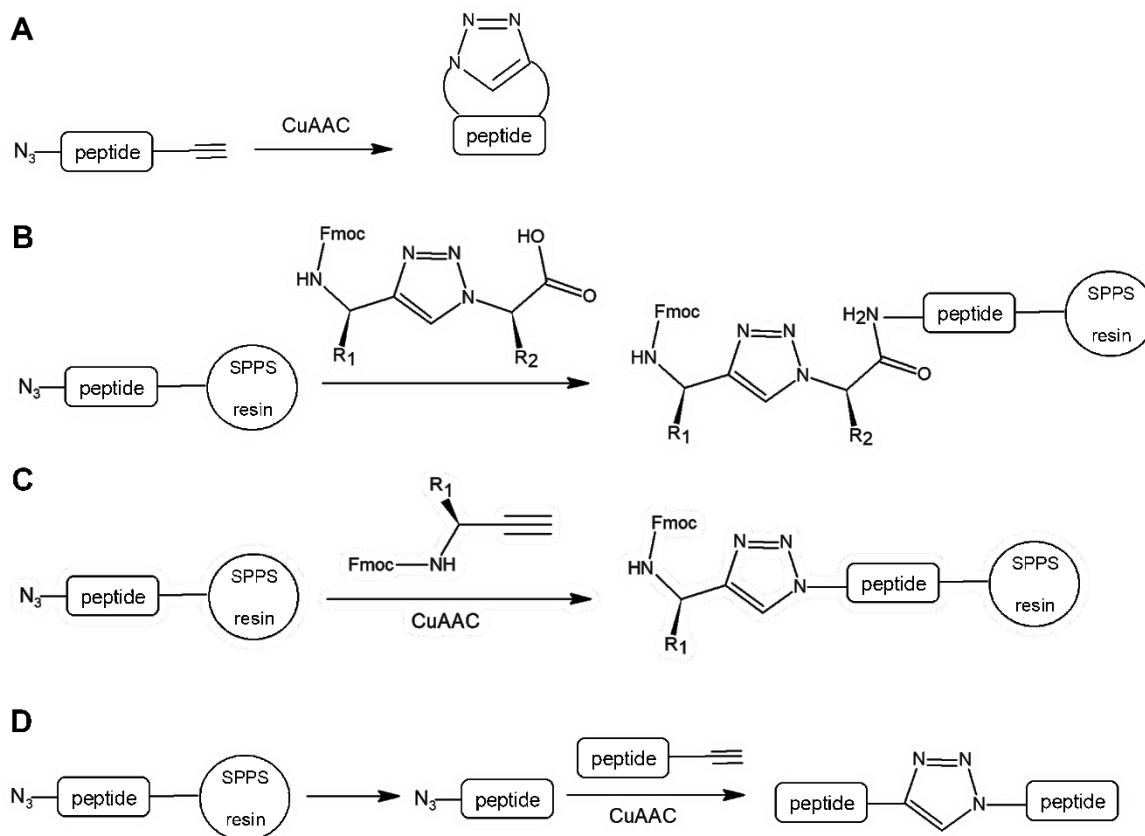
Figure 9 Synthetic approaches of triazolyl including cyclopeptidomimetics: (**A**) CuAAC in SPPS; (**B**) inclusion of triazole during SPPS; (**C**) connection of triazole to the solid support by CuAAC; (**D**) coupling of peptide chain fragment in solution after CuAAC [5,86].

Anyhow, the synthesis of the building blocks N^α-Fmoc-protected ω-azido and ω-ynoic-α-amino acids were shown to be involved in launching applicable synthetic procedures to develop a significant amount of "clickable" peptides [2,7,87].

According to the literature, microwave-assisted "click chemistry" is also common. Microwave irradiation decreases the reaction time, allows efficient internal heat transfer, and consequently increases the yield of the process. High temperature is quickly achieved. Thus, decomposition and polymerisation are avoided [78].

Ma and colleagues have described a microwave-assisted copper-mediated one-pot three-component synthesis of symmetrically substituted 1,2,4-triazoles between amines and aryl nitriles. This technique involves two equivalents of copper salts [66].

D'Ercole *et al.* have developed a reproducible and efficient microwave-assisted method for synthesising side chain-to-side chain cyclopeptides. They prepared the azide-alkyne cycloaddition catalysed by copper(I) ions in the solid phase. All essential parameters, *e.g.*, resin type, solvent, reaction time, catalytic system, and microwave energy, were optimised by a systemic one element at a time method [88].

Furthermore, 1,4-disubstituted 1,2,3-triazole is comparable to substituted imidazole due to its coordinative properties and amide bonds in molecular dimension and planarity. The triazolyl moieties are common ligands supporting donor sites for diverse metal ions coordination [77].

2.4   Application of the molecules possessing the triazolyl moieties

The chemical compounds containing triazoles have been widely studied for many pharmaceutical applications [5]. The 1,2,3-triazole derivatives present numerous bioactive functions, *i.e.*, against cancer, bacteria, fungi, or viruses, and as inhibitors of enzymes [89]. Some examples of the application of triazoles are presented below.

2.4.1   Triazole-modified compounds against microorganisms

Liu *et al.* analysed the antimicrobial properties of the [1,2,3]-triazolyl derivatives. They have applied "click chemistry" to transfer the Polybia-MPI (MPI), which is a natural antimicrobial peptide (AMP) isolated from the venom of the social wasp *Polybia paulista*.

It acquires weak haemolytic properties and activity against gram-negative and positive bacterial strains. The obtained results are presented in **Table 1**.

Table 1 Amino acid sequence and antibacterial properties of MPI and its analogues with minimal inhibitory concentrations (MIC) values given in µM; NA no antimicrobial activity [90].

Peptide	Sequence	*Escherichia coli*	*Staphylococcus aureus*	*Bacillus subtilis*	*Pseudomonas aeruginosa*
MPI	Ile-Asp-Trp-Lys-Lys-Leu-Leu-Asp-Ala-Ala-Lys-Gln-Ile-Leu-NH$_2$	32	32	8	NA
C-MPI-1	Ac-Ile-Asp-Trp-Lys-Lys-Leu-Leu-Lys-Ala-Ala-Lys-Pra-Ile-Leu-NH$_2$	64	64	8	NA
C-MPI-2	Ac-Ile-Lys-Trp-Lys-Lys-Leu-Leu-Pra-Ala-Ala-Lys-Gln-Ile-Leu-NH$_2$	128	256	128	NA
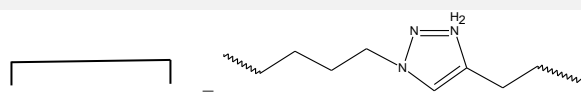
The authors have synthesised two intramolecular cyclic analogues, including the [1,2,3]-triazolyl moieties, C-MPI-1 and C-MPI-2, with various bridge orientations. The structure of C-MPI-1, cyclised at the *i* to *i*+4 positions, shows an enhanced helical tendency in H$_2$O, 50% trifluoroethanol (TFE), 30 mM sodium dodecyl sulphate (SDS), and improved stability against trypsin in comparison to parent peptide MPI. On the other hand, the structure of C-MPI-2, cyclised at the *i* to *i*+6 positions, lost helical motif in the same conditions. Consequently, the significance of the peptide helicity in antimicrobial properties was confirmed [90].

Furthermore, structures possessing the [1,2,3]-triazolyl cores play an essential role due to the extensive therapeutic applications in antifungal therapy. Therefore, triazole-containing medicines have been efficiently developed and used to treat several microbial infections for years [91]. Growing resistance to the existing antifungal drugs led to the development of innovative triazole analogues with progressive therapeutic indexes and increased antifungal spectrum [92].

Junior *et al.* proposed the glycotriazole-peptide analogues consisting of the [1,2,3]-triazolyl and monosaccharide moieties attached to amino acid residues presented in **Figure 10**.
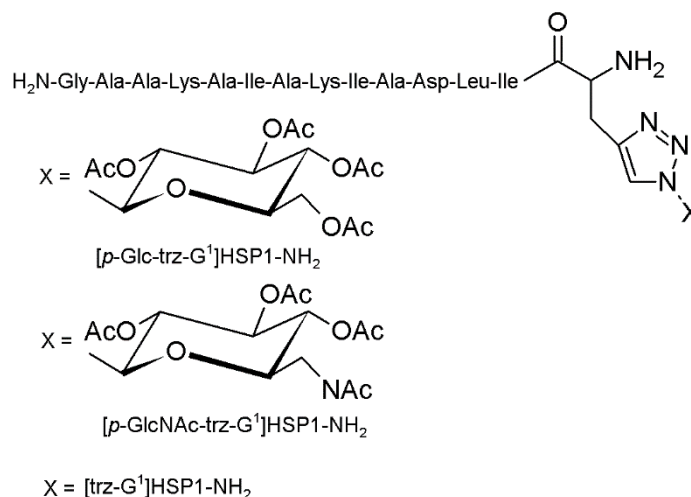

Figure 10 The glycotriazole-peptide derivatives [93].

They suggested the glycotriazole-peptide from hylaseptin-P1 (HSP1), which is AMP characterised by a 14-amino acid sequence C-terminal amide (HSP1-NH$_2$). In this sense, the triazolyl bridge bonded the peptide chain to the saccharide moiety. The antibacterial properties of HSP1-NH$_2$, [*p*-Glc-trz-G^1]HSP1-NH$_2$, [*p*-GlcNAc-trz-G^1]HSP1-NH$_2$, and [trz-G^1]HSP1-NH$_2$ were examined against gram-negative strains (*Pseudomonas aeruginosa*, *Escherichia coli*), gram-positive (*Staphylococcus aureus*, *Streptococcus agalactiae*) strains, and compared with chloramphenicol. The structures, except for *Streptococcus agalactiae*, demonstrated antibacterial activity against the examined bacteria. Interestingly, these tests showed that glycosylation stimulates slight antibacterial activity. Nevertheless, the glycotriazole-peptides and the [trz-G^1]HSP1-NH$_2$ presented improved antifungal abilities compared to HSP1-NH$_2$. The structure HSP1-NH$_2$ possesses no activity against *Candida spp.* strains. The triazole analogues demonstrated noticeably higher antifungal activity, indicating the significance of the triazole moiety in this procedure [93].

It is worth noting that structures containing the triazolyl moieties can be applied as treatments for HIV. Currently, inhibitors in antiretroviral therapies target the viral enzymes: integrase, protease, and transcriptase [94]. The virus can attack macrophages and T cells

by fusion of the viral membrane with the target cell membrane. In this sense, applying the virus to host cells is a great drug target. In this process, an essential function is presented by the glycoprotein from the viral envelope, derived from the proteolytic cleavage of a gp160 precursor into the gp120 surface protein and the gp41 transmembrane protein.

McFadden and colleagues described the peptide triazole derivative of 12p1, HNG-156, with a ferrocenyl triazole-substituted conjugate and attaching to gp120 with an equilibrium dissociation constant of 7 nM K_D, in contrast to the 2600 nM K_D value for 12p1. This study confirmed that the HNG-156 is non-cytotoxic and possesses anti-HIV type 1 (HIV-1) activity. Moreover, the triazole-modified peptide reacts with all analysed inhibitors [95].

Additionally, Rashad and co-workers studied the peptide triazoles, which can inhibit HIV-1 cell infection and suppress gp120 receptor binding. Furthermore, the peptide triazole analogues were stable to chymotrypsin and trypsin [96].

Likewise, triazole-modified peptidomimetics demonstrate anticancer properties. Sun *et al.* synthesised two cyclopeptide mimetics of a second mitochondria-derived activator of caspase by substituting two amide bonds with two triazole moieties. These peptidomimetics can bind to XIAP (blocking apoptotic pathways by binding with low nanomolar affinities and inhibiting caspase activity), cIAP-1, and cIAP-2 (inhibitor of cancer necrosis). Also, they can recover the activity of caspase-3/-7 and caspase-9, inhibited by XIAP [97].

According to the literature, substituted 1,2,4-triazole, *e.g.*, Letrozole, Anastrozole, and Vorozole, are important chemotherapeutics in breast cancer [98]. Baharloui and colleagues have described that both peptides GLTSK and GEGSGA, containing the triazolyl motifs, presented relevant anticancer properties against colon and breast cancer cells. In addition, the peptidomimetics containing the triazolyl cores demonstrated advanced cytotoxic activity on MDA-MB-231 cells rather than on MCF-7 cells [99].

Tahoori *et al.* synthesised a structure with high activity against lung cancer cells. This peptidomimetic has been discovered to be applied in tumour treatments by stimulating apoptosis in cancer cells recognised to have changed ras oncogene. The anticancer activity was observed *in vitro*, and peptidomimetics indicated a meaningful property against cancer cells with mutated ras oncogene such as A549, C26, and PC3 cells [100].

2.4.2   The structures possessing triazolyl cores with enzyme inhibition properties

Triazolyl-including peptidomimetics can be effective human enzyme inhibitors. Unfortunately, peptides are susceptible to enzymatic degradation, and owing to this barrier, several modifications must be used to improve the structural stability *in vivo* [101,102]. Incorporating triazolyl moiety into the peptide chain can increase cell life-time [103]. In this sense, the mentioned Huisgen cycloaddition is a promising approach to synthesising macrocycles or mimicking the β-strand conformation. These modifications can enhance peptide biostability and reduce conformation mobility, crucial in inhibitor designing [104].

Trabocchi *et al.* presented a library of peptidomimetic compounds with an N- or C-terminal guanidino group. All sequences were obtained *via* CuAAC, which developed sixteen unique 1,2,3-triazole analogues. They reported the data of *in vitro* inhibition tests with two different concentrations of each compound and later compared it with chloroamidine, a commercially available inhibitor of protein arginine deaminase 4 (PAD4). Five examined molecules were inactive, while the rest reached inhibitory effect at 1 and 10 mM concentration with 5-41% or 16-99%, respectively. Moreover, the chloroamidine demonstrated inhibition at 24% ($C_M = 1$ mM) and 36% ($C_M = 10$ mM). Molecular modelling studies have shown that the bond formation with [1,2,3]-triazolyl moieties and Arg^{374} or Trp^{347} residues is preferred, and this characterisation depends on the lengths of the side chains of amino acid residues [105].

Houghland and co-workers have synthesised ten unique peptidomimetics containing 1,2,3-triazole-linked lipids. This study has demonstrated that the replacement of effortlessly hydrolysed amide or ester linkages with the triazole bridge is accepted by the human ghrelin *O*-acyltransferase (GOAT). Furthermore, the attachment of hydrophobic fragments increases the potency and supports better effects in GOAT inhibition (IC$_{50}$ value of 0.7 µM) [106].

Guo and colleagues examined three series of 1,4-disubstituted 1,2,3-triazoles, which can be inhibitors of caspase-3 and caspase-7. It was observed that the N-terminal incorporation of the urea group performed the essential role of their activity. Moreover, molecular docking studies have proved that forming hydrogen bonds in the binding site caspase-3 is significant for inhibition [107].

Leyva *et al*. described a detailed study on caspases 1-3 and 6-9. They used a substrate activity screening (SAS) method to identify the substrates of caspase-6 and caspase-9. The reported groups in the most potent substrates were substituted with the pharmacophore, including the [1,2,3]-triazolyl core. The investigation led to three non-peptide inhibitors

with irrevocable character, which present high deactivating functions of caspases and low or no inhibition of other cysteine proteases [108].

In 2012, Valverde and colleagues explained studies about applying CuAAC to assemble unprotected peptide fragments into bioactive triazoles containing proteins. They have shown the value of the triazole moieties in developing secondary structures *via* hydrogen bonds as stabilising agents [80].

Lalmanach *et al.* have designed four compounds, among which the ones including the 1,4-disubstituted 1,2,3-triazole moiety or a semicarbazide bond, consequently substituting the C^α of glycine with a nitrogen atom. The screening tests resulted in visibly better outcomes for *aza*-Gly derivatives concerning triazolyl mimetics. Nevertheless, both groups displayed an engaging activity (K_i around nM *vs.* mM range, respectively). Molecular modelling studies justify the preference of the semicarbazide bond as discovered for the principal analogues [109].

Fittler and his research group have designed, synthesised, and analysed a library containing twenty-two chemical compounds to improve the inhibition activity of the sunflower trypsin inhibitor-1 (SFTI-1). Among these variations, sixteen studied structures were characterised as triazole analogues. Other modifications besides the triazolyl bridge substitution were applied, *i.e.*, non-natural amino acids coupling and sequence shortening. The nanomolar activity of the synthesised compounds was described by *in silico* experiments, suggesting a supplementary proton donor-acceptor interaction of basic ε^2-N in acidic residues and histidine in the active protease cleft [110].

Comparable research focused on replacing 1,4-disubstituted 1,2,3-triazoles into the peptide chain was reported by Empting *et al*. They have analysed the disulphide-bridged substitution to rigid the conformation and improve, leading to a more valuable activity than the STFI-1. One of the 1,5-disubstituted 1,2,3-triazole peptidomimetics demonstrated nanomolar inhibition activity, in line with the results of disulphide-bridged STFI-1 [111].

The cited literature highlights the most significant and recent studies, including the synthesis of triazolyl-containing peptidomimetics and their biological activity. The presented research explains the crucial role of the 1,2,3-triazole motif in peptide bioactivity.

Peptides that contain triazolyl moieties are a characteristic instance of peptidomimetics. They present all the benefits over standard peptides. Both effective synthetic techniques and bioactivity make these structures attractive and potential research objects. The structures possessing triazolyl motifs can be widely used as agents against cancer, bacteria, fungi, and viruses. It is worth mentioning that these modifications provide higher stability and bioactivity compared to non-modified structures [5].

2.5   Peptides antigens as biological targets

On the other hand, not only peptidomimetics possess significant roles in some biological systems or treatments for many diseases. Peptides also have many functions to play these valuable purposes. It is known that peptidomimetics have more advantages than natural or synthetic peptides, but they are also noteworthy in some cases. Peptides or proteins have established a favourable alternative to small-molecule scaffolds for some targets [112].

Peptides and antibodies (Abs) have entered a successful group in immunology since they were discovered. Peptide chemistry created the base of knowledge about protein structure, and Abs laid the basis for molecular immunology, even though the correlation between Abs and antigens (Ags) had to await innovations in peptide and protein chemistry. These advances led to the understanding that Abs and a primary group of Ags are themselves proteins. Peptides were also crucial for explaining the molecular biology of Ab specificity and biosynthesis, regarding B cell specificity and antigen presentation and T cell specificity and development [113].

Molecular biology still depends on applying peptides, antibodies, and peptide antibodies. This applies to research, diagnostics, and therapy and may become essential to preventing disorders, for instance, vaccination. In addition, new types of molecules are being developed to complete the traditional purpose of reagents, which may become helpful if the technologies can be more advanced [113].

In this scenario, I emphasised the recognition of series peptide antigens by patients with Multiple Sclerosis (MuSc).

2.6 Multiple Sclerosis

Multiple Sclerosis (MuSc) is the most common neurological and autoimmune disease affecting the CNS. MuSc indicates physical severe or intellectual incapacitation and neurological complications in young adults [114]. Multifocal regions of inflammation caused by focal T-lymphocytic, macrophage infiltrations, and death of oligodendrocytes are the significant causes of myelin sheath damage [115]. It results from forming CNS plaques composed of inflammatory cells and their products, transacted or demyelinated axons, and astrogliosis in grey and white matter. These lesions can crosstalk with the proper transport of nerve signals and lead to neuronal dysfunction, *e.g.*, autonomic and sensorimotor defects, ataxia, visual disturbances, fatigue, problems in thinking, and emotional difficulties [114].

It is expected that MuSc can become a common neurodegenerative disease, establishing the stage for pre-symptomatic diagnosis for other neurodegenerative disorders, especially Parkinson's or Alzheimer's disease [116].

There are four subtypes of MuSc: relapsing-remitting MuSc (RRMuSc), primary progressive MuSc (PPMuSc), secondary progressive MuSc (SPMuSc), and progressive relapsing MuSc (PRMuSc). Among these subtypes, RRMuSc is the most popular [117].

MuSc is more frequent in females, but this is not a rule. In the case series from the early 1900s, the sex ratio was almost identical. Since then, the sex ratio has progressively been rising, and now it is approximately 3:1 (female:male) in most technologically advanced countries [118]. There is an improving prevalence and frequency of MuSc in both developed and developing countries [119].

The aetiology of MuSc is still being determined. Nevertheless, it can be believed to be a multifactorial disorder, including a genetic predisposition linked with environmental impacts [120]. Inflammation of the grey and white matter tissues in the CNS due to focal infiltration of immune cells and their cytokines is the first reason for damage in MuSc. Many surveys have indicated that T helper cells (Th) adapt and interfere with the immune responses initiated by interaction between antigen-presenting cells (APCs) and T lymphocytes, which play an essential role in the beginning and progression of MuSc [121,122]. Moreover, B lymphocytes and their cytokines are other elements in the pathogenesis of MuSc.

Transforming growth factor-beta (TGF-β) or tumour necrosis factor-alpha (TNF-α), produced by these cells, can stimulate inflammation. In addition, mentioned cells can generate interleukin 10 (IL-10), an anti-inflammatory cytokine. Therefore, B lymphocytes have positive

and negative effects on the development of MuSc [123]. In addition, it is indicated that cytotoxic T cells (or CD8+ T cells) can be found in MuSc lesions [124]. These cells, *via* the production of cytolytic proteins such as perforin, mediate the suppression and deactivation of CD4+ T cells. Furthermore, these cells thoroughly improve vascular permeability and glial cell damage and trigger oligodendrocyte death, playing a crucial function in the pathogenesis of MuSc. In addition to CNS inflammation, the myelin repair procedure due to oligodendrocyte death is also limited [122].

It is known that many environmental factors cause the MuSc, such as viral agents, for example, Epstein-Barr virus (EBV) or human herpes virus type 6. Also, *Haemophilus influenzae* or *mycoplasma pneumonia* are potential bacterial triggering agents in MuSc [125,126]. Other factors that can cause MuSc are smoking cigarettes [127], deficiency of vitamins (mainly D and B_{12}) [128], diet [129,130], and exposure to UV radiation [131]. The external agents may have a nuclear antigen structurally homologous with myelin sheath components such as MBP, proteolipid protein (PLP), and myelin-associated glycoprotein. Therefore, myelin sheath lesions will form when these pathogens trigger immune cells [128]. Furthermore, the significant genetic risk connected with MuSc resides in DRB1-HLA*15 and/or other loci in solid connection imbalance with this allele. Heterozygotes for HLA-DRB1*15:01 have a probability ratio of MuSc more than three and homozygotes more than six, but the mechanism is unknown [132].

It is hypothesised that the role of HLA-DRB1*15:01 is *via* the presentation of antigens. Nevertheless, it cannot explain the protecting effects of the first class of alleles, such as HLA-A*02:01 [133].

MuSc is a voyage from being at risk through the asymptomatic illness, prodromal, and symptomatic stages [116]. Early recognition of MuSc is significant because it can give the occasion to pursue therapy and plans for the future. A precise diagnosis of MuSc is based on medical history and neurological examination using imaging techniques, *e.g.*, magnetic resonance imaging (MRI), lumbar punctures (LP) for analysis of cerebrospinal fluid (CSF), and analysis of blood samples [134]. MRI can identify any scar tissue formation and damage in the CNS. Evoked potential test that includes the visual, brain stems auditory, and somatosensory evoked possibilities present knowledge about demyelination in the CNS and optic nerve [128]. Additionally, analysis of CSF for MBP, immunoglobulin G (IgG) determinations [135], and analysis of blood samples for detection of deficiencies of the vitamins might be diagnostically valuable [136].

Owing to its heterogeneity, not completely specific MuSc biomarkers are available, thus hampering diagnosis and patient stratification. Bear in mind that current studies on B cells showed the significant role of antibodies in MuSc pathology. Identifying the antigenic targets characterised by specific antibodies in MuSc patient sera may improve patient stratification [104]. Some study indicates that the pathogenesis of MuSc has focused on the possible connection between MuSc and a plentiful protein found in CNS myelin, such as MBP [137].

2.7   Myelin Basic Protein

Myelin Basic Protein is the second most abundant protein, after the PLP, in CNS myelin [138], and it is a member of the family of intrinsically unstructured proteins [139,140]. Depending on interactions and environment, MBP can change its conformation [137]. It contains 30% of the total protein and approximately 10% of the dry weight of myelin. It is the only structural protein discovered to be necessary for creating CNS myelin.

MBP is attached to the cytosolic surface of the oligodendrocyte (OL) membrane, primarily by electrostatic interactions with negatively charged lipids [138]. It is presented in compact internodal myelin and is recognised to participate in the adhesion of the cytosolic surfaces of the multi-layered myelin sheath [141,142].

Furthermore, MBP plays essential functions, for instance, in signalling [143,144], in the nucleus [145], a regulatory role in the expression of other myelin proteins [146,147], and interactions with the cytoskeleton [148–151].

It is evidenced that MBP can attach to negatively charged lipid surfaces. It can bind to two lipid surfaces at once, probably by dimerising, and cause aggregation and adhesion of lipid vesicles [152–156] or multilayer formation [157–160]. Moreover, MBP can interact with polyanions such as microtubules *in vitro* [161,162], actin filaments [148,150,151,163,164] and binds to other proteins, *e.g.*, clathrin [165] or Ca^{2+}-calmodulin [148,149,166–169].

A myelin sheath, including MBP, appears in all vertebrates except the evolutionarily oldest (hagfish and lampreys, members of *Agnatha Cyclostomata*). The sequence of MBP is highly conserved from mammals (ten species sequenced) to chickens to clawed frogs [170]. MBP is also present in fishes, but shark MBP possesses only 44% homology with mammalian MBP [171,172].

Classic MBP, found in myelin, is a product of a larger gene complex called Golli (genes of oligodendrocyte lineage). It contains eleven exons in mice and ten in humans, including seven exons giving rise to classic MBP [173]. The main MBP isoform in the adult human and bovine CNS is 18.5 kDa, although, in rats and adult mice is 14 kDa. All isoforms include protein domains encoded by exons I, III, IV, and VII, while only the 21.5-, 20.5-, and 17.22-kDa forms have the domain encoded by exon II. The 21.5-, 20.2-, 18.5-, 17.24-, and 17.2-kDa types also contain exon VI, while the 17.22- and 14-kDa forms do not. The most considerable similarity between rodent and fish MBP is in exons I, III, and part of IV, which can be a functional core of MBP [174]. Fish express two isoforms of MBP, one lacking exon II and the other lacking exon II and exon Vb [171]. Expression of the mentioned isoforms is developmentally controlled, and they have several locations in myelin and cells, indicating that they may have separate roles. The isoforms, including the exon II-encoded domain, are expressed at high levels early in myelination and immature OLs in culture [175–177], even though the forms without this domain are the primary forms expressed later in myelination, in mature OLs, and adult myelin. Although the 18.5-kDa form is the main form in adult human myelin, exon II-containing forms are expressed during fetal development and remyelination [178].

2.7.1 Isomers of 18.5-kDa Myelin Basic Protein

The form of 18.5-kDa MBP exists as a series of charge isomers, named C1, C2, C3, C4, C5, C6, and C8 due to a variety of post-translational modifications that decrease their net positive charge, consist of deamidation, phosphorylation of serine or threonine [179,180] and citrullination (deimination of arginine to citrulline, Cit) [181].

C1 is the most highly positively charged and the least modified form. Analogue C2 is deamidated. The forms of C3-C6 can be changed by combinations of deamidation, phosphorylation, and deimination [179–181]. The structure of C8 differs from C1 by deimination. This is performed for 6-11 arginine residues, with a loss of net positive charge by one for every arginine to citrulline conversion [181,182] and modifying its hydrogen-bonding properties [183]. The phosphate groups of MBP turn over quickly, and the highest turnover was in the most mature myelin segments [184]. It can suggest that the phosphorylation of MBP plays a significant role in myelin function and structure [185]. Phosphorylation of MBP

in the myelin sheath is transformed in reaction to the nerve action potential [186–188] and OLs in culture in response to depolarisation or extracellular ligands [189–192].

It is worth noting that MBP can be phosphorylated *in vitro* by protein kinase A, protein kinase C, glycogen synthase kinase (GSK), mitogen-activated protein kinase (MAPK), calmodulin-dependent kinase, and all enzymes presented in myelin [193–197]. MBP from the brain of a patient suffering from MuSc was deamidated and less phosphorylated than regular MBP but included more methylated arginine residues [182]. The quantity of the deiminated form of MBP, C8, in myelin is the highest in children and reduces during growth. It might be suggested that it plays a role in the formation of myelin rather than myelin functions.

However, C8 occurs in more significant amounts in patients suffering from MuSc [181,182,198] and has been proposed to participate in the pathogenesis of MuSc [199].

2.7.2 Secondary structure of Myelin Basic Protein

All charge and size isoforms of MBP have been predicted to be intrinsically unstructured [170,200,201]. Experiments using circular dichroism (CD) spectroscopy have demonstrated that MBP possesses no ordered structure in solution [153,170]. Nevertheless, it has been expected to have a β-sheet structure [202], and particular fragments have been predicted to form amphipathic α-helices [104,202–204].

Using the mixture of charge isomers, MBP was presented *via* CD spectroscopy to obtain α-helical and β-sheet secondary structures interacting with lipids [205,206] and SDS micelles [207]. Moreover, the studies using cysteine substitution for Cys-specific spin labelling and electron paramagnetic resonance (EPR) spectroscopy have confirmed that the region 83-92 of recombinant murine 18.5-kDa C1 (rmC1), corresponding to residues 86-95 of human MBP, formed an amphipathic helix motif on binding to lipid vesicles [208]. The linear peptide, including this segment, has been managed to stimulate immunologic tolerance in patients with SPMuSc [209]. Molecular dynamics simulations showed that this amino acid sequence tended to form an α-helix in an aqueous solution, although this structure was temporary without stabilising factors [208].

MBP developed a stable α-helical core containing the region V^{83}-T^{92} in a mixture of 30% TFE [208,210]. Additionally, structure determination by solution nuclear magnetic resonance

(NMR) of an 18-meric peptide containing the segment Q^{78}-T^{95}, corresponding to murine numbering, confirmed that this region could be α-helical in dodecylphosphocholine micelles and a mixture of 30% TFE-d_2 [211].

2.8 Experimental autoimmune encephalomyelitis in Multiple Sclerosis

The most used experimental animal model for MuSc is experimental autoimmune encephalomyelitis (EAE). EAE is a neuropathological and immune condition containing demyelination, CNS inflammation, gliosis, and axonal loss, all essential elements of MuSc pathology [212]. EAE is generated by stimulating a T-cell-mediated immune response against myelin antigens [213]. There are two types of EAE, adoptive transfer (AT) and active, caused by various initiation techniques. AT EAE is induced by immunising a model animal with myelin-specific CD4+ T cells from a donor animal [213]. Conversely, active EAE is stimulated by immunising with myelin peptides, *e.g.*, MBP and an array of tissue.

Even though MBP has not been determined to be the primary autoantigen in MuSc, MBP-specific autoreactive T cells have been observed in the blood of MuSc patients at a higher rate than in healthy people [214].

2.9 Cross-reactivity between viral antigens and MBP epitopes

Cross-reactivity to exogenous self-antigens and antigens, characterised as molecular mimicry, has been a suggested mechanism, fundamental and impairing, of many autoimmune disorders. This develops on the hypothesis that exposure to an external antigen with an identical amino acid sequence or structure to host antigens can affect an autoimmune response [137].

The theory of molecular mimicry related to viral and microbial pathogens in MuSc pathogenesis has been expected, particularly related to the EBV, and some of the studies have shown that MBP can be a possible target autoantigen. It has been demonstrated that cross-reactions between EBV and MBP can happen, but there are also cross-reactions between MBP and other viruses. There is a solid relationship between MuSc and EBV. EBV infection in adolescence and young adulthood is one of the well-known environmental hazard factors in MuSc [215].

It has been described that autoantibodies from MuSc patient sera identify MBP and recruit inflammatory cells to focal regions, thus targeting CNS myelin elements and changing their stability [216].

2.9.1   Myelin Basic Protein as possible epitope in Multiple Sclerosis

Extensive study has been performed on MBP and its potential role as a source for autoantigenic epitopes in MuSc. Unquestionably, there are differences in the isoform composition and structure of MBP, as well as in compact myelin, during the pathogenesis of MuSc [217–219].

The mechanism at the molecular level of these changes needs to be made apparent. An abnormal isoform composition of MBP probably leads to damaged membrane interactions and the loosening of the rigid structure of myelin. This may further lead to the noted anti-MBP immunoactivity and the presence of MBP in the CSF [137].

MBP in serum or the CSF is a symptom of myelin damage in general, and analysis for it may be appropriate for diagnosing different neurodegenerative disease states and spinal cord demyelination [220].

In this sense, studies of anti-MBP antibodies in MuSc have been mainly analysed, reporting controversial results ranging from 0 to 100% seropositivity [221]. Specifically, RRMuSc patients have been described to be seropositive to anti-MBP(84-100) antibodies [222]. Moreover, anti-MBP antibodies have been detected in sera and CSF in 85% of RRMuSc patients and 45% of MuSc patients, respectively, compared to 2% in non-MuSc controls [223,224].

Furthermore, the role of anti-MBP antibodies and myelin-reactive autoantibodies have been discussed [137]. This issue can be generated by various factors, for instance, including doubtful differences at the molecular level in the composition and structure of MBP isoforms and in compact myelin during the pathogenesis of MuSc [218,219]. The theory of atypical isoform composition of MBP, leading to the loosening of the rigid myelin structure and reduced membrane interactions, might lead to the noted anti-MBP immune reactivity and the presence of MBP in the CSF. Then, changes in the MBP sequences applied in immunosorbent assays could clarify anti-MBP antibody recognition in sera samples and their low affinity. Cells secreting high-affinity anti-myelin antibodies have been explained in CSF from MuSc

patients, especially when compared to circulating anti-MBP antibodies, which demonstrated low affinity [225,226]. In any case, the involvement of anti-MBP antibodies with earlier and more common disease relapses highlights their fascinating role in MuSc [227].

2.10 Structures of peptides and proteins

The additional principal issue of peptides or proteins is their conformational preferences. It is known that there exist four types of structures: primary, secondary, tertiary, and quaternary [228].

The primary structure categorises the amount and sequence of the amino acid residues in a peptide or protein chain. The secondary structure defines ordered conformations of periodic, *e.g.*, α-helix or β-sheet, or non-periodic nature such as turns. Frequently, these structures are stabilised by hydrogen bonds between donors (NH) and acceptors (CO) hydrogen bonds of peptide bonds. The 3D arrangement of secondary structure components is recognised as the tertiary structure [228].

The conformation of a polypeptide chain in β-sheets or α-helices is determined not only by hydrogen bonds but also by other interactions that can stabilise the peptide chain, for instance, metal chelation by various groups within a protein fold or the disulphide bonds [228]. The quaternary structure of a protein is the association of numerous protein chains or subunits into a directly packed arrangement. Each of the subunits has its primary, secondary, and tertiary structure. The subunits are kept together by van der Waals forces and hydrogen bonds between nonpolar side chains [229].

However, the weak peptide forces, such as van der Waals forces, hydrogen bonds, or intramolecular hydrophobic interactions, are insufficient for a stable secondary structure conformation. Additional modifications of the backbone, N- or C-termini, or side chains to mimic the structures of natural products and stabilisation of secondary structures are commonly applied tools in peptide chemistry [230,231].

Likewise, chemical modification efficiently produces peptide analogues with the preferred structures. The enhanced stability and activity have resulted in the presentation of various peptide drugs [232].

2.10.1 Peptide cyclisation

Cyclisation is a systematic method of peptide modification involving numerous approaches, such as head-to-tail, backbone-to-side chain, and side chain-to-side chain [233–235]. The cyclisation of peptides can increase cell permeability [236–238] and proteolytic stability [239,240] and allow stabilisation and mimicking of the peptide secondary structure. A single peptide sequence cannot form a loop or turn structures without being attached to other peptides. However, cyclisation enables the formation of these secondary structures by pre-organising intramolecular interactions [241]. It should be noted that peptide cyclisation is frequently used to stabilise other secondary structures, *i.e.*, α-helices or β-sheets [242–244].

2.10.2 Stabilisation and peptide mimicking of α-helices

Helices are one of the most popular systems of peptide and protein secondary structures [245], which are formed by intramolecular hydrogen bonds [246]. The α-helix can be stabilised by replacing hydrogen bonds *via* covalent bonds or building cross-links through side chains. In the α-helix motif, the side chains of amino acids at positions i, $i+4$, and $i+7$ are on the same side, and building cross-links through i and $i+4$ or i and $i+7$ efficiently approach backbone atoms and support to create hydrogen bonds in helical structures [247–249].

Excellent strengths have been made to explore different cross-links, such as the formation of disulphide bonds by substituting amino acid residues with cysteine or homocysteine [250], lactam-based with the construction of a lactam bridge through the side chain of aspartic or glutamic acid with lysine residue [251], and biselectrophilic linkers [252,253].

Worth to mention that stapled peptides represent a modern new cross-linking approach introduced to stabilise the α-helix structure, using non-natural electrophilic amino acids to replace residues at i and $i+4$ or i and $i+7$ position and form ligations with nucleophilic cross-links [239,254,255]. The hydrogen bonds surrogate modification approach requires the replacement of one hydrogen bond of the α-helix peptide by a covalent bond to change the helical structure [232].

2.10.3 Mimicking of β-sheets and β-strands in peptides

The motifs of β-sheets and β-strands represent another class of secondary structures of peptides and proteins based on mimicking the turns. The modification of peptides to stabilise β-sheets is achieved by introducing D-amino acid residues, *e.g.*, D-Pro, to form a turn structure in the peptide sequence. D-Pro-L-Pro models are a well-widespread scaffold for stabilising antiparallel β-hairpins in various effective protein-protein interactions (PPI) inhibitors [256,257]. Furthermore, the macrocyclisation of amyloid β-sheet mimics has also been applied to create β-strand or β-sheet structures [258–261].

3   AIM AND OBJECTIVES OF DOCTORAL DISSERTATION

Peptides and peptidomimetics are fascinating groups of chemical compounds. These structures can be applied as drugs and synthetic hormones or inhibit some enzymes. Moreover, they can form various secondary structures such as α-helices or β-turns.

With all these considerations in mind, my attention was focused on the studies based on secondary structures to develop peptides and peptidomimetics containing biological activity. It is well-known that the conformation of peptides and their analogues radically impact their bioactivity.

Furthermore, the presented study aims to replace the disulphide-containing bridge in native oxytocin with $1H$-[1,2,3]triazol-1-yl-containing bridge to attend to the requirement for metabolically stable OT-derived drug candidates and chemical probes with desired pharmacological activities. It was designed a series of $C\alpha^1$-to-$C\alpha^6$ side chain-to-side chain disubstituted-1,4- or 4,1-($1H$-[1,2,3]triazol-1-yl)-bridged OT analogues presenting a systematic permutation of the ring size, location, and orientation of the triazolyl moieties (**Figure 11**).

H$_2$NCHCO-Tyr-Ile-Gln-Asn-NHCHCO-Pro-Leu-Gly-NH$_2$

1,4-($1H$-[1,2,3]-triazol-1-yl)

	m	n	m+n
I	4	1	5
II	3	2	5
III	2	3	5
IV	1	4	5
V	2	1	3
VI	1	2	3
VII	1	1	2

H$_2$NCHCO-Tyr-Ile-Gln-Asn-NHCHCO-Pro-Leu-Gly-NH$_2$

4,1-($1H$-[1,2,3]-triazol-1-yl)

	m	n	m+n
IR	4	1	5
IIR	3	2	5
IIIR	2	3	5
IVR	1	4	5
VIR	2	1	3
VIR	1	2	3
VIIR	1	1	2
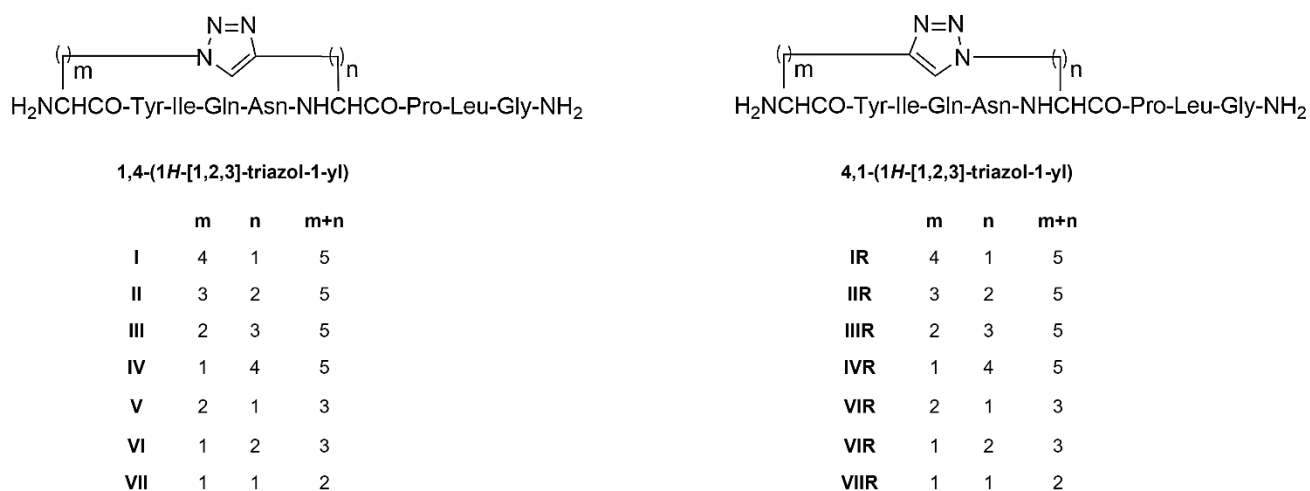
Figure 11 Structural permutations of oxytocin analogues relative to the *i-i*+5 CuAAC-based intramolecular macrocyclisation in which m+n=5, 3 or 2.

Moreover, I have reported studies on the role of the sequence and structure of synthetic MBP peptides (**Table 2**) that have been used to identify specific antibodies in MuSc patient sera. Therefore, the studies of the relationship between the structures and the bioactivity of the series of synthetic MBP peptides were discussed.

Table 2 Synthesised MBP peptides [104].

Peptide	Fragment	Sequence
1	MBP(81-106)	`-----TQDENPVVHFFKNIVTPRTPPPSQGK----------`
2	MBP(76-116)[a]	`SQHGRTQDENPVVHFFKNIVTPRTPPPSQGKGRGLSLSRFS`
3	MBP(76-96)[a]	`SQHGRTQDENPVVHFFKNIVT--------------------`
4	MBP(97-116)[a]	`--------------------PRTPPPSQGKGRGLSLSRFS`
5	MBP(81-92)	`-----TQDENPVVHFFK-----------------------`
6	MBP(99-106)	`--------------------TPPPSQGK----------`

[a]*Peptide sequence is N-terminal acetylated and C-terminal amide.*

In order to achieve the presented goals, the following objectives have been identified:

- Structure optimisation of analogues of OT and native OT by molecular modelling.
- Synthesis, purification, and analysis of peptides and peptidomimetics.
- Conformational studies of peptides and peptidomimetics.
- Biological activity assays of peptides and peptidomimetics.

4 EXPERIMENTAL SECTION

4.1 Materials

Fmoc-L-Pra-OH, (2*S*)-2-(Fmoc-amino)-5-hexynoic acid (Fmoc-L-Hex(5-ynoic)-OH), Fmoc-L-Ala(β-N$_3$)-OH, Fmoc-L-azido-homoalanine (Fmoc-L-hAla(γ-N$_3$)-OH), Fmoc-L-Nva(δ-N$_3$)-OH and Fmoc-L-Nle(ε-N$_3$)-OH were purchased by MERCK KGaA (Darmstadt, Germany). Fmoc-protected amino acids and Rink-amide Wang resin, *N,N'*-diisopropylcarbodiimide (DIC), OxymaPure® (ethyl cyanohydroxyiminoacetate), 2-(1*H*-benzotriazol-1-yl)-1,1,3,3-tetramethyluronium hexafluorophosphate (HBTU), Fmoc-Lys(Boc)-Wang Tentagel® resin were purchased from Iris Biotech GmbH (Marktredwitz, Germany). (2S-2-Fmoc-amino)-7-octanoic acid (Fmoc-L-Oct(7-ynoic)-OH) was purchased by Acrotein ChemBio^{Inc} (Hoover, U.S.A.). (2*S*)-2-(Fmoc-amino)-6-hexynoic acid (Fmoc-L-Hept(6-ynoic)-OH) was purchased by Ambeed (Arlington, U.S.A.). Peptide-synthesis grade *N,N*-dimethylformamide (DMF), acetonitrile (ACN), trifluoroacetic acid (TFA) were purchased from Carlo Erba (Milan, Italy). Piperidine, diisopropyl ether (*i*Pr$_2$O), triisopropyl silane (TIS), and deuterium oxide were purchased from Sigma-Aldrich (Milan, Italy). Tentagel® S RAM was purchased from Rapp Polymere (Tuebingen, Germany). 2,2,2-trifluoroethanol (TFE) was purchased from Alfa Aesar (Kandel, Germany). Myelin Basic Protein (MBP) was purchased from Merck (Milan, Italy). 2,2,2-trifluoroethanol-d$_3$ (TFE-d$_3$) was purchased from Deutero (Kastellaun, Germany).

4.2 Methods

4.2.1 Molecular modelling

The structure optimisation of native OT and its analogues **I-VII** and **IR-VIIR** were performed at the DFT level with B3LYP functional and 6-31g(d,p) level of theory. To determine the atomic charge was the Merz Kollman scheme. The Polarisable Continuum Model (PCM) was used to estimate the impact of solvent on the conformation of examined peptides and using water as a solvent. The *Gaussian09* software was applied for all *ab initio* calculations. The structures were visualised using *BIOVIA Discovery Studio Visualizer*

software. The initial structure of OT was downloaded from PDB (PDB ID: 2MGO) [262]. Subsequently, the [1,2,3]-triazolyl moieties were substituted in the structures into disulphide bonds. Moreover, cysteine residues were replaced with modified amino acids with alkyne or azide functions.

4.2.2 Methods of synthesis

All presented syntheses and CuAAC reactions were performed at the Interdepartmental Research Unit of Peptide and Protein Chemistry and Biology, Department of Chemistry "Ugo Schiff" at the University of Florence with the support of Dr. Francesca Nuti.

4.2.2.1 Synthesis of linear oxytocin precursors

The OT linear precursor peptides **I'-VI'** and **IR'-VIR'** were performed on Rink-amide Wang resin (0.64 mmol/g, 250 mg) and in the case of linear peptides **VII'** and **VIIR'** on Tentagel® S RAM (0.23 mmol/g, 435 mg) by microwave-assisted solid-phase peptide synthesis (MW-SPPS) following the Fmoc/*t*Bu strategy, using the Liberty Blue™ automated microwave peptide synthesiser (CEM Corporation, Matthews, NC, U.S.A.). Fmoc deprotections were performed with a solution of 20% piperidine in DMF (2 M). Peptide assembly was performed by repeating the MW-SPPS standard coupling cycle for each amino acid, using Fmoc-protected amino acids (2.5 equiv, 0.4 M in DMF), OxymaPure® (2.5 equiv, 1 M in DMF), and DIC (2.5 equiv, 3 M in DMF). The coupling of unnatural amino acids N^α-Fmoc-Xaa(ω-N$_3$)-OH was performed using the protocol described by D'Ercole *et al.* [88]. Both deprotection and coupling reactions were performed in a Teflon vessel with microwave energy and nitrogen bubbling. Unclear peptide coupling steps were checked by the ninhydrin test explained by Kaiser [263]. Cleavage of OT linear peptides **I'-VII'** and **IR'-VIIR'** from the resin and simultaneous deprotection of the amino acid side chains were carried out with a mixture of TFA:TIS:H$_2$O (95:2.5:2.5, v:v:v, 1 mL/100 mg of resin-bound peptide) for 3 h with vigorous shaking at RT. The resin was filtered and washed with TFA. The filtrate was concentrated under N$_2$ with the addition of cold *i*Pr$_2$O resulting in a precipitate that was separated by centrifugation, dissolved in H$_2$O, and lyophilised [264].

4.2.2.2 Synthesis of analogues of oxytocin I-VI and IR-VIR

Purified OT linear peptide precursors **I'-VI'** and **IR'-VIR'** (>95% purity) were subjected to CuAAC reaction using the same conditions as those reported by Le Chevalier *et al.* [7]. The conversion of the purified OT linear peptide precursors to the required 1,4- or 4,1-(1*H*-[1,2,3]-triazol-1-yl) containing cyclo-peptides was performed in a mixture of H_2O:*t*BuOH (2:1, v:v), in the presence of 4.4-fold molar excess of $CuSO_4 \cdot 5H_2O$ and ascorbic acid, by *in situ* formation of Cu(I) from Cu(II) salts. The mixture was stirred overnight at RT. Then, the solution was concentrated and lyophilised. The intermolecular macrocyclisation was monitored by RP-HPLC ESI-MS. Complete conversion of all OT linear precursors into the desired (1*H*-[1,2,3]triazol-4-yl)-containing cyclopeptides **I-VI** (**Table 3**) and (1*H*-[1,2,3]triazol-1-yl)-containing cyclopeptides **IR-VIR** (**Table 4**) was achieved after 18 hours [264].

4.2.2.3 Synthesis of analogues of oxytocin VII and VIIR

Peptide-resin **VII'** (0.1 mmol) (**Table 3**) and peptide-resin **VIIR'** (0.1 mmol) (**Table 4**) were subjected to microwave-assisted CuAAC reaction as reported by D'Ercole *et al.* [88]. The reaction was applied using CuBr (1.2 equiv) and sodium ascorbate (1.5 equiv) diluted into a mixture of DMSO and DMF, DIPEA (5 equiv), and 2,6-lutidine (5 equiv) at 55°C for 10 min. The monitoring of the intermolecular macrocyclisation was performed by a mini-cleavage.

The peptide was cleaved following the general cleavage protocol, purified, and analysed as described for peptide precursors **I'-VI'** and **IR'-VIR'** [264].

4.2.2.4 Synthesis of MBP peptides

All MBP peptides (**1-6**) were synthesised in solid-phase using a MW-SPPS on a Liberty Blue™ automated peptide synthesiser (CEM Corporation, Matthews, NC, U.S.A.), following the Fmoc/*t*Bu methodology [265–267]. Tentagel® S RAM resin (loading 0.23 mmol/g) was used for the synthesis of peptides **1**, **5**, and **6**. Fmoc-Lys(Boc)-Wang Tentagel® resin

(loading 0.23 mmol/g) was used for the synthesis of peptides **2**, **3**, and **4**. Fmoc-deprotections were performed with a solution of 20% (v:v) piperidine in DMF (2 M). Peptide assembly was performed by repeating the standard MW-SPPS coupling cycle for each amino acid, using Fmoc-protected amino acids (2.5 equiv, 0.4 M in DMF), OxymaPure® (2.5 equiv, 1 M in DMF), and DIC (2.5 equiv, 3 M in DMF). Doubtful peptide coupling steps were tested by micro-cleavages performed with a microwave apparatus CEM Discover™ single-mode MW reactor (CEM Corporation, Matthews, NC, U.S.A.) or by the ninhydrin test [263].

Resins with peptides **2-4** were N-terminal acetylated before cleavage, using two portions of Ac_2O in a DMF solution for 10 min at RT. Final cleavage and side-chain deprotections were performed using a mixture of $TFA:TIS:H_2O$ (95:2.5:2.5, v:v:v) at RT. After 2.5 h, each resin was filtered off, and the solution was concentrated, flushing with N_2. Each peptide was precipitated from cold Et_2O, centrifuged, and lyophilised [104].

4.2.3 Techniques of purification of synthesised products

All presented data from the purification of obtained products **I**-**VII**, **IR**-**VIIR**, and **1-6** were received at the Interdepartmental Research Unit of Peptide and Protein Chemistry and Biology, Department of Chemistry "Ugo Schiff" at the University of Florence with the support of Dr. Francesca Nuti.

4.2.3.1 Purification of oxytocin linear peptide precursors

Lyophilised crude linear peptides **I'-VI'** and **IR'-VIR'** were purified by Biotage® Isolera™ Systems instrument (Uppsala, Sweden) on SNAP Ultra C18 column (25 g) at 20 mL/min using a gradient 0-60% of B. The used eluent system: A (0.1% TFA in H_2O) and B (0.1% TFA in ACN) [264].

4.2.3.2   Purification of analogues of oxytocin

The crude 1*H*-[1,2,3]-triazolyl-containing cyclopeptides **I-VII** and **IR-VIIR** were purified by Biotage® Isolera™ Systems instrument (Uppsala, Sweden) on SNAP Ultra C18 column (25 g) at 20 mL/min using a gradient 0-60% of B. The used eluent system: A (0.1% TFA in H_2O) and B (0.1% TFA in ACN).

The copper salts were removed by elution with H_2O before initiating the gradient [264].

4.2.3.3   Purification of MBP peptides

The crude peptides **1-6** were purified by RP-HPLC on an Isolera One Flash Chromatography (Biotage, Uppsala, Sweden) using a SNAP Ultra C18 column (25 g) at 20 mL/min. The used eluent system: A (0.1% TFA in H_2O) and B (0.1% TFA in ACN).

The second step of purification of the MBP peptides **1-6** was performed by semipreparative RP-HPLC on a Waters instrument (Separation Module 2695, detector diode array 2996) using a Sepax Bio-C18 column (Sepax Technologies, Newark, U.S.A.) (5 µM, 250 mm × 10 mm) at 4 mL/min. The used eluent system: A (0.1% TFA in H_2O) and B (0.1% TFA in ACN) [104].

4.2.4   Analytical characterisation of purified products

All presented data of analytical characterisation of obtained products **I-VII**, **IR-VIIR**, and **1-6** were received at the Interdepartmental Research Unit of Peptide and Protein Chemistry and Biology, Department of Chemistry "Ugo Schiff" at the University of Florence with the support of Dr. Francesca Nuti.

Characterisation of the OT, OT cyclopeptides **I-VII** and **IR-VIIR** was performed by analytical HPLC using a Waters ACQUITY HPLC coupled to a single quadrupole ESI-MS (Waters® ZQ Detector, Waters Milford, MA, U.S.A.) with a BEH C18 column (5 µm, 2.1 mm × 50 mm) at 35°C, λ=215 nm, at 0.6 mL/min with eluent systems: A (0.1% TFA in H_2O) and B (0.1% TFA in ACN). Gradient elution was performed with a flow of 0.6 mL/min and started at 10% B, with a linear increase to 60% B in 5 min.

Characterisation of the MBP peptides **1-6** was performed by analytical HPLC using a Waters ACQUITY HPLC coupled to a single quadrupole ESI-MS (Waters® ZQ Detector, Waters Milford, MA, U.S.A.) supplied with a BEH C18 column (1.7 μm, 2.1 mm × 50 mm) at 35 °C, λ=215 nm, at 0.6 mL/min with solvent systems: A (0.1% TFA in H_2O) and B (0.1% TFA in ACN). Gradient elution was performed with a flow of 0.6 mL/min and started at 10% B, with a linear increase to 90% B in 5 min. Data were acquired and processed using *MassLynx* software (Waters, Milford, MA, U.S.A.).

The mass analysis of the OT cyclopeptides **I-VII** and **IR-VIIR** was performed on a Single Quadrupole ESI-MS Micromass ZQ coupled to RP-HPLC system Waters Alliance 2695 Separation Module equipped with a Photodiode Array Detector Waters PDA 2996 (Waters, MA, U.S.A.). Data were acquired and processed using *MassLynx* software (Waters, Milford, MA, U.S.A.) [104,264].

The HPLC chromatograms and ESI-MS spectra of all obtained products are reported in Supplementary material as **Figure S1-S42**.

4.2.5 Immunoassays of MBP peptides

Immunoassays, particularly inhibition ELISA and SP-ELISA, were performed and interpreted by MSc Michael Quagliata and Dr. Feliciana Real-Fernandez at the Interdepartmental Research Unit of Peptide and Protein Chemistry and Biology, Department of Chemistry "Ugo Schiff" at the University of Florence.

4.2.5.1 Sample sera collection

Fifteen MuSc patients were recruited in the Multiple Sclerosis Clinical Care and Research Centre at the Department of Neurosciences, Reproductive Sciences, and Odontostomatology at the University of Naples "Federico II".

The RRMuSc patients were previously diagnosed after a LP, CSF analysis, and MRI examination and achieved the established international diagnostic criteria [268,269]. The presented studies were performed in accordance with the Declaration of Helsinki.

The completed experimental protocols were accepted by the Ethics Committee in 2006 (protocol n. 120/06) and 2017 (protocol n. 160/17).

Blood samples were drawn during the regular follow-up of patients, while the healthy control samples were carried out during blood donations or routine health checks. Sera samples were obtained for diagnostic reasons from patients and healthy controls who had given their informed consent. Blood samples were centrifuged at 4000 rpm for 10 min, and sera supernatant was stored at -20°C until use [104].

4.2.5.2 Set-up of the coating conditions

All MBP peptides **1-6** were dissolved in buffer carbonate (pH 9.8) or PBS (pH 7.2), independently. Plates were coated using a buffer without peptide to evaluate the influence of peptide in the obtained signals. Polystyrene 96-well ELISA plates were coated with 100 µL/well of a 10 µg/mL solution of synthetic peptide antigens **1-6** diluted in tested buffers. After overnight incubation at 4°C, plates were washed thrice using a washing buffer. Nonspecific binding sites were blocked with 100 µL/well of FBS buffer (10% FBS in washing buffer) or 5% bovine serum albumin (BSA) buffer at RT for 1 h. The blocking buffer was removed, and plates were incubated overnight at 4°C with buffer as blank, expected positive and negative sera (diluted 1:100 in 10% FBS buffer or 2.5% BSA buffer, 100 µL/well). After three washes, plates were treated with 100 µL/well of anti-human IgG or IgM alkaline phosphatase-conjugated specific antibodies diluted in FBS buffer 1:3000 (IgG) and 1:200 (IgM) for all tested peptide antigens **1-6**. After 3 h of incubation at RT and three washes, 100 µL of substrate buffer (1 mg/mL pNPP, 0.01 M MgCl$_2$ in carbonate buffer, pH 9.6) was added to each well. The colourimetric reaction was carried out by adding 100 µL of substrate reaction solution (1 mg/mL pNPP, 0.01 M MgCl$_2$ in carbonate buffer, pH 9.6) to each well, and plates were read at 405 nm using a TECAN plate reader. After 30 min, the reaction was stopped with 1 M NaOH solution (50 µL/well), and the absorbance was read in a multichannel ELISA reader (Tecan Sunrise, Männedorf, Switzerland) at 405 nm. Antibody titer values were calculated as (mean Abs of serum duplicate) - (mean Abs of blank duplicate). The graphical representation of calculated mean values is shown in Supplementary material as **Figure S43-S49** [104].

4.2.5.3 Inhibition ELISA

Nunc-Immuno MicroWell 96-well polystyrene ELISA plates (NUNC Maxisorb, product code M9410, Merck, Milan, Italy) were coated with a solution of 10 μg/mL of the peptide antigens **1-6** in 0.05 M pure carbonate buffer with pH 9.6 adding 100 μL/well and incubated at 4°C overnight. After five washes with a washing buffer (0.9% NaCl, 0.05% Tween 20) using an automatic Hydroflex microplate washer (Tecan Italia, Milan, Italy). Nonspecific binding sites were blocked with 100 μL/well of FBS buffer solution (10% FBS in washing buffer) at RT for 1 h [270]. Semi-saturating sera dilution was calculated in preliminary titration curves (absorbance 0.7). Seven different concentrations of each synthetic antigenic peptide probe were used as inhibitors. Then, sera samples at the selected dilution were incubated in parallel with increasing concentrations of antigens (range 1×10^{-10} to 1×10^{-4} M) for 1 h at RT. All competitive experiments were performed in triplicate. After three washes with washing buffer, uninhibited antibodies were identified by adding 100 μL/well of alkaline phosphatase-conjugated to anti-human immunoglobulin G or M (IgG and IgM, Merck, Milano, Italy) diluted 1:3000 (IgG) and 1:200 (IgM) in FBS buffer. Then the microplates were incubated for 3 h at RT and, after three washes with washing buffer, 100 μL of substrate solution consisting of 1 mg/mL *p*-nitrophenyl phosphate *p*NPP (Merck, Milan, Italy) and 0.01 M $MgCl_2$ in carbonate buffer (pH 9.6) were added. After approximately 30 min, the reaction was stopped with 1 M NaOH solution (50 μL/well), and the absorbance was read in a multichannel ELISA reader (Tecan Sunrise, Männedorf, Switzerland) at 405 nm. Antibody titer values were calculated as (mean Abs of serum triplicate) - (mean Abs of blank triplicate), graphically representing the absorbance inhibition percentage. As references, one positive and one negative serum were included in each plate for further normalisation. Each experiment was performed at least twice on different days. Within-assays and between-assays coefficients of variations were below 10%. Calculated half maximal inhibitory concentrations (IC_{50}) are reported for each antigen [104].

4.2.5.4 SP-ELISA

Immunoassays were performed to evaluate IgM or IgG antibodies in sera by SP-ELISA. For this purpose, the synthetic peptide antigens **1-6** were coated on 96-well ELISA plates (NUNC Maxisorb, product code M9410, Merck, Milan, Italy). Coating conditions were set up separately for each peptide. Polystyrene 96-well ELISA plates were coated with 100 μL/well of a 10 μg/mL solution of synthetic peptide antigens **1-6** diluted in 0.05 M pure carbonate buffer (pH 9.6), individually. After overnight incubation at 4°C, plates were washed thrice using a washing buffer. Nonspecific binding sites were blocked with 100 μL/well of FBS buffer solution (10% FBS in washing buffer) at RT for 1 h. FBS buffer was removed, and plates were incubated overnight at 4°C with sera (diluted 1:100 in FBS buffer, 100 μL/well). After three washes with washing buffer, plates were treated with 100 μL/well of anti-human IgG or IgM alkaline phosphatase-conjugated specific antibodies diluted in FBS buffer 1:3000 (IgG) and 1:200 (IgM) for all tested antigens. After 3 h of incubation at RT and three washes with washing buffer, 100 μL of substrate buffer (1 mg/mL pNPP, 0.01 M $MgCl_2$ in carbonate buffer, pH 9.6) was added to each well. The colourimetric reaction was carried out by adding 100 μL of substrate reaction solution (1 mg/mL pNPP, 0.01 $MgCl_2$ M in carbonate buffer, pH 9.6) to each well, and plates were read at 405 nm using a TECAN plate reader. After 30 min, the reaction was stopped with 1 M NaOH solution (50 μL/well), and the absorbance was read in a multichannel ELISA reader (Tecan Sunrise, Männedorf, Switzerland) at 405 nm. Antibody titer values were calculated as (mean Abs of serum triplicate) - (mean Abs of blank triplicate), graphically representing the calculated mean values. As references, one positive and one negative serum were included in each plate for further normalisation. Each experiment was performed at least twice on different days. Within-assays and between-assays coefficients of variations were below 10% [104].

4.2.6   Circular dichroism spectroscopy

4.2.6.1   Circular dichroism of oxytocin and its analogues

CD spectra of oxytocin and its analogues **I-IV** and **IR-IVR** were recorded by Prof. Dr. Maud Larregola at the PeptLab@UCP at the Université de Cergy-Pontoise associated with Interdepartmental Research Unit of Peptide and Protein Chemistry and Biology of the University of Florence.

Moreover, CD spectra of oxytocin and the second series of analogues of oxytocin **V-VII** and **VR-VIIR** were registered at the Department of Bioorganic Chemistry at the Wrocław University of Science and Technology.

CD spectra were recorded on JASCO J-815. The CD experiments were registered in H_2O between 270 and 185 nm at 25°C. The CD spectra were registered with the following parameters: 0.2 nm resolution, 1.0 nm bandwidth, 20 mdeg sensitivity, 0.25 s response, 100 nm·min^{-1} scanning speed, 5 scans, and 0.02 cm cuvette path length. The CD spectra of solvents were recorded and subtracted from the raw data. The spectra were corrected by a baseline that was measured with the identical solvent in the same cell. The CD intensity is given as mean residue molar ellipticity (θ) [deg·cm^2·dmol^{-1}] [104].

The residue molar ellipticity (θ) was calculated according to:

$$\theta = \frac{\left(\frac{deg}{C \cdot l \cdot AA}\right)}{10}$$

θ − residue molar ellipticity [deg·cm^2·dmol^{-1}]

C − concentration $\left[\frac{mol}{dm^3}\right]$

l − cell path length [cm]

AA − number of amino acid residues

4.2.6.2   Circular dichroism of MBP peptides

All presented CD spectra of synthetic MBP peptides **1-6** were recorded at the Department of Bioorganic Chemistry at the Wrocław University of Science and Technology.

CD spectra were recorded on JASCO J-815 with increasing temperature from 10 to 60°C in increments of 5°C between 270 and 185 nm. The CD experiments were registered in H_2O, a mixture of H_2O:TFE (50:50, v:v) and PBS (phosphate buffered saline, pH 7.4, containing: sodium chloride, potassium chloride, sodium phosphate dibasic, potassium phosphate monobasic). The CD spectra were registered with the following parameters: 0.2 nm resolution, 1.0 nm bandwidth, 20 mdeg sensitivity, 0.25 s response, 100 nm·min^{-1} scanning speed, 5 scans, and 0.02 cm cuvette path length. The CD spectra of solvents were recorded and subtracted from the raw data. The CD spectra were corrected by a baseline that was measured with the identical solvent in the same cell. The CD intensity is given as mean residue molar ellipticity (θ) [deg·cm^2·dmol^{-1}] calculated in the same way presented above. Furthermore, in studied peptides, the helix contents were determined [271].

Helix content (%) was calculated according to [271]:

$$\% = 100 \cdot \left(\frac{[\theta]_{222}}{-39500 \cdot \left(1 - \frac{2.57}{n}\right)} \right)$$

$[\theta]_{222}$ – residue molar ellipticity at 222 nm

n – number of peptide bonds

4.2.7   NMR studies of obtained peptides and peptidomimetics

4.2.7.1   NMR studies of oxytocin and its analogues

The NMR spectra of oxytocin and its analogues **I-VII** and **IR-VIIR** were recorded and interpreted by Prof. Dr. Maud Larregola at the PeptLab@UCP at the Université de Cergy-Pontoise associated with the Interdepartmental Research Unit of Peptide and Protein Chemistry and Biology of the University of Florence and Prof. Dr. Olivier Lequin in the Laboratory of Biomolecules at the Sorbonne University.

Lyophilised peptides were dissolved at a concentration of 2 to 3 mM in 550 µL of H_2O:D_2O (90:10, v:v) containing 50 mM deuterated sodium succinate, pH 5. Sodium 4,4-dimethyl-4-silapentane-1-sulphonate-d_6 (DSS) was added at a final concentration of 0.11 mM for chemical shift calibration. NMR experiments were recorded on Bruker Avance III 500 MHz spectrometer equipped with a TCI ^{1}H/^{13}C/^{15}N cryoprobe with a Z-axis gradient. NMR spectra were processed with *Topspin 3.2* software (Bruker) and analysed with the *NMRFAM-SPARKY* software [272]. ^{1}H, ^{13}C and ^{15}N resonances were assigned using 1D ^{1}H WATERGATE, 2D ^{1}H-^{1}H TOCSY (DIPSI-2 isotropic scheme of 72 ms duration), 2D ^{1}H-^{1}H ROESY (300 ms mixing time), 2D ^{1}H-^{13}C HSQC, 2D ^{1}H-^{13}C HSQC-TOCSY and 2D ^{1}H-^{15}N HSQC spectra recorded with range between 5 to 25°C. ^{1}H chemical shift was referenced against DSS. ^{1}H, ^{13}C and ^{15}N chemical shift signals were referenced indirectly. The chemical shift deviations (CSD) were calculated as the differences between observed chemical shifts and random coil values reported in water [273]. The temperature gradients of the amide proton chemical shifts were derived from 1D ^{1}H WATERGATE experiments recorded from 5 to 25°C. ^{3}J$_{HN-H\alpha}$ were measured on 1D ^{1}H WATERGATE spectra.

^{1}H, ^{13}C, and ^{15}N resonances of selected peptidomimetics were assigned using scalar coupling and dipolar coupling correlation experiments. The turn propensities of the different peptides were investigated by analysing ^{3}J$_{HN-H\alpha}$ coupling constants, characteristic sequential, medium-range ROEs, and the temperature dependence of amide protons. Structures of effective forms of studied peptides were calculated on the basis of ROE-based distance restraints and ^{3}J coupling-based dihedral angle restraints [264].

4.2.7.2   NMR structure calculations of oxytocin and its analogues

The NMR structure calculations of oxytocin and its analogues **I-VII** and **IR-VIIR** were performed and interpreted by Prof. Dr. Maud Larregola at the PeptLab@UCP at the Université de Cergy-Pontoise associated with the Interdepartmental Research Unit of Peptide and Protein Chemistry and Biology of the University of Florence and Prof. Dr. Olivier Lequin in the Laboratory of Biomolecules at the Sorbonne University.

Inter-proton distance restraints were derived from ROESY cross-peak volumes integrated using the *NMRFAM-SPARKY* software. Upper bounds for proton pairs were calculated using the most intense inter-residual HN-H$^{\alpha}$ correlation as a reference (distance set to 2.2 Å). ROE cross-peak volumes involving chemically equivalent protons were divided by the multiplicity of protons, and distance restraints were calculated using the r^{-6} average. An additional tolerance of 10% was applied to the upper bounds for backbone protons and 20% for side chain protons. The lower bounds were set to the sum of the van der Waals radii of protons. Φ angle restraints were derived from $^{3}J_{HN-H\alpha}$ coupling constants using a Karplus relationship. The force constants for distance and dihedral angle restraints were set to 20 kcal·mol^{-1}·Å^{-2} and 50 kcal·mol^{-1}·rad^{-2}, respectively.

Structures were calculated using the *Amber 14* software. Noncanonical amino acid residues were parameterised using general Amber force field (gaff) atom types, and partial charges were computed *via* the AM1-BCC method implemented within the *Antechamber* software. Peptides were built using the ff14SB force field. A set of one hundred structures was calculated by simulated annealing *in vacuo* using NMR-derived experimental restraints and dihedral angle restraints to fix the *trans* configuration of amide bonds. The best twenty structures exhibiting the lowest potential energy and minimal restraint violations (<0.2 Å and <5° for distances and dihedral angles restraints, respectively) were selected to represent the final NMR ensemble [264].

4.2.7.3   NMR studies of MBP peptides

Firstly, the NMR spectra of peptides **1** and **2** were recorded and interpreted by Prof. Dr. Alfonso Carotenuto and Dr. Diego Brancaccio at the Department of Pharmacy at the University of Naples "Federico II".

The samples for NMR studies of peptides **1** and **2** were prepared by dissolving the appropriate amount of peptide in 50 mM potassium phosphate buffer (pH 6.5), 10% D_2O, and 100 mM DPC-d_{38}. NMR spectra were recorded on a Varian INOVA 600 MHz spectrometer equipped with a z-gradient 5 mm triple-resonance probe head. The spectra were recorded at 25°C and were calibrated relative to TSP (0.00 ppm) as the internal standard. One-dimensional (1D) NMR spectra were recorded in the Fourier mode with quadrature detection. The water signal was suppressed by gradient echo [274]. 2D DQF-COSY [275,276], 2D ^1H-^1H TOCSY [277], and 2D ^1H-^1H NOESY [278] spectra were recorded in the phase-sensitive mode. Data block sizes were 2048 addresses in T2 and 512 equidistant T1 values. Before the Fourier transformation, the time domain data matrices were multiplied by shifted sin2 functions in both dimensions. A mixing time of 70 ms was used for the 2D ^1H-^1H TOCSY experiments. 2D ^1H-^1H NOESY experiments were run with a mixing time of 100 ms [104].

Moreover, the following data obtained in NMR studies were recorded and interpreted at the Department of Bioorganic Chemistry at the Wrocław University of Science and Technology with the support of Dr. Michał Jewgiński.

All lyophilized MBP peptides **1-6** were dissolved in a mixture of H_2O:D_2O (90:10, v:v) and TFE-d_3:D_2O:H_2O (50:10:90, v:v:v). NMR spectra were recorded on a Bruker Advance 600 MHz spectrometer. Chemical shifts are given in ppm relative to residual solvent signals. NMR spectral signal assignment and integration were carried out with *Topspin 3.2* software (Bruker) and analysed with the *NMRFAM-SPARKY* software. ^1H- and ^{13}C-NMR spectra as well as ^1H-^1H-COSY, ^1H-^1H-TOCSY, ^1H-^1H-NOESY, ^1H-^1H-ROESY, ^1H-^{13}C-HSQC, and ^1H-^{13}C-HMBC spectra were used for the signal assignments. ^1H-^1H-NOESY experiments were carried out with a mixing time of 200 to 350 ms. Temperature experiments were recorded in the range of 288 to 313 K.

4.2.7.4   NMR structure calculations of MBP peptides

All molecular dynamics calculations were performed and interpreted at the Department of Bioorganic Chemistry at the Wrocław University of Science and Technology by Dr. Michał Jewgiński.

Determination of the structural preferences of the analysed MBP peptides **5** and **6** was based on molecular modelling methods using linear simulated annealing molecular dynamics and molecular mechanics. The computational techniques and topological data for individual building blocks were established primarily on experimental data. The applied experimental data were distance constraints and constraints imposed on the torsion angles of the main chains of peptides.

Moreover, the distance constraints were defined based on correlation signals of 2D [1]H-[1]H-NOESY spectra, using as reference distances between geminal protons of methylene groups according to the equation presented below to determine the inter-proton distances [279].

The distance between peaks was calculated according to [279]:

$$r_{ij} = r_{ref}(\frac{a_{ref}}{a_{ij}})^{1/6}$$

r_{ij} – the distance between peaks,

r_{ref} – known reference distance between peaks,

a_{ref} – the volume of the reference cross peaks,

a_{ij} – the volume of the cross peaks.

The found distance constraints were sorted, due to the calculated distances, into three categories:

    a.   strong (1.8 – 2.5 Å),

    b.   medium (1.8 – 3.5 Å),

    c.   weak (1.8 – 5.0 Å).

Worth to mention that the conformational analyses were carried out in two stages. In the first stage, a stretched conformation was generated based on the amino acid sequence, and then, using the linear annealing method, molecular dynamics were carried out by gradually cooling the system from 3500 K to 25 K in steps of 12.5 K.

According to this procedure, one thousand independent structures were generated. For the data found in this method, the structures were clustered by the positions of the main chain atoms: N(H)-Cα-C(O). A different number of amino acids was used for clustering, depending on the flexibility of the main chain.

Furthermore, conformation refinement was performed using structural constraints for the structures representative of the obtained clusters (NOE, $J_{HNH\alpha}^{3}$). In this technique, one thousand independent conformations were determined for each arrangement, which were subsequently clustered based on the positions of the main chain. Finally, the analyses of torsion angles were performed for the obtained clusters.

4.2.8 Pharmacological experiments of oxytocin and its analogues

All pharmaceutical assays of oxytocin and its analogues **I**-**VII** and **IR**-**VIIR** were performed and analysed by MSc Bernhard Retzl, MSc Nataša Tomašević, and Prof. Dr. Christian W. Gruber in the Center for Physiology and Pharmacology at the Medical University of Vienna.

4.2.8.1 Sample sera collection

A sample of sera from a 40th-week pregnant woman was collected by Prof. Dr. Maria E. Street at the Department of Medicine and Surgery at the University of Parma.

One serum sample from a 40th-week pregnant woman was used as control and obtained within the study protocol 2020_0119314, approved by the AVEN ethics committee in Reggio Emilia on 15/10/2020. The study was performed according to the Declaration of Helsinki, and written informed consent was obtained as appropriate.

4.2.8.2 Stability assay

Stock solutions (1 mg/mL) of native OT and analogues of oxytocin **IV** and **IVR** were prepared in H_2O and stored at 4°C until use. These three peptide solutions (0.1 mg/mL) were prepared by diluting the respective stock solutions in phosphate buffer at pH 7.2. Each peptide solution (50 μL) was added to the 40th-week pregnant serum (300 μL) and incubated at 37°C. A reference peptide was used as an internal standard. At selected times (1, 3, 5, 20, 24, 48 h), an aliquot (30 μL) of each peptide was taken and quenched with a solution of H_2O:ACN (1:1) with 0.1% TFA (70 μL). The vial containing the solution was cooled at 0°C for 5 min. After centrifugation (11000 rpm, 10 min), the supernatants were analysed (2×10 μL, injection) by RP-HPLC-MS at 215 nm. Data analysis (n = 2) was performed using Prism Version 6, a nonlinear fit one-phase decay model [264].

4.2.8.3 Membrane preparation

HEK293 cells stably expressing the receptor of interest [262] were seeded in 10-cm dishes. At about 80% confluency, the cell monolayer was rinsed with ice-cold PBS, mechanically detached with a cell scraper, resuspended in 5 mL of ice-cold PBS, and harvested by centrifugation at $300 \times g$ and 4°C. The pellet was resuspended in 1 L of ice-cold hypotonic buffer (50 mM TRIS, 5 mM $MgCl_2$, 0.1% BSA) supplemented with a complete protease inhibitor cocktail. Cells were subsequently disrupted by four 10-s ultrasonication cycles using a benchtop ultrasonic cleaner filled with ice-cold water. Membranes were pelleted by centrifugation at $38000 \times g$ and 4°C for 30 min, resuspended in ice-cold hypotonic buffer, aliquoted, and stored at -80°C. The protein concentration was determined with the BCA assay [264].

4.2.8.4 Radioligand binding experiments

For radioligand binding experiments, ligands were incubated with HEK293 cell membranes stably expressing oxytocin GFP-tagged receptors for 1 h at 37°C. The unbound ligand was

removed by rapid filtration over glass fibre filters using a cell harvester (Skatron). Non-specific binding was determined in 10 μM of unlabelled OT or AVP. Data were expressed as a percentage of specific displacement of [^{3}H]-OT/AVP that was normalised between nonspecific and total binding. One-point displacement experiments were measured in technical duplicates, and heatmaps were created in *Python 3* software using the seaborn module [280]. For concentration-response experiments, samples were measured in technical duplicates and fitted with a three-parameter model (hill slope = 1) in *GraphPad Prism* software [264].

4.2.8.5 Second messenger formation

The formation of the second messenger IP-3 was measured with an IP$_1$ Tb kit (Cisbio, Codolet, France) according to the protocol of the manufacturer with minor changes [281]. HEK293 cells stably expressing the GFP-tagged oxytocin receptor were seeded in white 348-well plates (Greiner bio-one) at a cell density of 10^4 cells per well. After 48 h, the cell culture medium was removed, and 5 μL of stimulation buffer was added, followed by incubation for 30 min. Then, the peptide solutions at indicated concentrations prepared in the stimulation buffer were added, and the plate was incubated for 1 h at 37°C and measured as outlined below.

The antagonism of sample **IVR** at the OTR was characterised by Schild regression analysis [281,282]. Briefly, concentration-response curves of OT were measured in the presence and absence of analogue **IVR**. The cells were pre-treated with the peptidomimetic **IVR** (100 nM, 300 nM, 1 μM and 3 μM) for 30 min at 37°C followed by co-incubation of OT for an additional 30 min at 37°C. The reaction was terminated by adding 5 μL of IP$_1$-1-d$_2$ and 5 μL of Ab-cryptate. After 1 h of incubation at 37°C, fluorescence was measured on a Flexstation 3 (Molecular Devices, San Jose, CA, U.S.A.) and quantified using the 665/620 nm ratio. The samples were measured in technical triplicates. The data were normalised between the response of the positive control (10 μM of oxytocin) with the negative control (stimulation buffer) and fitted by nonlinear regression using *GraphPad Prism* software. The logarithm of the concentration ratio (A′/A-1) was plotted against the logarithm of the respective concentration of analogue **IVR** to generate the pA2 value (functional inhibitory affinity) [264].

5 RESULTS AND DISCUSSION

5.1 Synthesis and design of studied peptides and peptidomimetics

Solid-Phase Peptide Synthesis is a valuable method for the preparation of amino acid chains of peptides or peptidomimetics, in particular oxytocin and its analogues or synthetic MBP peptides. The sequences of required structures were well-known, so it accelerated the whole experimental process.

The main advantage of using this method is reducing the time of the syntheses because MW-SPPS synthesised all products presented in this PhD thesis. On the other hand, using high-priced reagents in excess is necessary during the SPPS, especially in synthesising analogues of OT with modified amino acids possessing azide or alkyne functions.

Additionally, after the SPPS, it was necessary to purify obtained products. The purification of analogues of OT was complicated due to the low stability of modified amino acid residues. This issue was not observed in the case of the series of synthetic MBP peptides because these structures own typical amino acid sequences.

It is worth noting that many reagents applied during the SPPS harm the environment. This is a huge disadvantage of using this technique, although the mentioned technique has more benefits than drawbacks.
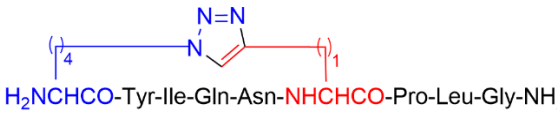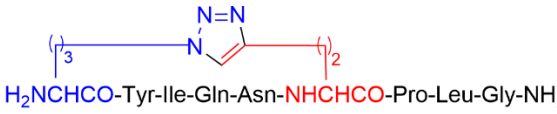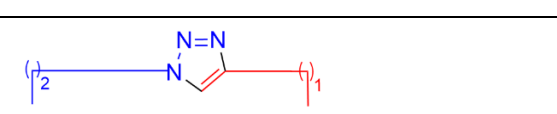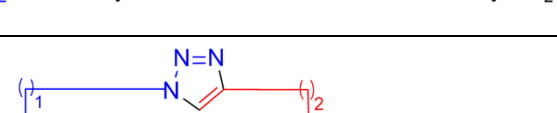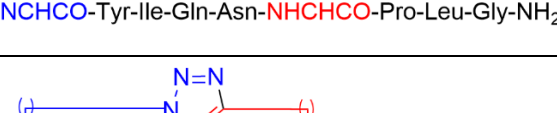
5.1.1 Synthesis strategy of analogues of oxytocin

In this study, it was designed a series of 1,4- or 4,1-disubstituted-($1H$-[1,2,3]triazol-1-yl)-bridged i-to-$i+5$ side chain-to-side chain OT homologues that vary in the size of the heterodetic ring-forming linker connecting $C\alpha^1$-to-$C\alpha^6$, the location of the [1,2,3]triazol-1-yl moiety in the linker $C\alpha^1$-$(CH_2)_m$-1,4-/4,1-disubstituted-($1H$-[1,2,3]triazol-1-yl)-$(CH_2)_n$-$C\alpha^6$ where m+n=5 (m and n=1, 2, 3 and 4), m+n=3 (m and n=1 or 2) or m+n=2 (m and n=1) and its orientation in the linker (**Table 3** and **Table 4**).

The synthesis was carried out by the MW-SPPS technique following the Fmoc/tBu methodology [2,88]. It was used N^α-Fmoc-ω-azido- and N^α-Fmoc-ω-ynoic-α-amino acids as building blocks to generate two sets of precursors that will differ in the order of incorporating these two complementing blocks. Locating the N^α-Fmoc-ω-azido- and N^α-Fmoc-ω-ynoic-α-

amino acids in positions 1 and 6, respectively, will generate the set of 1,4-disubstituted-(1*H*-[1,2,3]triazol-4-yl)-bridged analogues (**Table 3**, precursors **I'-VII'**). On the other hand, placing the same complementing building blocks in the reversed order, namely positions 6 and 1, respectively, will generate the set of 4,1-disubstituted-(1*H*-[1,2,3]triazol-1-yl)-bridged analogues (**Table 4**, precursors **IR'-VIIR'**) [264].
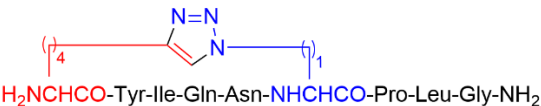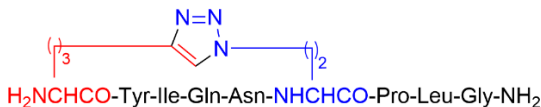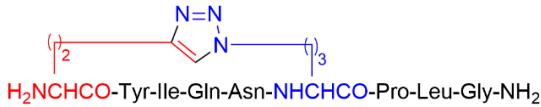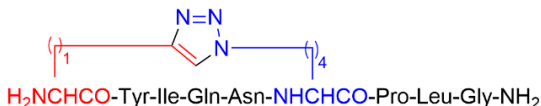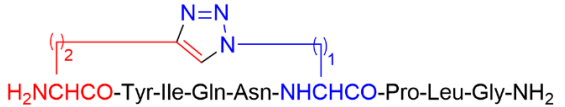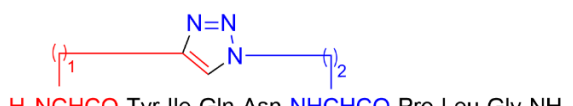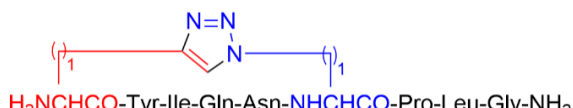
Table 3 Sequences of the linear precursors H-Xaa[1]-Tyr[2]-Ile[3]-Gln[4]-Asn[5]-Yaa[6]-Pro[7]-Leu[8]-Gly[9]-NH$_2$ (**I'-VII'**) and the 1,4-(1*H*-[1,2,3]-triazol-1-yl) containing cyclo-peptides (**I-VII**), {[H-Ala(&[1])-Tyr[2]-Ile[3]-Gln[4]-Asn[5]-Ala(&[2])-Pro[7]-Leu[8]-Gly[9]-NH$_2$]} {[1-[&[1](CH$_2$)$_m$]-1*H*-1,2,3-triazol-4-yl]-(CH$_2$)$_n$&[1]]} with m+n=5, 3 or 2 and m and n=1-4, 1-2, or 1 [264].

	Linear Precursor		[1,2,3]-triazolyl containing cyclo-peptides
I'	*H-Nle(ε-N₃)-Tyr-Ile-Gln-Asn-Pra-Pro-Leu-Gly-NH₂*	**I**	H$_2$NCHCO-Tyr-Ile-Gln-Asn-NHCHCO-Pro-Leu-Gly-NH$_2$
II'	*H-Nva(δ-N₃)-Tyr-Ile-Gln-Asn-Hex(5-ynoic)-Pro-Leu-Gly-NH₂*	**II**	H$_2$NCHCO-Tyr-Ile-Gln-Asn-NHCHCO-Pro-Leu-Gly-NH$_2$
III'	*H-hAla(γ-N₃)-Tyr-Ile-Gln-Asn-Hept(6-ynoic)-Pro-Leu-Gly-NH₂*	**III**	H$_2$NCHCO-Tyr-Ile-Gln-Asn-NHCHCO-Pro-Leu-Gly-NH$_2$
IV'	*H-Ala(β-N₃)-Tyr-Ile-Gln-Asn-Oct(7-ynoic)-Pro-Leu-Gly-NH₂*	**IV**	H$_2$NCHCO-Tyr-Ile-Gln-Asn-NHCHCO-Pro-Leu-Gly-NH$_2$
V'	*H-hAla(γ-N₃)-Tyr-Ile-Gln-Asn-Pra-Pro-Leu-Gly-NH₂*	**V**	H$_2$NCHCO-Tyr-Ile-Gln-Asn-NHCHCO-Pro-Leu-Gly-NH$_2$
VI'	*H-Ala(β-N₃)-Tyr-Ile-Gln-Asn-Hex(5-ynoic)-Pro-Leu-Gly-NH₂*	**VI**	H$_2$NCHCO-Tyr-Ile-Gln-Asn-NHCHCO-Pro-Leu-Gly-NH$_2$
VII'	*H-Ala(β-N₃)-Tyr-Ile-Gln-Asn-Pra-Pro-Leu-Gly-NH₂*	**VII**	H$_2$NCHCO-Tyr-Ile-Gln-Asn-NHCHCO-Pro-Leu-Gly-NH$_2$

All amino acid residues are presented in the L configuration.

CONSTRAINED SECONDARY STRUCTURES TO DEVELOP BIOACTIVE PEPTIDES AND PEPTIDOMIMETICS

Table 4 Sequences of the linear precursors H-Yaa^1-Tyr^2-Ile^3-Gln^4-Asn^5-Xaa^6-Pro^7-Leu^8-Gly^9-NH$_2$ (**IR'-VIIR'**) and the 4,1-(1H-[1,2,3]-triazol-1-yl) containing cyclo-peptides (**IR-VIIR**), {[H-Ala(&^{1})-Tyr^2-Ile^3-Gln^4-Asn^5-Ala(&^{2})-Pro^7-Leu^8-Gly^9-NH$_2$]} {[1-[&^{1}(CH$_2$)$_m$]-1H-1,2,3-triazol-4-yl]-(CH$_2$)$_n$&^{1}]} with m+n=5, 3 or 2 and m and n=1-4,1-2, or 1 [264].

	Linear Precursor		[1,2,3]-triazolyl containing cyclo-peptides
IR'	H-*Oct(7-ynoic)*-Tyr-Ile-Gln-Asn-*Ala(β-N₃)*-Pro-Leu-Gly-NH₂	**IR**	H₂NCHCO-Tyr-Ile-Gln-Asn-NHCHCO-Pro-Leu-Gly-NH₂
IIR'	H-*Hept(6-ynoic)*-Tyr-Ile-Gln-Asn-*hAla(γ-N₃)*-Pro-Leu-Gly-NH₂	**IIR**	H₂NCHCO-Tyr-Ile-Gln-Asn-NHCHCO-Pro-Leu-Gly-NH₂
IIIR'	H-*Hex(5-ynoic)*-Tyr-Ile-Gln-Asn-*Nva(δ-N₃)*-Pro-Leu-Gly-NH₂	**IIIR**	H₂NCHCO-Tyr-Ile-Gln-Asn-NHCHCO-Pro-Leu-Gly-NH₂
IVR'	H-*Pra*-Tyr-Ile-Gln-Asn-*Nle(ε-N₃)*-Pro-Leu-Gly-NH₂	**IVR**	H₂NCHCO-Tyr-Ile-Gln-Asn-NHCHCO-Pro-Leu-Gly-NH₂
VR'	H-*Hex(5-ynoic)*-Tyr-Ile-Gln-Asn-*Ala(β-N₃)*-Pro-Leu-Gly-NH₂	**VR**	H₂NCHCO-Tyr-Ile-Gln-Asn-NHCHCO-Pro-Leu-Gly-NH₂
VIR'	H-*Pra*-Tyr-Ile-Gln-Asn-*hAla(γ-N₃)*-Pro-Leu-Gly-NH₂	**VIR**	H₂NCHCO-Tyr-Ile-Gln-Asn-NHCHCO-Pro-Leu-Gly-NH₂
VIIR'	H-*Pra*-Tyr-Ile-Gln-Asn-*Ala(β-N₃)*-Pro-Leu-Gly-NH₂	**VIIR**	H₂NCHCO-Tyr-Ile-Gln-Asn-NHCHCO-Pro-Leu-Gly-NH₂

All amino acid residues are presented in the L configuration.

It was synthesised the fourteen linear peptide precursors **I'-VII'** and **IR'-VIIR'** employing N^α-Fmoc-ω-azido-α-amino acids and N^α-Fmoc-ω-ynoic-α-amino acids to replace the protected cysteine residue building blocks in the stepwise assembly of the fully protected resin-bound precursors [87,283].

The linear unprotected peptide precursors **I'-VII'** and **IR'-VIIR'** were obtained by MW-SPPS following the Fmoc/*t*Bu strategy [7]. Deprotection and cleavage from resin generated the OT linear precursors **I'-VII'** and **IR'-VIIR'** that were then submitted to CuAAC-mediated solution phase intramolecular macrocyclisation procedure as reported by Le Chevalier *et al.* and Rostovtsev with coworkers [7,75]. Following the mentioned procedure, it successfully converted the linear precursors **I'-VI'** and **IR'-VIR'** to the respective analogues of oxytocin **I-VI** and **IR-VIR** with yields ranging from 15-45% (**Figure 12**).

However, when applied to the linear OT precursors **VII'** and **VIIR'**, the same procedure did not generate the anticipated respective cyclopeptides **VII** and **VIIR**. In this series, the cyclic OT analogues **VII** and **VIIR** present the shortest bridge (-CH_2-1,4-/4,1-1*H*-([1,2,3]triazol-1-yl)-CH_2-), which could lead to reduced and ineffective solution phase intramolecular cyclisation. On the other hand, performing the intramolecular on-resin MW-assisted CuAAC-mediated macrocyclisation following the method reported by D'Ercole *et al.* [88] yielded the anticipated macrocyclic products **VII** and **VIIR** in 15% and 40%, respectively (**Figure 12**). The critical on-resin "infinite" dilution of the resin-bound linear precursor enabled the effective CuAAC-mediated intramolecular cyclisation and yielded the expected products [264].
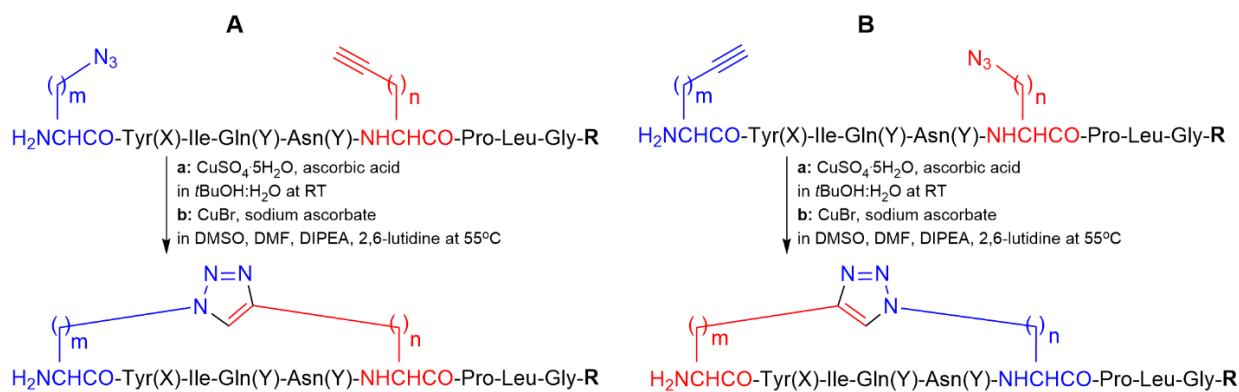
Figure 12 General procedure CuAAC intramolecular macrocyclisation of (**A**) 1,4- or (**B**) 4,1-disubstituted-(1*H*-[1,2,3]-triazolyl containing OT analogues carried out: (**a**) in solution (**R** = NH_2) [7] or (**b**) by on-resin microwave-assisted strategy (**X** = tBu; **Y** = Trt; **R** = Tentagel® S RAM resin) [88].

Worth to mention that the entire series of 1,4-/4,1-(disubstituted-(1*H*-[1,2,3]-triazolyl)-containing OT analogues **I-VII** and **IR-VIIR** were purified and characterised by RP-HPLC-MS

analysis (**Table 5**). Moreover, the native oxytocin was synthesised by the Fmoc/*t*Bu SPPS strategy and used as a reference compound in the biological assays.

Table 5 Analytical characterisation data for peptides **I-VII** and **IR-VIIR**.

Orientations	Peptides permutations (m+n=)	HPLC (R_T, min)[a]	ESI-MS (*m/z*) found[b] (calcd)	HPLC purity (%)	Quantity (mg)
	oxytocin	3.53	1007.63 (1008.15)	96	5
1,4-(1*H*-[1,2,3]triazol-1-yl)	**I** (4+1=5)	3.58	1052.85 (1052.56)	95	7
	II (3+2=5)	3.37	1052.86 (1052.56)	96	6
	III (2+3=5)	3.42	1052.87 (1052.56)	95	2
	IV (1+4=5)	3.62	1052.86 (1052.56)	96	6
	V (2+1=3)	3.65	1024.83 (1024.62)	98	6
	VI (1+2=3)	3.38	1024.95 (1024.62)	95	4
	VII (1+1=2)	3.48	1010.78 (1010.5)	98	5
4,1-(1*H*-[1,2,3]triazol-1-yl)	**IR** (4+1=5)	3.58	1052.82 (1052.56)	97	5
	IIR (3+2=5)	3.25	1052.93 (1052.56)	96	7
	IIIR (2+3=5)	3.48	1052.88 (1052.5)	95	2
	IVR (1+4=5)	3.68	1052.74 (1052.56)	98	25
	VR (2+1=3)	3.65	1024.82 (1024.62)	96	20
	VIR (1+2=3)	3.45	1024.83(1024.62)	97	22
	VIIR (1+1=2)	3.55	1010.79 (1010.5)	98	15

[a]*Analytical HPLC gradients at 1 mL·min^{-1} 10-60% B in 5 min; solvent systems: A (0.1% TFA in H$_2$O), B: (0.1% TFA in ACN);* [b]*Detected as [M+H]$^+$.*

5.1.2   Design of the series of MBP peptides

According to the literature, there is an immunodominant sequence in a specific region of MBP. Ota *et al.* reported that the sequence of MBP(83-101) is a potential immunodominant T-cell epitope limited to HLA-DR2b (DRB1*15:01) in MuSc [284]. Furthermore, Kim *et al.* described that MBP(89-101) has two registers for binding to DR2a and DR2b [285]. Likewise, other authors identified MBP(87-106) [286] and MBP(83-101) [287] as T-cell epitopes inside the MBP protein.

With this idea in mind, to cover the whole immunodominant region of MBP, it was synthesised and analysed the peptide MBP(81-106) (**1**). Additionally, believing that the sensitivity of the peptide-based ELISA might be restricted when short antigen sequences are applied, it was designed the extended sequence MBP(76-116) (**2**) to reach better antigen exposition in the SP-ELISA [267]. To explain the amino acid residues mainly involved in the B-cell epitope recognition, the whole sequence of MBP(76-116) (**2**) was divided into two parts: MBP(76-96) (**3**) and MBP(97-116) (**4**). Amino- and carboxy-termini of peptides were acetylated and amidated to remove free terminal charges, which are absent in the native protein sequence and may interfere with antibody recognition [288]. Moreover, the shorter sequences of MBP(81-92) (**5**) and MBP(99-106) (**6**) were synthesised to test them in competitive ELISA [104].

All sequences of amino acid residues of a series of MBP peptides **1-6** are presented in **Table 2**. It should be noted that analytical characterisation data of presented peptides **1-6** are reported in **Table 6**.

Table 6 Analytical characterisation data for MBP peptides **1-6**.

Peptide	Fragment	Purification gradient method (%)	HPLC gradient (% B)[a] R_T (min)	HPLC purity (%)	ESI-MS (*m/z*) found[c] (calcd)
1	MBP(81-106)	0-60 in 25min	5-95 3.90 min	>95	979.4 (979.1)[c]
2	MBP(76-116)*	20-60 in 25min	5-60 3.88 min	>95	1151.9 (1151.5)[d]
3	MBP(76-96)*	10-60 in 25min	5-95 4.10 min	>95	832.7 (832.6)[c]
4	MBP(97-116)*	20-60 in 25min	5-95 3.32 min	>95	723.3 (723.2)[c]
5	MBP(81-92)	0-60 in 25min	5-95 3.63min	>95	731.4 (731.3)[e]
6	MBP(99-106)	0-10 in 10min	1-20[b] 1.55 min	>95	811.6 (811.9)[f]

Gradient times: [a]10min, [b]5min; ESI-MS: detected as [c]$[M+3H]^{3+}$, [d]$[M+4H]^{4+}$, [e]$[M+2H]^{2+}$, [f]$[M+H]^+$.
*Peptide sequence was N-terminal acetylated and C-terminal amide.

5.2   Biological activity of MBP peptides

5.2.1   SP-ELISA

Fifteen sera from MuSc patients were screened by synthetic MBP peptides **1-6** as antigens in SP-ELISA. Preliminary tests were performed to set the best conditions for coating the various peptide antigens onto the ELISA plates. Consequently, it was evaluated IgG and IgM antibody titres to each relevant peptide, observing a nonspecific IgG antibody reactivity against peptide MBP(99-106) (**6**) (**Figure 13A**). Moreover, this nonspecific IgG antibody reactivity was also observed against peptide MBP(81-106) (**1**) but to a lesser extent.
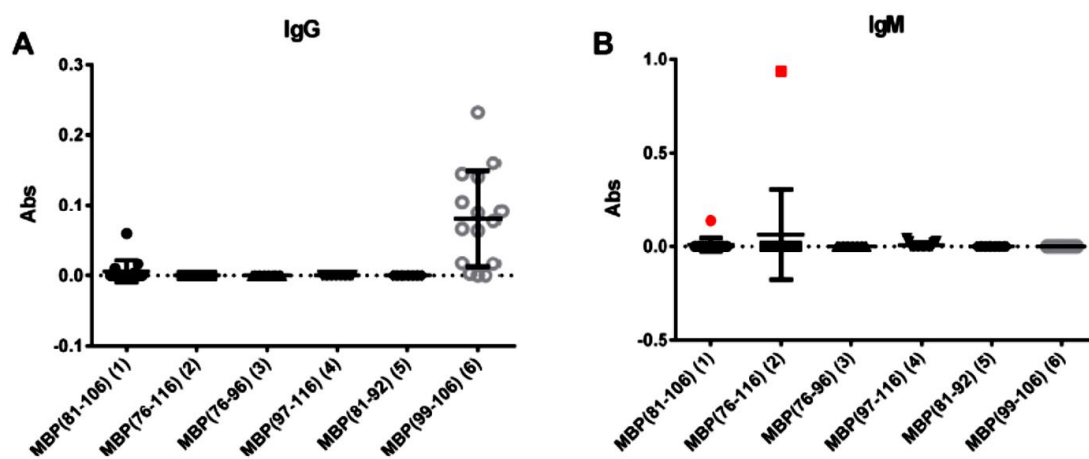
Figure 13 Mean antibody titers to MBP peptide antigens for (**A**) IgGs and (**B**) IgMs of MuSc patient sera. IgM antibody responses of the MuSc serum to the coated peptides MBP(81-106) (**1**) and MBP(76-106) (**2**) are marked in red [104].

A deeper analysis of obtained data suggested that MBP(99-106) (**6**) contains too short amino acid sequence to be effectively coated and/or exposed on the ELISA plate, favouring the nonspecific signals observed. Inconsistent peptides **2-5** did not detect IgG-type antibodies.

On the other hand, IgM antibodies were detected in one representative patient serum with peptide MBP(76-116) (**2**) and, in a lesser way, with peptide MBP(81-106) (**1**) (**Figure 13B**). Remarkably, whereas the intensity of IgMs signal is evident for peptide MBP(76-116) (**2**), the peptide MBP(81-106) (**1**) slightly recognised IgMs and IgGs.

This discovery can be justified by the peptide MBP(76-116) (**2**), which may include an extended epitope or features an optimal exposition on the ELISA plate, not obtained by the peptide MBP(81-106) (**1**), but essential to capture IgM antibodies. This remarkable result suggests that the structures of MBP(81-106) (**1**) may reproduce the proper antigen presentation, such as the one observed in the whole protein, thus enabling optimal antibody recognition of IgM antibodies.

Furthermore, it was noted that the peptide MBP(76-116) (**2**) can detect a stable, high, and reproducible IgM antibody titer. A further explanation for the low reactivity mainly observed for both IgMs and IgGs with most of the tested samples stems from the observation that a high percentage of patients are under immunosuppressive treatment and are not in the primary phase of the disease. Egg *et al.* reported that anti-MBP IgM antibodies decrease in patients with longer disease duration [289]. Likewise, it should be mentioned that the recognised representative patient is not following any immunosuppressive treatment [104].

5.2.2   Inhibition ELISA

The attention was focused on the IgM antibody response to peptide MBP(76-116) (**2**) to confirm the specificity of the observed signals in a competitive SP-ELISA. To this purpose, MBP(76-116) (**2**) was coated on the ELISA plate, and all the synthesised MBP peptides **1-6**, including MBP(76-116) (**2**) itself, were separately tested at various concentrations as inhibitors of IgM antibody binding in the representative serum (**Figure 14A**).
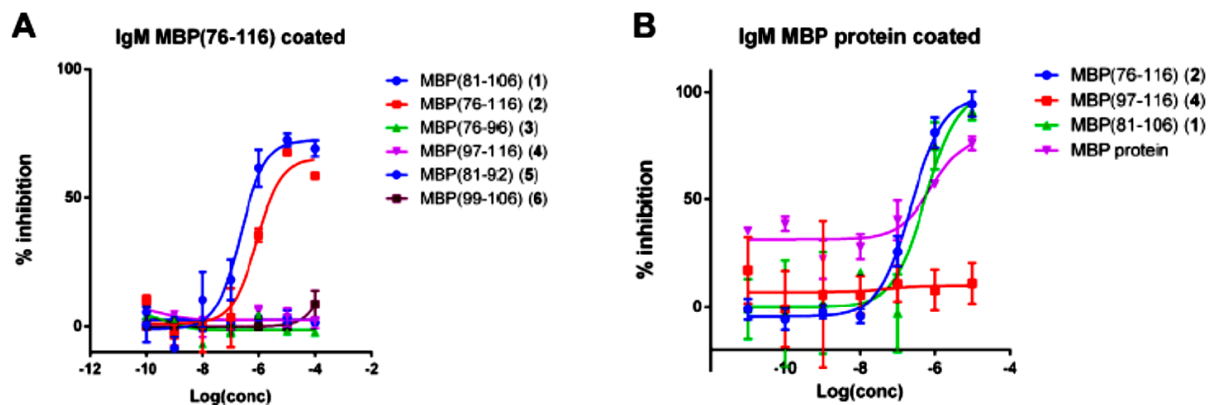
Figure 14 Competitive ELISA obtained coating (**A**) the peptide antigen MBP(76-116) (**2**) or (**B**) the MBP protein Inhibition curve of IgMs using peptides and protein as inhibitors at different concentrations. Results show the inhibition activity % (ordinate axis) of the reference MuSc serum for IgMs *vs.* antigen concentrations on a logarithmic scale (abscissas axis). Antibody titer values were calculated as (mean Abs of serum triplicate) - (mean Abs of blank triplicate), graphically representing the calculated mean values ± the standard deviation [104].

The presented results showed that peptides MBP(81-106) (**1**) and MBP(76-116) (**2**) were able to inhibit IgM antibody binding to MBP(76-116) (**2**) in the analysed MuSc serum, showing an IC_{50} of $(2.2 \pm 0.18) \cdot 10^{-7}$ and $(8.4 \pm 0.24) \cdot 10^{-7}$, respectively. All calculated IC_{50} values are presented in **Table 7**.

Table 7 Calculated IC_{50} values of anti-MBP(76-116) or anti-MBP protein IgM antibodies of MuSc serum to MBP(76-116) (**2**) and MBP(81-106) (**1**). Values are reported as a 95% confidence interval for the calculated mean IC_{50} ± the standard error (SEM) [104].

Coated antigen	Inhibitor	IC_{50} (IgM)
MBP(76-116) (**2**)	MBP(81-106) (**1**)	$(2.2 \pm 0.18) \cdot 10^{-7}$
	MBP(76-116) (**2**)	$(8.4 \pm 0.24) \cdot 10^{-7}$
MBP protein	MBP(81-106) (**1**)	$(5.5 \pm 0.31) \cdot 10^{-7}$
	MBP(76-116) (**2**)	$(2.3 \pm 0.07) \cdot 10^{-7}$
	MBP protein	$(7.9 \pm 0.34) \cdot 10^{-7}$

These results confirmed that IgM antibody response to peptide MBP(76-116) (**2**) is concentration-dependent and assesses the specificity of the IgM recognition, previously observed in SP-ELISA.

Furthermore, it was performed the inhibition experiments coating the MBP protein and using peptides MBP(81-106) (**1**), MBP(76-116) (**2**), MBP (97-116) (**4**), and the MBP protein as inhibitors (**Figure 14B**). Results demonstrated the cross-reactivity between peptides MBP(81-106) (**1**), MBP(76-116) (**2**) and the whole MBP protein. The peptides could inhibit IgM antibody binding to MBP protein in the tested MuSc serum with comparable IC_{50} (**Table 7**). The greater affinity observed in the competitive experiment with peptide MBP(81-106) (**1**) suggests that the elongation of the sequence featured by peptide MBP(76-116) (**2**) is essential for antibody recognition in SP-ELISA and the shortened sequence MBP(81-106) (**1**) is recognised more efficiently by antibodies in the solution conditions of the competitive experiment [104].

Considering these results, it was decided to study the secondary structures of all synthetic MBP peptides **1-6** by circular dichroism spectroscopy, described later in this doctoral dissertation.

5.3   Conformational analysis

The three-dimensional (3D) structure of a peptide or a protein is essential to biological activity. Pauling and Corey confirmed by X-ray crystallography of amino acids, amino acid amides, and linear peptides that the C-N bond length in a peptide bond is shorter than a regular single bond. The significance delocalisation confers limited double bond character onto the C-N bond. The conformation of the peptide backbone is characterised by the three torsion angles such as φ [C(=O)-N-Cᵅ-C(=O)], ψ [N-Cᵅ-C(=O)-N], and ω [Cᵅ-C(=O)-N-C] (**Figure 15**) [228].
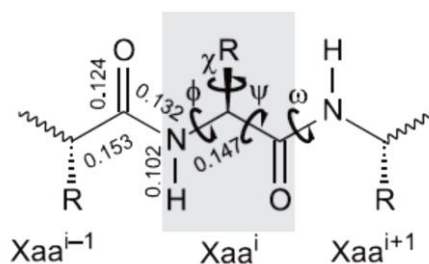
Figure 15 Torsion angles such as φ, ψ, ω and bond lengths of the amino acid Xaa[1] in peptides [228].

The free rotation around the C-N amide bond is limited because of the partial double bond character with a rotational barrier of approximately 105 kJ·mol^{-1}. Therefore, two rotamers of the peptide bond exist: the *trans*-configured peptide bond ($\omega = 180°$) and the *cis*-configured peptide bond ($\omega = 0°$) (**Figure 16**). The former is energetically favoured by 8 kJ·mol^{-1} and is found in most peptides that do not contain proline. In cases where the amide group of the imino acid proline participates in a peptide bond, the energy of the *trans*-configured Xaa-Pro bond is enhanced. Subsequently, the energy difference between the *trans* and *cis* isomers reduces [228].
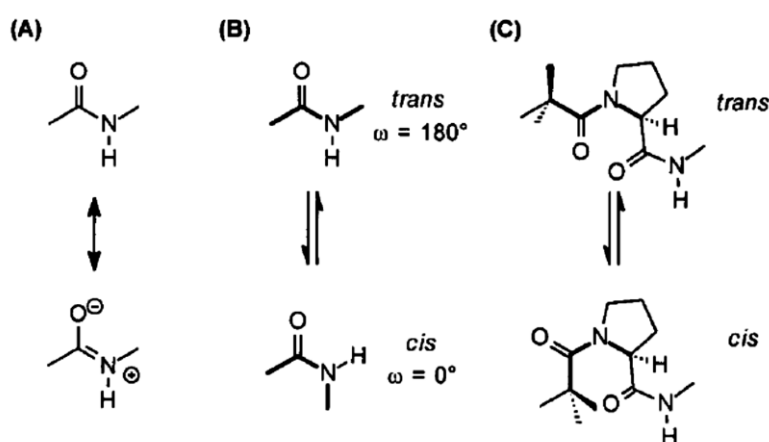
Figure 16 (**A**) Resonance stabilisation; (**B**) *cis/trans* isomerisation of the peptide bond; (**C**) *cis/trans* isomers of a Xaa-Pro bond [228].

The structure of peptides or proteins plays a crucial role in their activity. For instance, peptides are able to adopt multiple flexible conformations in solution. It is known that there are various methods of analysing peptide configurations, for example, NMR or CD spectroscopy.

5.3.1   Structure optimisation of oxytocin and its analogues

In this PhD thesis, it was applied *in silico* methods such as structure optimisation to calculate the most stable conformations of oxytocin and its analogues **I-VII** and **IR-VIIR**. The mentioned computational technique was used to observe structural changes in studied structures, especially distances between the atoms, dihedral angles, energy, entropy, molar heat

capacity, or superposition. The obtained data of oxytocin and its analogues **I-VII** and **IR-VIIR** are presented in Supplementary material as **Table S1-S4**.

It was performed and analysed two categories of data compared above. **Figure 17Figure *19*** shows all illustrations of obtained optimised structures.
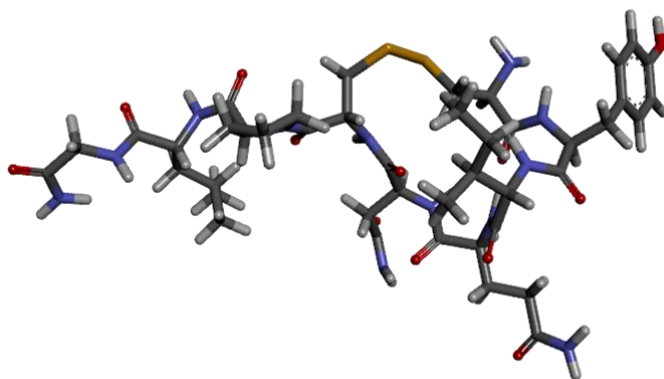
Figure 17 Optimised structure of oxytocin.
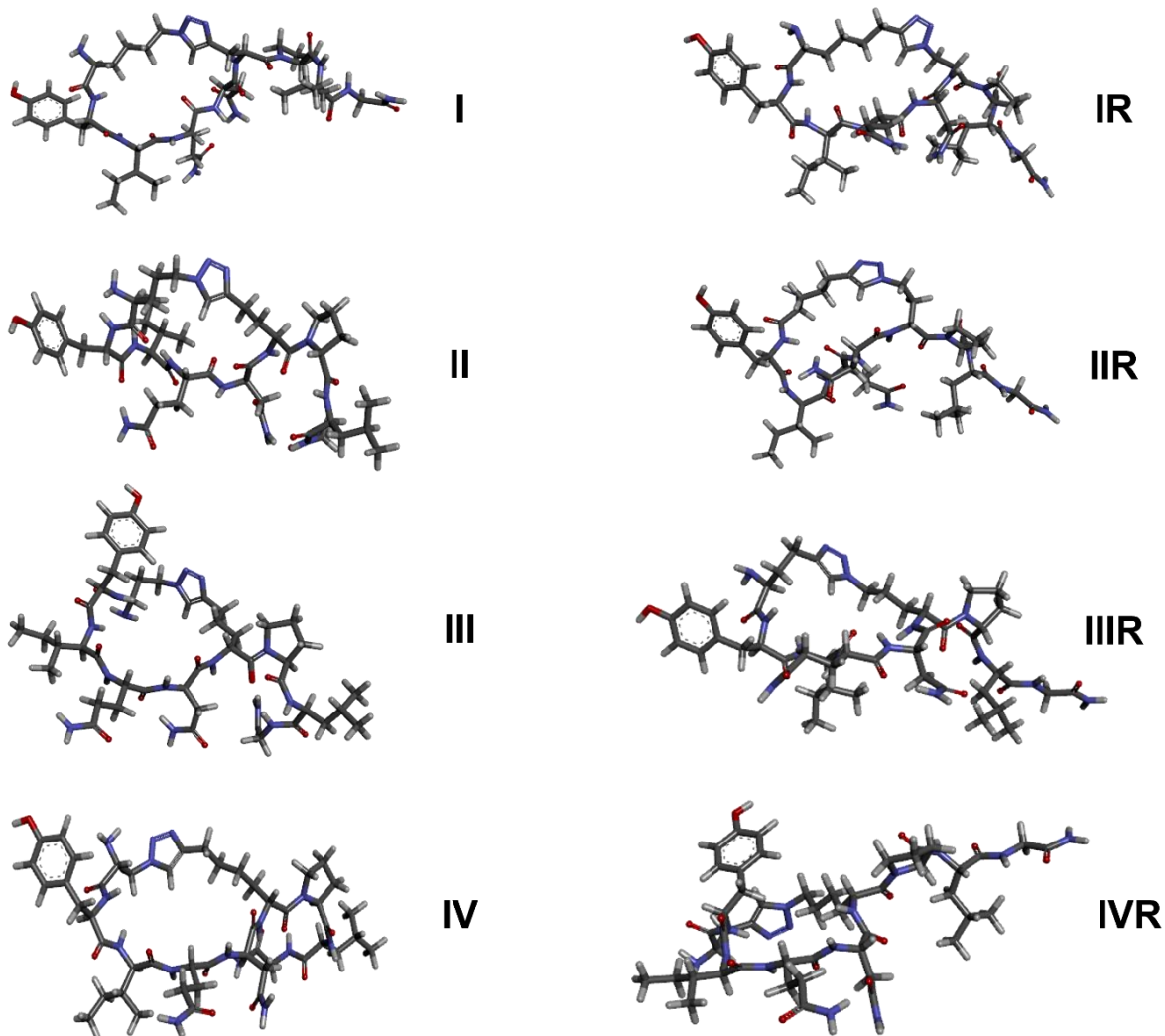
Figure 18 Optimised structures of analogues of oxytocin **I-IV** and **IR-IVR**.
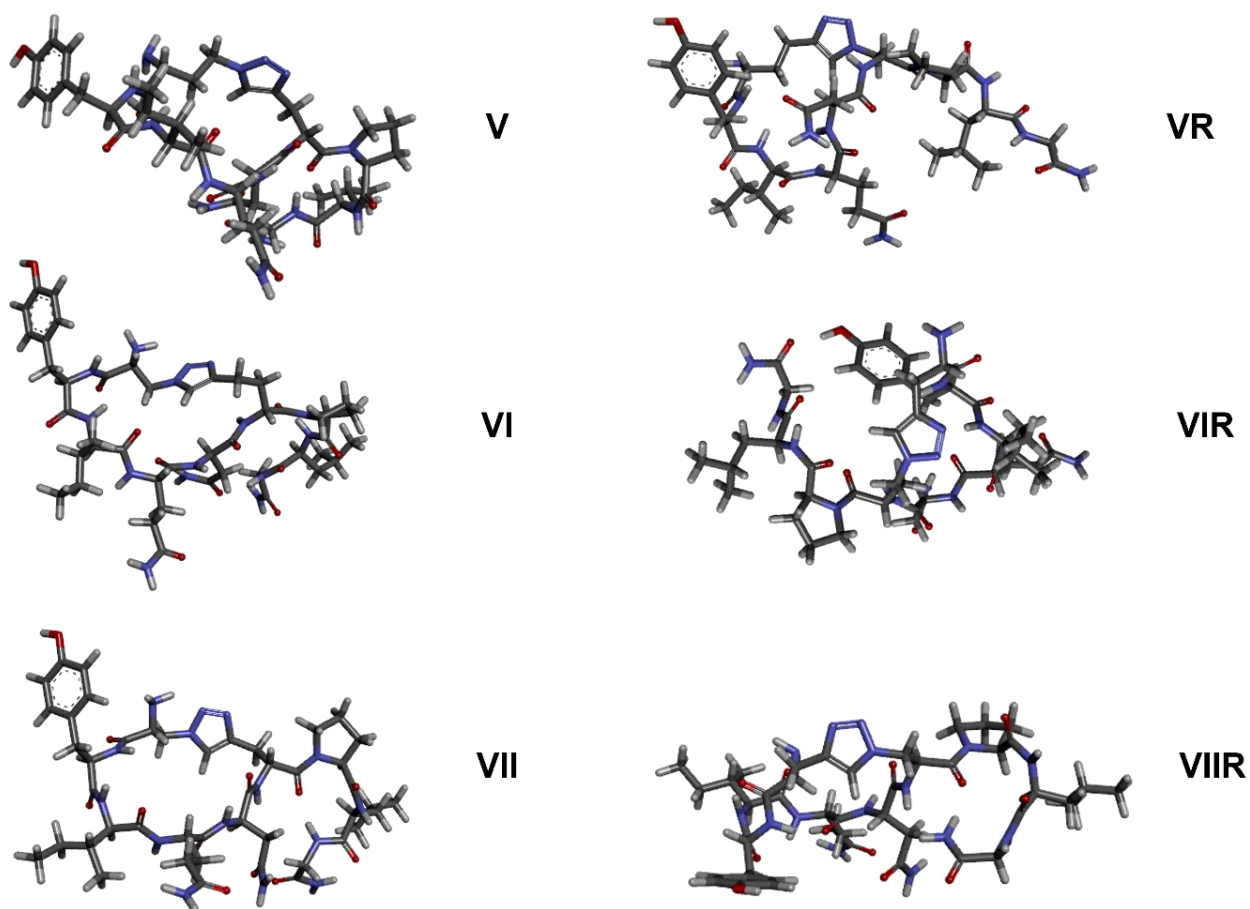
Figure 19 Optimised structures of analogues of oxytocin **V-VII** and **VR-VIIR**.

At the beginning, acetylated oxytocin downloaded from PDB (OT(PDB)) and analogues of oxytocin as zwitterions (**Table S1-S2**) were compared. Then, the native oxytocin (OT) was compared with OT analogues as neutral structures without any charges (**Table S3-S4**).

Calculated values in each pair of compounds, for example, **I-IR** or **II-IIR**, are comparable. Furthermore, the significant differences in dihedral angles and atom distances near the triazolyl bridge are visible between OT(PDB) and analogues **I-VII** and **IR-VIIR**. This is the reason for the dimension of the triazolyl bridge.

Additionally, the most favourable RMS values possess the peptidomimetics named **II**, **III**, and **IIR**, **IIIR**. Based on this knowledge, the mentioned structures are better mimetics of native oxytocin because the RMS values are closer to 1.0. The most energy-efficient peptidomimetics are named **I**, **II**, **III**, and **IIIR**, **IVR**, **IIR**.

Moreover, the values of angles at the N-terminus of the peptide chain are related because of the location of proline and leucine residues out of the loop. Glycine possesses different values of dihedral angles because this amino acid is located at the N-termini of the peptide sequence. It is probably incorporated in structure optimisation.

Likewise, at the beginning of structure optimisation, the calculations were performed with acetylation of the N-terminus of the peptide chain of OT analogues. After analysis of obtained data, it was observed that acetyl groups had blocked the rotation of the atoms of studied compounds and demonstrated the lowest energy values.

Noteworthy, the structures with neutral charges are not flexible, and these molecules cannot rotate. Moreover, hydrogen bonds form between some atoms of amino acid residues, especially in the loop. The hydrogen bonds are responsible for stabilising the structures. It should be noted that the analogues of OT, which m+n=2 or 3, such as **VI**, **VIR**, and **VII**, **VIIR** are the most rigid among the other ones.

As presented above, the differences between calculated dihedral angles of compounds are caused by the conformation preferences of analysed peptidomimetics. All changes in distances between atoms or dihedral angles are directly connected with the length of the triazolyl bridge, especially the presence of -CH$_2$ groups in the surroundings of the 1,2,3-triazoles.

5.3.2   CD spectroscopy

Circular dichroism spectroscopy is a quick, easy, and valuable technique for characterising the secondary structures of peptides. For the UV region ranging from 180 to 240 nm α-helices, β-sheets, and random coil motifs can be observed. Each secondary structure gives specific signals on the CD spectra [290]. This method is based on the changes in the absorption of left- and right-handed circularly polarised light by a chiral molecule.

The differential absorbance (ΔA) is described as:

$$\Delta A = A_L - A_R = (\varepsilon_L - \varepsilon_R) \cdot C \cdot l$$

A_L – left-handed circularly polarised light absorption

A_R – right-handed circularly polarised light absorption

ε – molar extinction coefficients $\left[\frac{cm^2}{mol}\right]$

C – concentration $\left[\frac{mol}{cm^3}\right]$

l – path length [cm]

5.3.2.1 CD spectroscopy of analogues of oxytocin

According to the CD spectra registered in water, all analysed oxytocin analogues displayed characteristic signals for random coil structures, especially analogues **I-III** (**Figure 20**). Worth to mention that analogue **IV** presented a tendency to form β-turn conformation, which was also observed in native oxytocin (**Figure 20**).
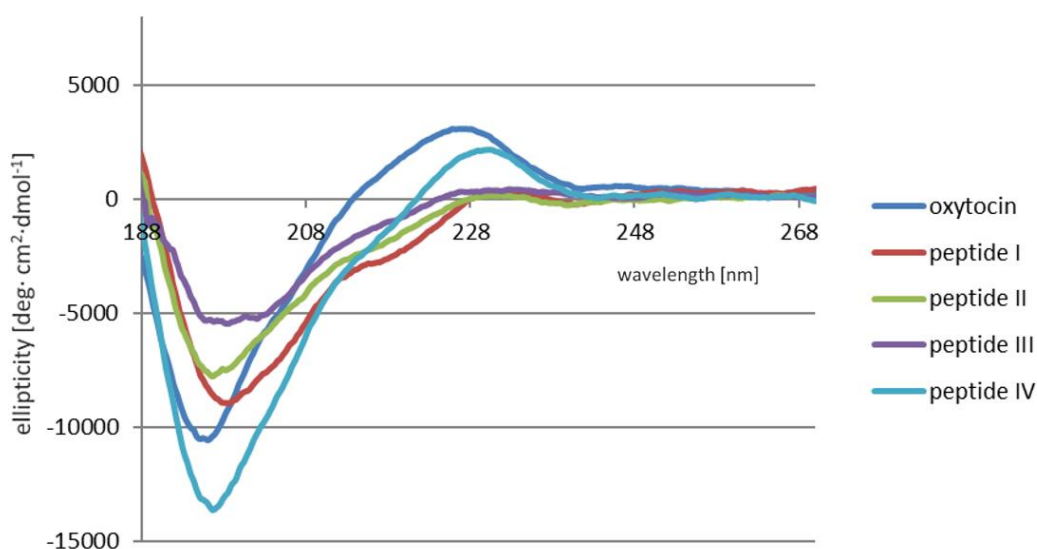
Figure 20 CD spectra of oxytocin and its analogues **I-IV** measured in the water [264].

Moreover, similar shapes of CD spectra, prepared in water, and comparable signals are observed for analogues **IR-IVR** (**Figure 21**).
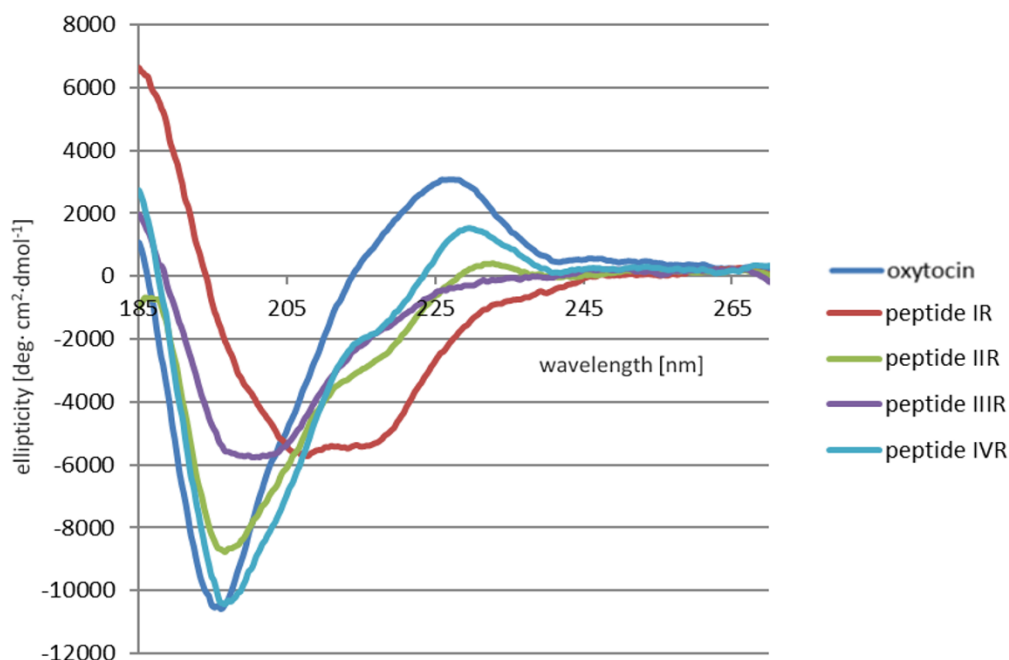
Figure 21 CD spectra of oxytocin and its analogues **IR-IVR** measured in the water [264].

Based on the presented CD spectra, peptidomimetic **IR** demonstrated a tendency to form α-helix motif because it displayed one signal at around 190 nm ($\pi\rightarrow\pi^*$ transition) and two signals at about 210 nm and 220 nm ($\pi\rightarrow\pi^*$ and $n\rightarrow\pi^*$ transitions). Peptidomimetics **IIR** and **IIIR** showed random coil conformations.

Moreover, native oxytocin and analogue **IVR** presented β-turn structures, which were also observed in the case of analogue **IV**. These peptidomimetics possessed the same amount of -CH$_2$ groups in the surroundings of the triazolyl bridge, although they differed in the orientation of the triazoles.

In order to obtain complete information about conformational preferences *via* CD spectroscopy, the analysis of the second series of peptidomimetics **V-VII** (**Figure 22**) and **VR-VIIR** (**Figure 23**) was prepared.
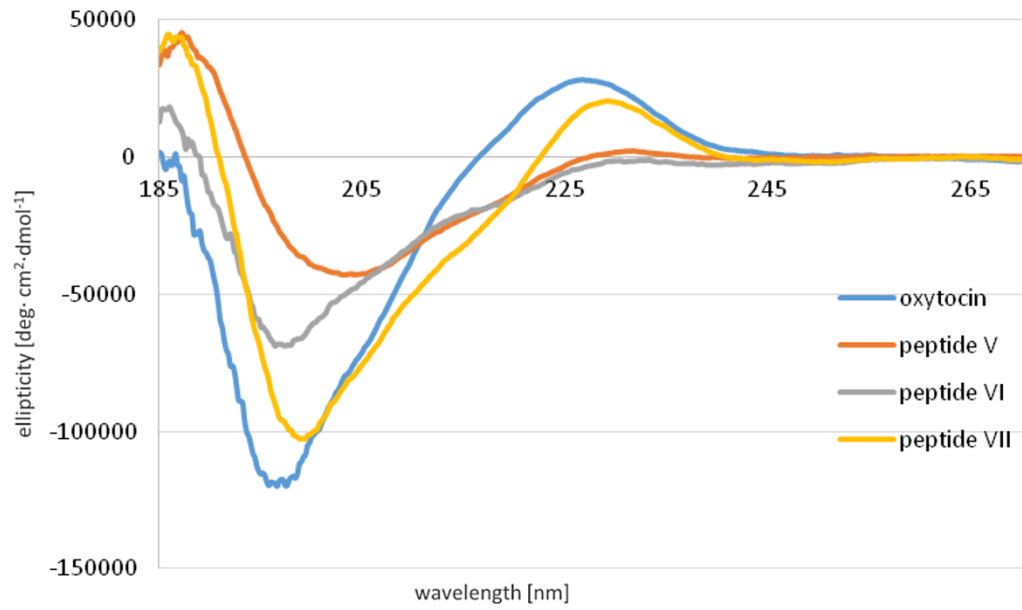
Figure 22 CD spectra of oxytocin and its analogues **V-VII** measured in the water [264].
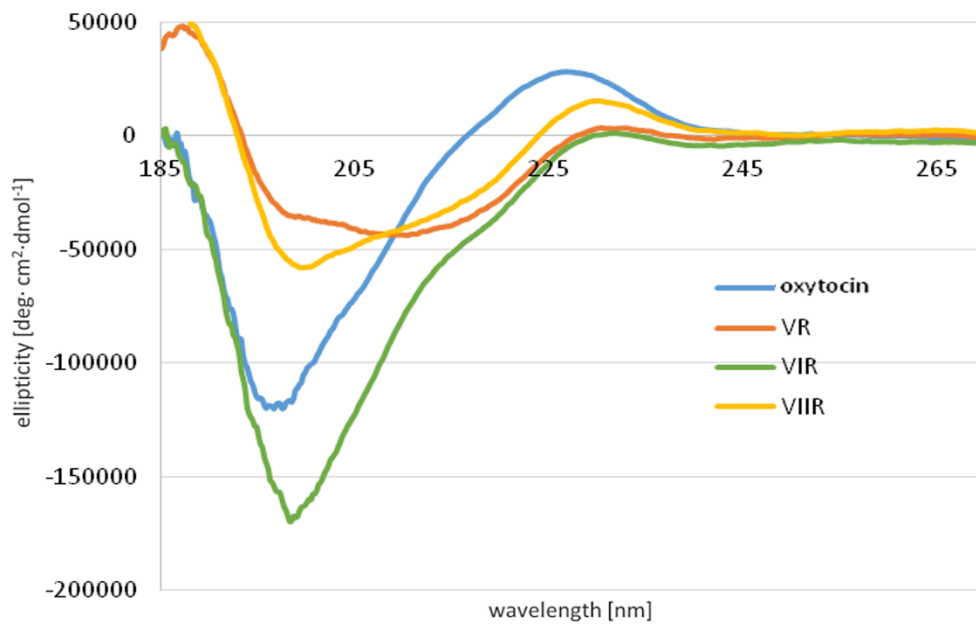
Figure 23 CD spectra of oxytocin and its analogues **VR-VIIR** measured in the water [264].

Comparison of the analogues **V** and **VR** with **VI** and **VIR**, which had the same dimension of the triazolyl bridge (m+n=3), nevertheless possessed another alignment of the -CH$_2$ groups in the surrounding of the triazole (**V** and **VR**: m,n=2,1; **VI** and **VIR**: m,n=1,2), showed that arrangement of -CH$_2$ groups demonstrated the effect on forming the secondary structures from β-turn for peptidomimetics **V** and **VR** to random coil for analogues **VI** and **VIR**.

Furthermore, according to the presented CD spectra, the most similar structure resembling native oxytocin is shown in analogue **VII**. It can be relevant with comparable quantities of atoms in both structures.

Worth to note that all analysed peptidomimetics **I-IV** *vs.* **IR-IVR** and **V-VII** *vs.* **VR-VIIR** were able to form related structures with the same amount of -CH$_2$ groups in the surrounding of the triazolyl bridge though the different orientation of the triazole, *e.g.*, **VI** and **VIR** demonstrated random coil conformations. Peptidomimetics **V** and **VR** possessed the tendency to present β-turn structures. Additionally, analogues **VII** and **VIIR** displayed unordered structures in water. In this case, the orientation of the triazolyl ring did not impact the representation of the secondary structures.

Given the circumstances, if the structure possesses fewer -CH$_2$ groups in the surrounding triazolyl bridge, it will be more ordered and partake less flexible conformation, affecting the above secondary structures of analysed compounds [264].

5.3.2.2   CD spectroscopy of MBP peptides

The analysis of the conformational preferences *via* CD experiments of peptides MBP(81-106) (**1**) and MBP(76-116) (**2**) presents that these peptides seem to be randomly structured in water (**Figure 24**).
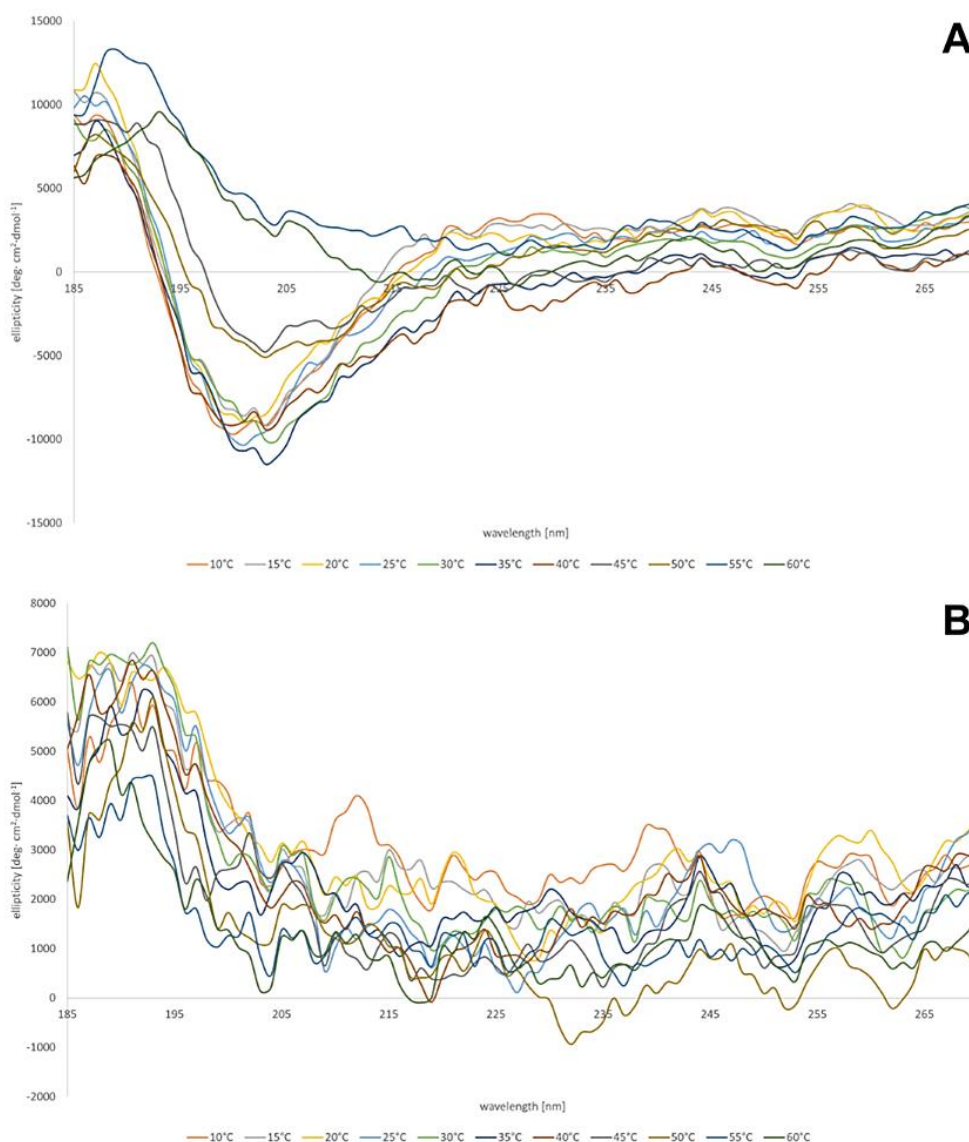
Figure 24 CD spectra of the peptides (**A**) MBP(81-106) (**1**) and (**B**) MBP(76-116) (**2**) measured in water at various temperatures [104].

Furthermore, it was examined the conformational behaviour of these peptides in a mixture of H$_2$O:TFE (50:50, v:v), which is an established stabilising agent [291]. Besides, using fluoroalcohol requires additional stability by eliminating the water molecules from the surroundings of the peptides [292]. The spectra obtained in the solvent mixture displayed two signals at 220 nm and 210 nm (n→π* and π→π* transitions) and one signal at 190 nm (π→π* transition) (**Figure 25**, **Figure 26**) that is characteristic of helical structures [208,293–295].
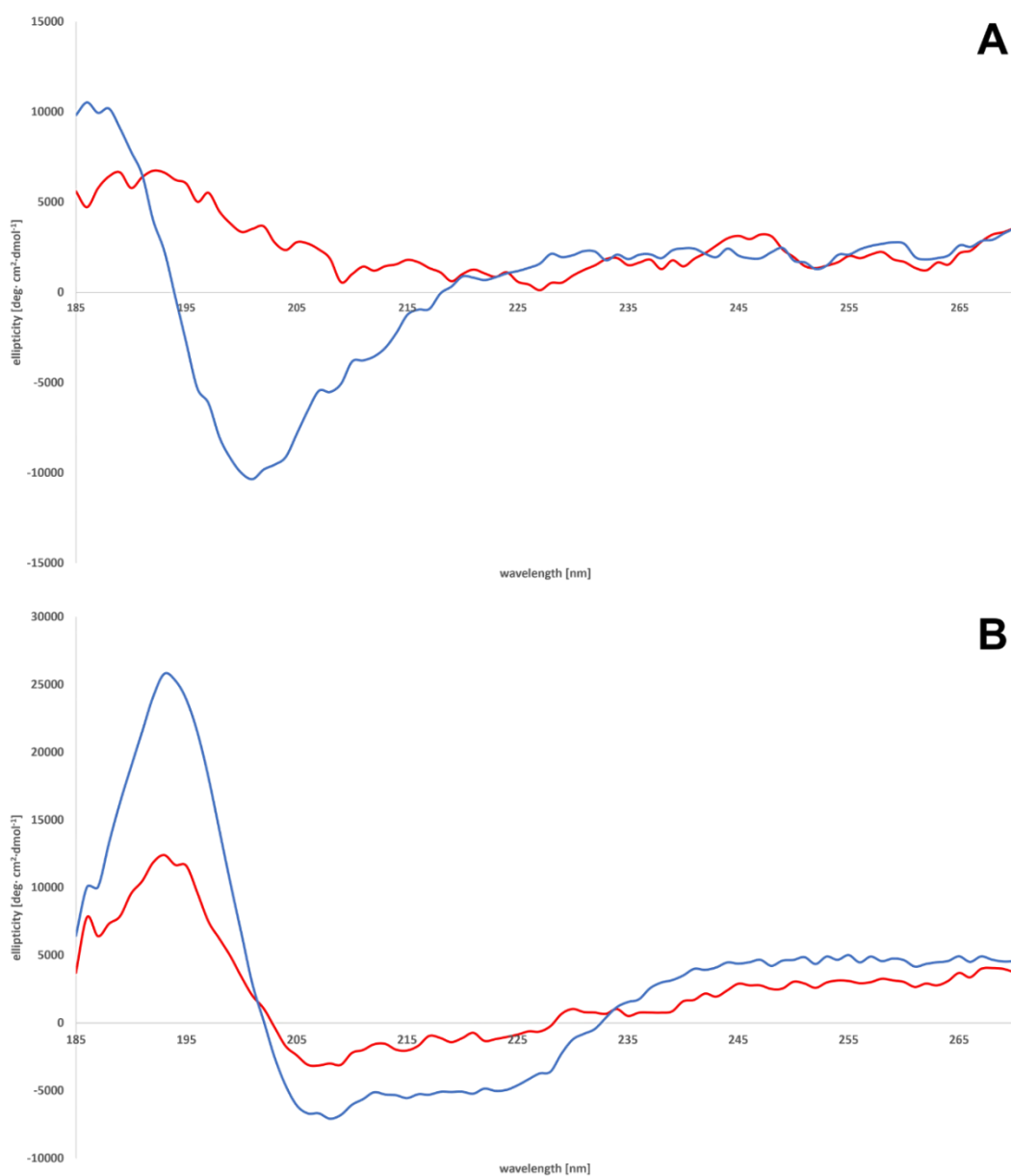
Figure 25 CD spectra of peptides MBP(81-106) (**1**) (blue line) and MBP(76-116) (**2**) (red line) measured in (**A**) water and (**B**) mixture of H_2O:TFE (50:50, v:v) at 25°C [104].

Based on these amino acid sequences, the peptides tend to form helical structures [208,294,296]. Additionally, it may be assumed that there were no spectral differences in secondary peptide structure at various temperatures (**Figure 24**, **Figure 26**).
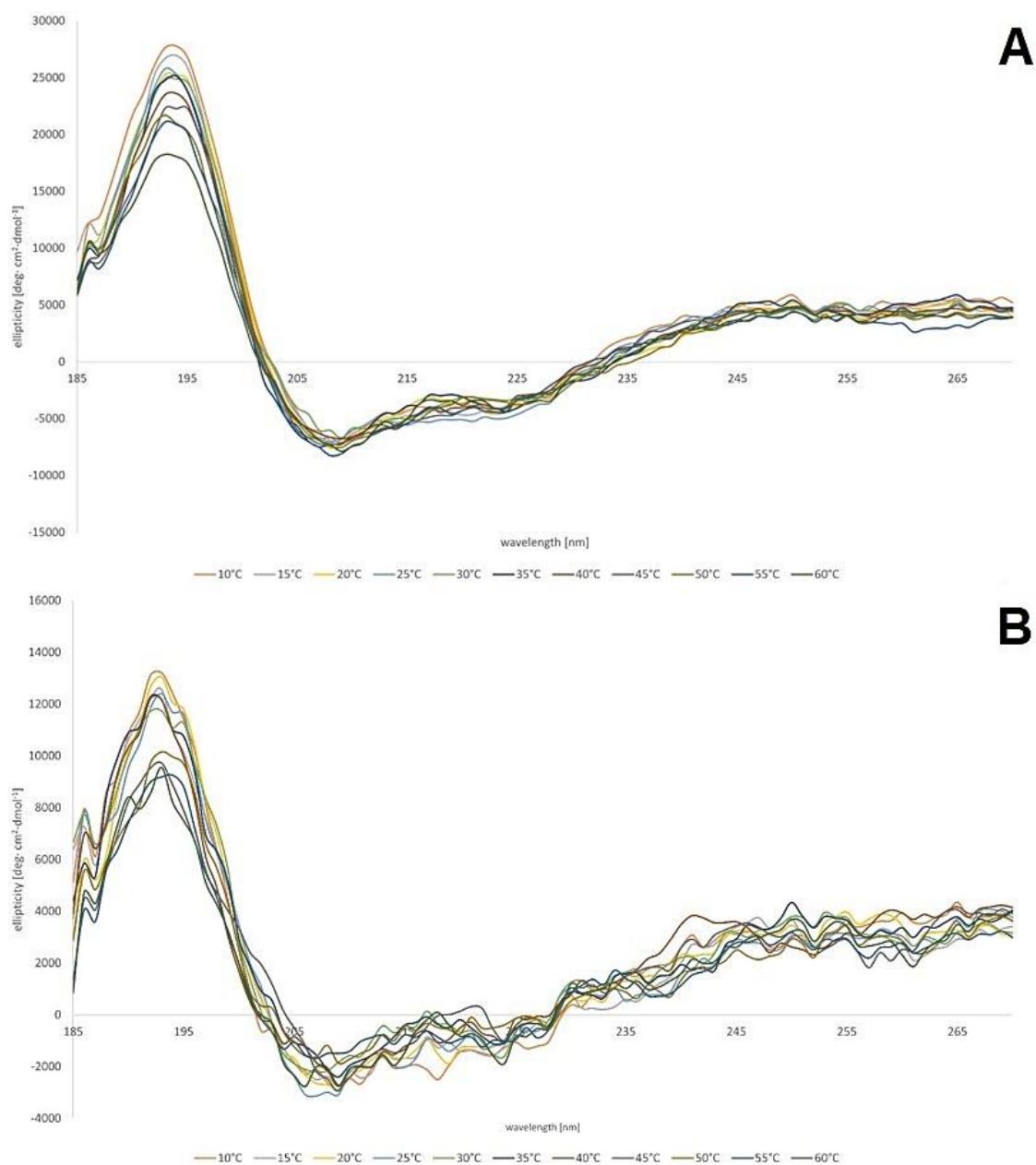
Figure 26 CD spectra of the peptides (**A**) MBP(81-106) (**1**) and (**B**) MBP(76-116) (**2**) measured in a mixture of H_2O:TFE (50:50, v:v) at various temperatures [104].

Remarkably, the peptide MBP(81-106) (**1**) demonstrates a higher tendency to form a helical conformation, as compared to the longer peptide MBP(76-116) (**2**) (**Figure 25**) [271]. The elongation at the N- and C-termini of the peptide initiates the disability in forming the helix

motif. Moreover, a different agent stabilising the α-helical structure in the peptide MBP(81-106) (**1**) is the presence at the N- and C-termini of positively and negatively charged amino acid residues able to form salt bridges [297]. Inconsistent, the peptide MBP(76-116) (**2**) contains many positively charged amino acids, such as arginine residues, which can produce a destabilised effect on helix conformation by electrostatic repulsion [298].

Additionally, it was examined the conformational preferences of peptides MBP(81-106) (**1**) and MBP(76-116) (**2**) in PBS, which is the most applied solvent to maintain physiological pH. Demonstrated data suggest that peptides **1** and **2** show random coil structures (**Figure 27**).
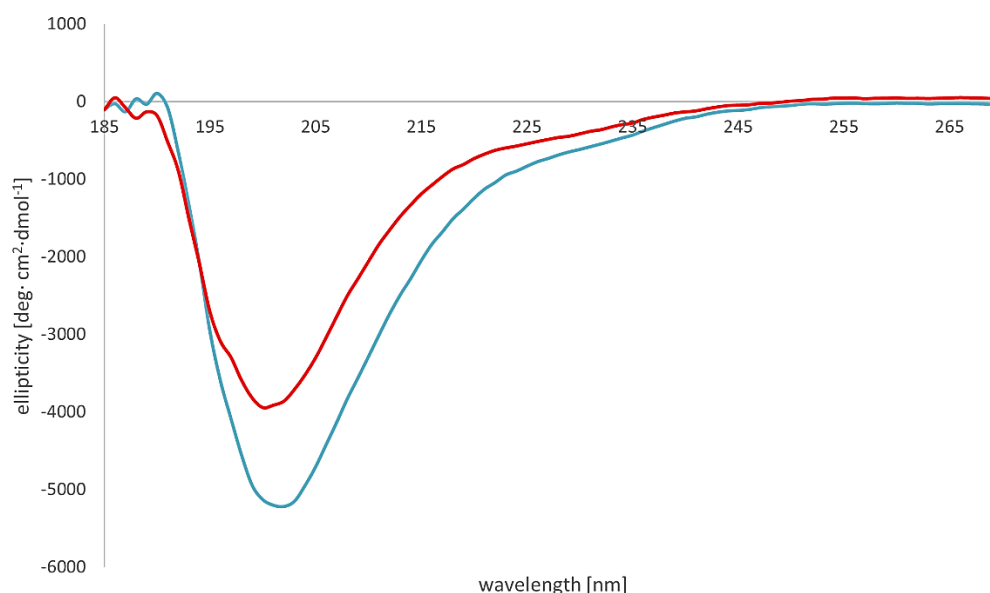
Figure 27 CD spectra of peptides MBP(81-106) (**1**) (blue line) and MBP(76-116) (**2**) (red line) measured in PBS at 25°C [104].

The presented spectra demonstrated a signal at approximately 200 nm characteristic for unordered peptides. Nevertheless, peptide MBP(81-106) (**1**) demonstrates a more ordered structure, as can be inferred by the small but essential shift at a higher wavelength of the minimum of MBP(81-106) (**1**) compared to MBP(76-116) (**2**) [299,300]. Likewise, there were no differences in secondary structure at various temperatures for peptide MBP(81-106) (**1**) (**Figure 28**).
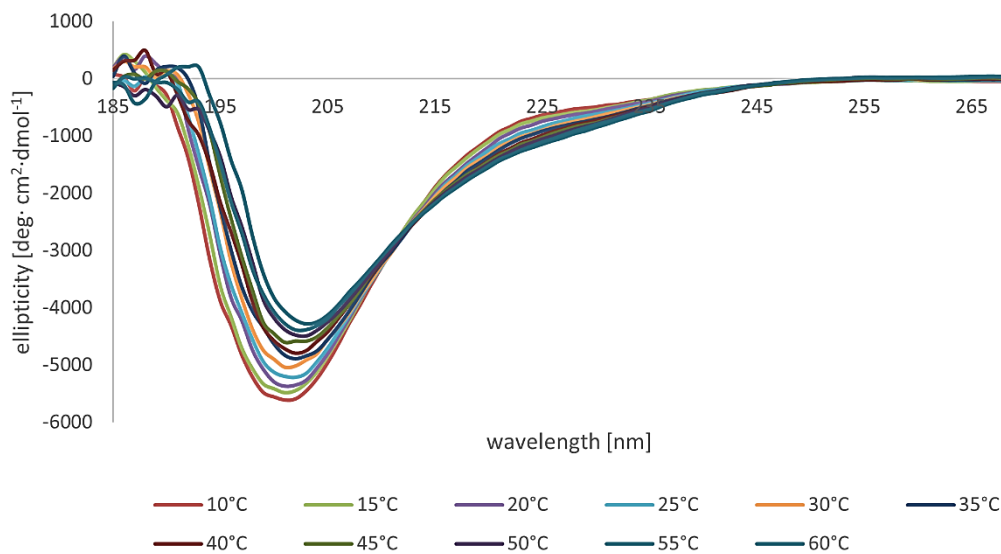
Figure 28 CD spectra of peptide MBP(81-106) (**1**) measured in PBS at various temperatures [104].

In contrast, raising the temperature of MBP(76-116) (**2**) led to a shift of the minimum to lower wavelength and a substantial reduction of the signal intensity (**Figure 29**).
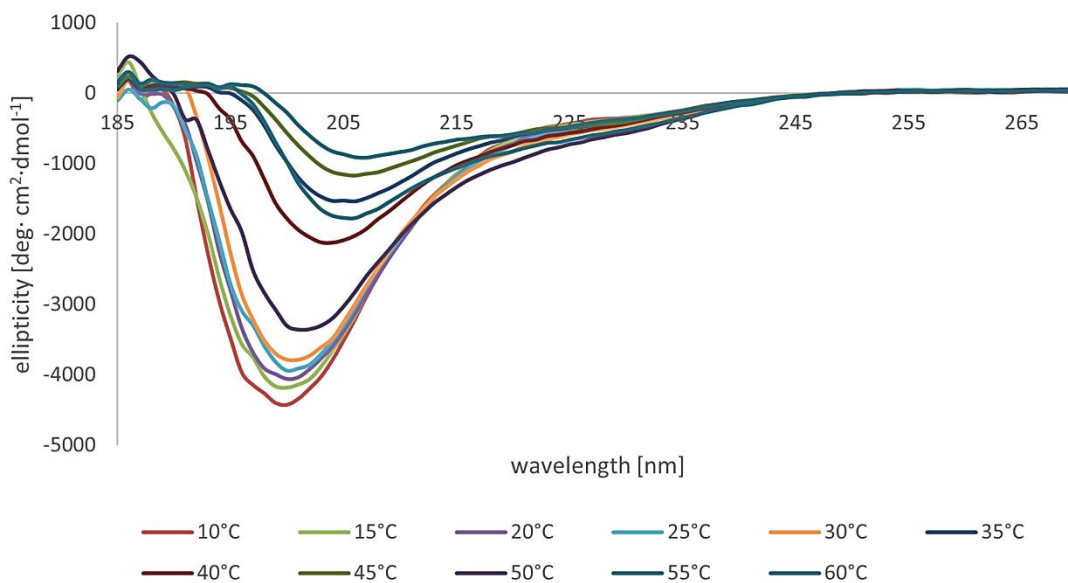
Figure 29 CD spectra of peptide MBP(76-116) (**2**) measured in PBS at various temperatures [104].

This result can derive from a temperature-induced peptide self-aggregation, which is possible in β-structures with a minimum of approximately 205 nm. The incomplete aggregation can account for the decreased ability of peptide MBP(76-116) (**2**) to interact with the IgM antibodies [104].

Based on previously obtained data for peptides MBP(81-106) (**1**) and MBP(76-116) (**2**), CD experiments were performed to define the conformational preferences of all examined MBP peptides **1-6**. Presented spectra indicated that all analysed peptides **1-6** form unordered structures in water (**Figure 30**).
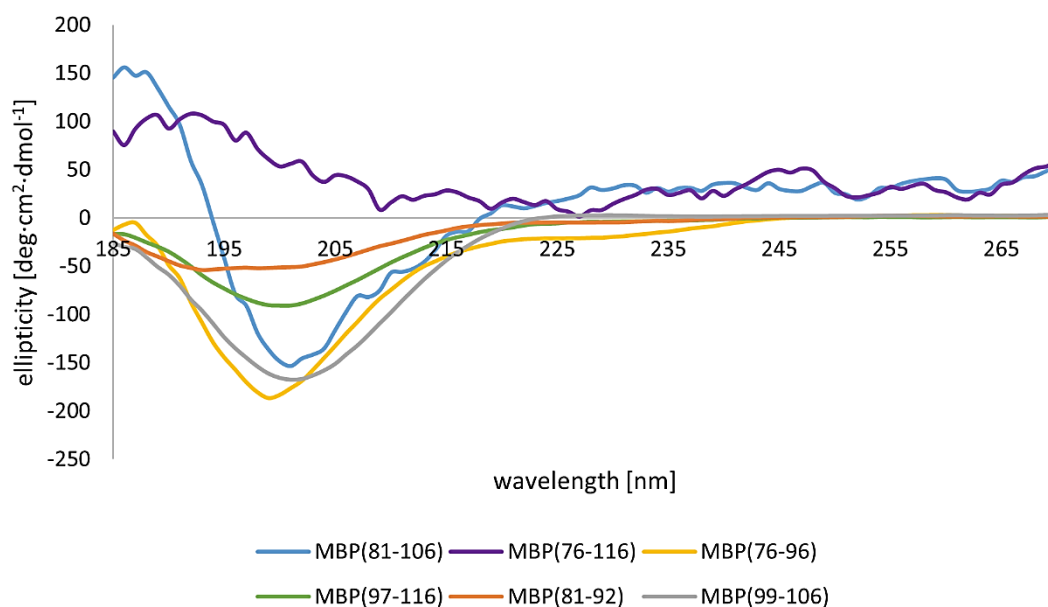
Figure 30 CD spectra of peptides MBP(81-106) (**1**) (blue line), MBP(76-116) (**2**) (violet line), MBP(76-96) (**3**) (yellow line), MBP(97-116) (**4**) (green line), MBP(81-92) (**5**) (orange line), and MBP(99-106) (**6**) (grey line) measured in water at 25°C.

CD spectra of all examined MBP peptides **1-6** registered in an aqueous solution show that their conformations are predominantly random coils. CD spectra of MBP peptides **3-6** measured in water at various temperatures are reported in Supplementary material as **Figure S50-S53**.

Moreover, the conformational behaviour of these peptides was studied in a mixture of H$_2$O:TFE (50:50, v:v). The CD spectra obtained in the solution of 50% TFE presented two

signals at 220 nm and 210 nm (n→π* and π→π* transitions) and one signal at 190 nm (π→π* transition), especially for peptides **1-3** (**Figure 31**).
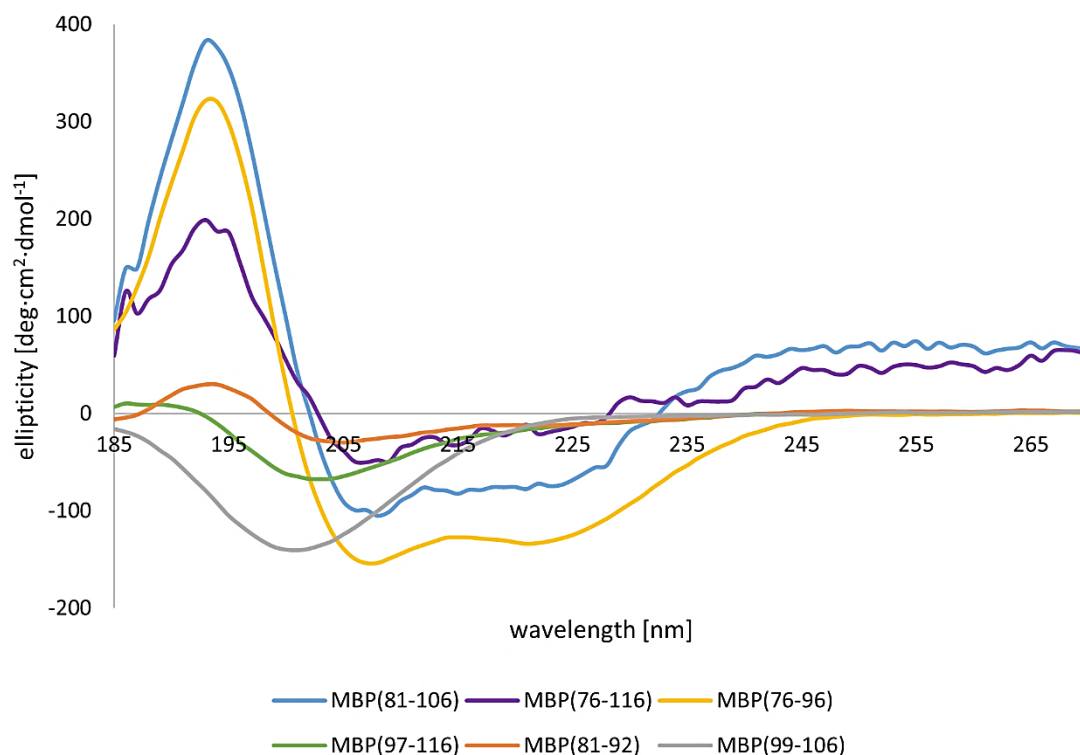
Figure 31 CD spectra of peptides MBP(81-106) (**1**) (blue line), MBP(76-116) (**2**) (violet line), MBP(76-96) (**3**) (yellow line), MBP(97-116) (**4**) (green line), MBP(81-92) (**5**) (orange line), and MBP(99-106) (**6**) (grey line) measured in a mixture of H_2O:TFE (50:50, v:v) at 25°C.

According to the literature, the presented signals are characteristic of helical structures. Some of the studied peptides demonstrate a tendency to form helical structures, *i.e.*, MBP(81-106) (**1**). On the other hand, the CD spectrum of MBP(76-96) (**3**) shows the characteristic signals for helical conformation (**Figure 32**).
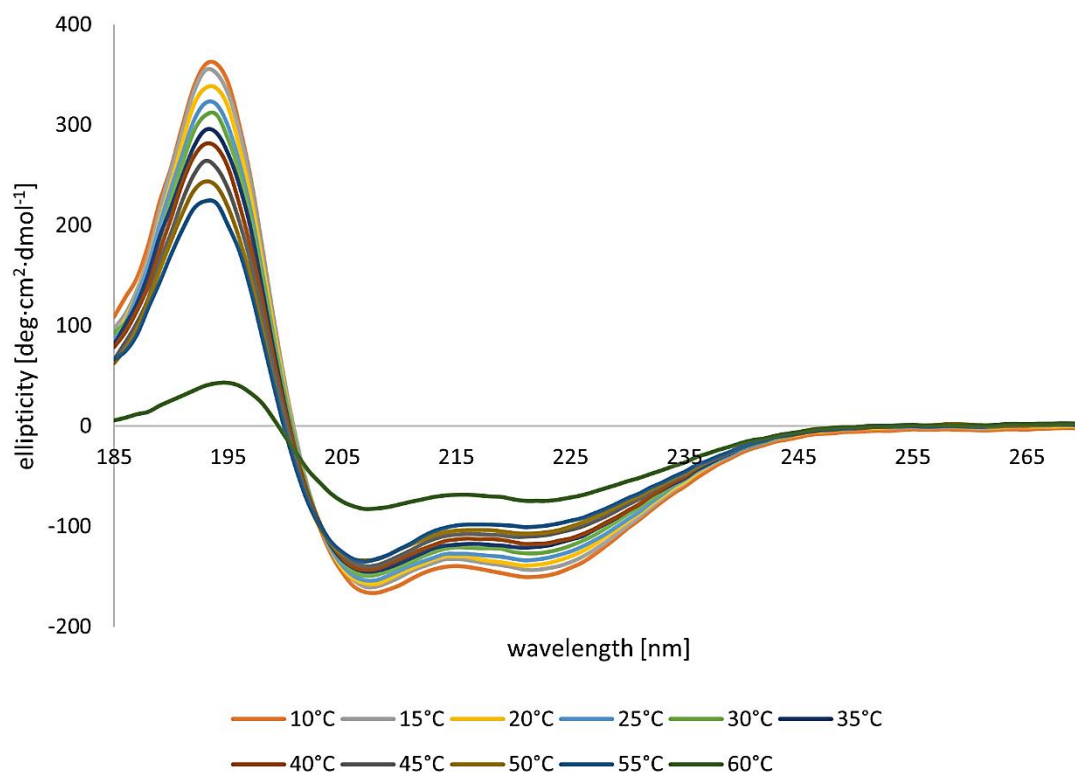
Figure 32 CD spectra of the peptide MBP(76-96) (**3**) measured in a mixture of H_2O:TFE (50:50, v:v) at various temperatures.

The maximum at around 195 nm and the minimums corresponding to 210 nm and 220 nm present that peptides MBP(81-106) (**1**) and MBP(76-116) (**2**) form α-helix structures. Although, MBP(81-106) (**1**) has a higher tendency to form helical conformation than MBP(76-116) (**2**) in 50% TFE [104]. The peptides MBP(97-116) (**4**), MBP(81-92) (**5**), and MBP(99-106) (**6**) can create random coil structures in a mixture of 50% TFE (**Figure 31**, **Figure S54-S56**). Mainly, differences in secondary peptide structure were not observed at different temperatures for experiments carried out in the water and a mixture of H_2O:TFE (50:50, v:v). The elongation at the N- and C-termini of the peptides causes the disability in forming the helix, for example, from MBP(76-96) (**3**) to MBP(76-116) (**2**). Worth to mention that, in the case of some peptides, *i.e.*, MBP(76-96) (**3**) at 60°C started the denaturation process because, at this temperature, the shape of the spectrum suggested that the compound demonstrated no ordered structure (**Figure 32**, bottle green line).

Moreover, it was performed the predictions of the secondary structures based on *DichroWeb* (**Table 8**) [295] and the calculation of the helix content of all synthetic MBP peptides **1-6** (**Table 9**) [271].

Table 8 Calculated secondary structures of synthetic MBP peptides **1-6** based on *DichroWeb* at 25°C (solutions from the CDSSTR method, using reference dataset: 3) [295].

	Conditions	Helix 1 [%]	Helix 2 [%]	Strand 1 [%]	Strand 2 [%]	Turns [%]	Unordered [%]	Total [%]
MBP(81-106) (1)	H_2O	-1	6	26	16	19	32	98
	H_2O:TFE (1:1)	2	7	23	11	22	35	100
MBP(76-116) (2)	H_2O	3	2	36	14	23	21	99
	H_2O:TFE (1:1)	-1	1	24	9	25	40	98
MBP(76-96) (3)	H_2O	16	8	21	13	18	24	100
	H_2O:TFE (1:1)	43	15	12	11	7	12	100
MBP(97-116) (4)	H_2O	0	3	24	15	26	31	99
	H_2O:TFE (1:1)	-1	3	29	14	24	29	98
MBP(81-92) (5)	H_2O	-2	7	26	17	23	27	98
	H_2O:TFE (1:1)	0	3	25	13	25	32	98
MBP(99-106) (6)	H_2O	6	-2	21	13	30	30	98
	H_2O:TFE (1:1)	0	2	27	16	24	29	98

Table 9 Calculated helix content of MBP peptides **1-6** [271].

| Peptide | Conditions of experiments | | | |
| | H$_2$O | | H$_2$O:TFE (1:1) | |
	$[\theta]_{222}$	Helix content [%]	$[\theta]_{222}$	Helix content [%]
MBP(81-106) (1)	10.1	-0.03	-71.9	0.20
MBP(76-116) (2)	16.8	-0.05	-21.1	0.06
MBP(76-96) (3)	-21.8	0.06	-126.9	0.37
MBP(97-116) (4)	-7.8	0.02	-15.3	0.04
MBP(81-92) (5)	4.7	0.02	-12.0	0.04
MBP(99-106) (6)	-3.3	0.01	-10.8	0.04

According to the results obtained in the mentioned methods, the peptide MBP(76-96) (**3**) has the highest helix content of all examined peptides. Based on these calculations, I can assume that the rest of the analysed MBP peptides **1**, **2**, **4-6** form random coil structures in a water solution.

Furthermore, the peptides **1-3** are able to create α-helical structures in a mixture of H$_2$O:TFE (50:50, v:v). Peptide MBP(81-92) (**5**) shows a tendency to form a helix structure in a solution of 50% TFE. On the other hand, peptides **4** and **5** can demonstrate random coil structures in these conditions.

All obtained results from predictions based on *DichroWeb* (**Table 8**) or calculations of the helix content (**Table 9**) are in accordance with performed CD experiments.

5.3.3 NMR spectroscopy

5.3.3.1 NMR studies of oxytocin and its analogues

The conformational space of oxytocin and its fourteen analogues **I-VII** and **IR-VIIR** was analysed by NMR spectroscopy in water. NMR structures were generated by molecular dynamics calculations under distance and dihedral angle restraints derived from ^{1}H-^{1}H Rotating-Frame Overhauser Effects (ROEs) and $^{3}J_{HNH\alpha}$ coupling constants, respectively. **Figure 33** presents the conformational ensembles obtained for all peptides examined in this study.

Moreover, a superimposition of each analogue displaying the lowest RMSD with the structure of OT is also included in the Supplementary material (**Figure S57** and **Table S7**) to demonstrate the degree of structural difference or similarity to OT. All ^{1}H, ^{13}C, and ^{15}N chemical shifts of oxytocin and its analogues **I-VII** and **IR-VIIR** at various temperatures performed in $H_2O:D_2O$ (90:10, v:v) are reported in Supplementary material as **Table S8-S22**.
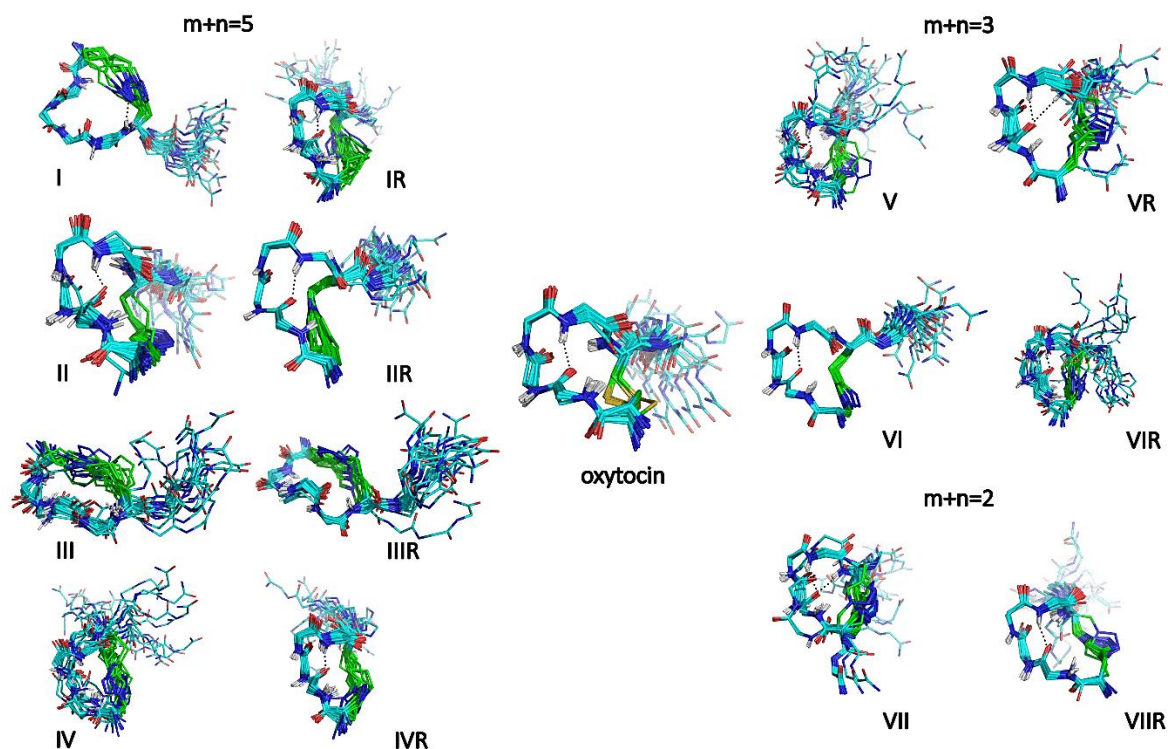
Figure 33 Superimposition of the twenty lowest energy structures of OT and its analogues **I-VII** and **IR-VIIR** prepared in water [264].

Firstly, OT conformation was studied at 5°C in water as a reference to validate the molecular mechanics calculations protocol. As in the previously published NMR structure (PDB ID: 2MGO) [262], it was confirmed that oxytocin preferentially adopts a type I β-turn conformation in water centred on Ile^3-Gln^4 residues. This is supported by observing characteristic ROEs (Ile^3 HN/Gln^4 HN, Gln^4 HN/Asn^5 HN, and Tyr^2 H^δ/Gln^4 HN) (**Table S5**).

Moreover, a typical hydrogen bond between the carbonyl group of Tyr^2 and the HN group of Asn^5 is observed in the NMR structures (**Figure 33**). The analysis of amide proton temperature coefficients indicates that HN protons in Asn^5 and Cys^6 are more sequestered from solvent than in other amino acid residues ($\Delta\delta HN/\Delta T$ of -5.5 and -5.1 ppb/K, respectively, in comparison with an average value of -7.5 ppb/K) (**Table S6**). This is in agreement with the orientation of both HN groups towards the interior of the peptide macrocycle in the NMR structures.

The NMR analysis of OT analogues **I-VII** and **IR-VIIR** reveals some similarities with OT in H^α and C^α chemical shifts, with sequential HN/HN ROEs and some medium-range ROEs

indicative of the existence of folded conformations. Interestingly, all peptides show a deshielding of Tyr[2] H^{α}, a shielding of Ile[3] and Gln[4] H^{α} protons, and a deshielding of Ile[3] and Gln[4] C^{α} carbons (**Table S5** and **Figure S57**).

However, differences can be observed in the ROE correlations and the amide proton temperature coefficients, reflecting different turn propensities and stabilities. A type I β-turn conformation centred on Ile[3]-Gln[4] is observed in the NMR structures of ten analogues among the fourteen studied (**Figure 33**, **Table S8-S22**). Some analogues also populate inverse γ-turn conformations on Asn[5] (**III**, **IIIR**, **VIR**) or a type I β-turn shifted on Gln[4]-Asn[5] (**VII**). The analogue **IR** has a 3$_{10}$ helical folding with a double-turn conformation. In all structures, the exocyclic C-terminal Pro[7]-Leu[8]-Gly[9]-NH$_2$ extension is highly labile, as supported by near random coil values of the H^{α} and C^{α} chemical shifts (**Figure S57**) and negative temperature coefficients of amide protons (**Table S6**). Moreover, the calculated chemical shift deviations (CSD) for OT and its analogues are demonstrated in **Figure S58**.

It should be highlighted that peptidomimetics **IV** and **IVR** possess the most interesting pharmacological properties, which are discussed below. In both analogues, the disulphide bridge is replaced by a longer 1*H*-[1,2,3]triazolyl-containing bridge, where m+n=5 (m=1, n=4), as compared with the -CH$_2$-S-S-CH$_2$- presented in OT and the location of the 1*H*-[1,2,3]triazolyl moiety in the bridge is removed by only one methylene from the N-proximal bridgehead. The only difference between peptidomimetics **IV** and **IVR** is the 1*H*-[1,2,3]triazolyl orientation 1,4- *vs.* 4,1-, respectively. Moreover, the studied compounds share a typical CD signature with OT, exhibiting a positive contribution around 230 nm characteristic of turn conformations (**Figure 20**, **Figure 21**). Nevertheless, a different picture emerges from the NMR analysis. While analogue **IVR** shows all diagnostic ROEs of a type I β-turn centred on Ile[3]-Gln[4], similar to OT. On the other hand, peptidomimetic **IV** lacks Ile[3] HN/Gln[4] HN and Tyr[2] H^{δ}/Gln[4] HN ROE correlations (**Table S5**), which appear more flexible than analogue **IVR** [264].

5.3.3.2   Comparison with the active conformation of OT in the OTR binding site

A recent publication of the structure of the oxytocin receptor OTR-OT-G-protein complex (PDB ID: 7QVM) allows the comparison of the receptor-bound conformation of OT to the NMR structure in an aqueous solution [300]. Even if a β-turn conformation is observed in both structures, it is essential to note that the turn position is shifted from Ile^3-Gln^4 in water to Tyr^2-Ile^3 in the stabilised mutant $[D^{153}Y]$OTR-OT bound conformation. In it, Ile^3 is buried in a hydrophobic pocket formed by side-chain residues of transmembrane helices (TMs) **II-VI** and **VII**, and the Tyr^2 penetrates deeply into a pocket lined up by TMs **II**, **III**, **VI**, and **VII** [301].

In addition, the cryo-electron microscopy (cryo-EM) structure of wild-type OTR in complex with OT and G protein (PDB ID: 7RYC) also reveals that Tyr^2 of OT sits deep within the receptor core alongside TM **VII** and TM **II**, and Ile^3 occupies a hydrophobic pocket formed on TM **V** [302]. Activation of the OTR leads to a perturbation of TM **VII**, resulting in partial unfolding and the formation of a kink near the extracellular receptor side [301]. This indicates that the predominant conformation of OT in water may not be the bioactive conformation and that binding to OTR implies conformational selection of otherwise a weakly populated conformer in solution and/or an induced fit conformational transition.

To get insight into the steric impact of the 1*H*-([1,2,3]triazolyl)-containing cyclisation on the putative bound conformation, it was decided that peptidomimetics **IV** and **IVR** fit the receptor-bound OT conformation. The superimposition of peptidomimetic **IIR** adopting the receptor-bound conformation of OT indicates that the 1*H*-[1,2,3]triazol-1-yl ring would be centred at the C^α atom of Cys^6 in OT. Still, it will impose a steric clash between Pro^7 in OT and W^{188} in the extracellular loop 2 (ECL2) connecting TMs **IV-V** (**Figure 34**).

Conversely, in the analogues **IV** and **IVR**, the triazole moieties, like the disulphide bridge, are removed only by one -CH_2- from the N-proximal bridgehead and occupy the position of S^γ atom in Cys^1 of OT, and like OT, it is facing the apolar OTR residues M^{315} and L^{316} in TM **VII**. Comparing the orientations of the exocyclic C-terminal tripeptide extension in the analogue **IIR** with the orientation of the same tripeptides in the analogues **IV** and **IVR** reveals the latter is closely aligned with that of OT and unlike the one in compound **IIR**, does not experience the steric hindrance imposed by the proximity to W^{188}. The exocyclic C-terminal amidated extension of OT is facing ECL2 and ECL3 of the cognate receptor and is crucial for its activation. Nevertheless, the lack of perfect overlap of the C-terminal extension of OT

with those of the weakly active analogues **IV** and **IVR** may account for their weak affinity to the OTR [264].
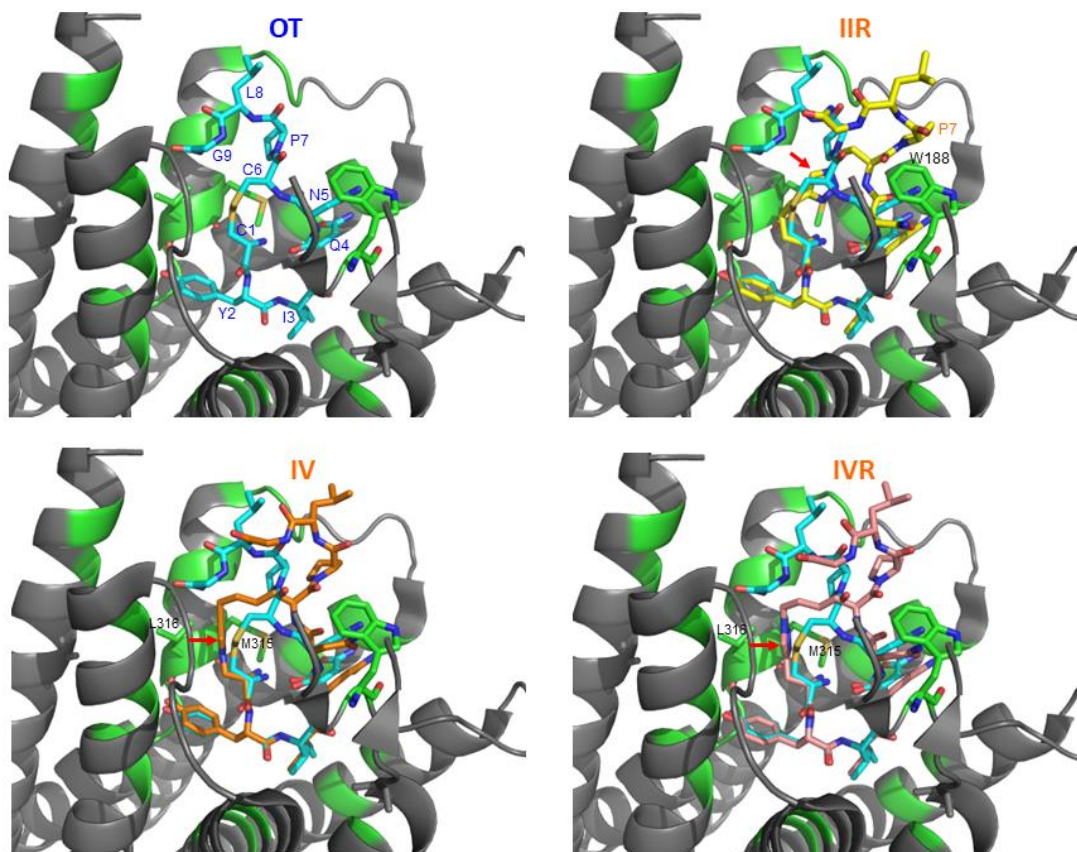
Figure 34 Superimposition of analogues **IIR** (yellow), **IV** (orange), and **IVR** (pink) onto OT (cyan) in the OTR (PDB ID: 7QVM). Residues of OTR in close contact with OT ligand (distance <5 Å) are marked in green. Only the side chains of W[188], M[315], and L[316] are shown. Analogues **IIR**, **IV**, and **IVR** were modelled by constraining dihedral angles to enforce the bioactive conformation of OT. The 1*H*-[1,2,3]-triazolyl rings in peptidomimetics **IIR**, **IV**, and **IVR** are indicated by an arrow [264].

5.3.3.3 NMR studies of MBP peptides

Firstly, the conformational behaviour of peptides MBP(81-106) (**1**) and MBP(76-116) (**2**) was analysed in a DPC micelle (100 mm) by NMR spectroscopy.

Almost completed ^{1}H NMR assignments were obtained for MBP(81-106) (**1**). Unfortunately, in the case of MBP(76-116) (**2**), some amino acid residues could not be assigned as a result of strong signals overlapping (**Table S23-S24**) [104].

According to chemical shift values (**Table S23-S24**) and NOE interaction patterns (**Figure S59**), it can be assumed that MBP(81-106) (**1**) and MBP(76-116) (**2**) possess stable helical structures along residues 87-96, while the remaining regions did not demonstrate diagnostic parameters of any secondary structure. It is believed that peptides **1** and **2** present random coil conformations.

Moreover, the demonstrated results are in agreement with data reported in the literature about a 36-residue peptide fragment of murine MBP corresponding to residues 76-111 [294].

Comparing the chemical shift values of peptides MBP(81-106) (**1**) and MBP (76-116) (**2**), which are not drastically different, the helical structure turns out to have the same stability regardless of the amino acid sequence length. Furthermore, the superposition of selected regions of the NOESY spectra of two analysed peptides **1** and **2** demonstrates graphic evidence of this result (**Figure S59**) [104].

Afterwards, it was performed NMR studies of peptides **1-6** in a mixture of $H_2O:D_2O$ (90:10, v:v) and TFE-d_3:D_2O:H_2O (50:10:90, v:v:v) to confirm the synthesised structures and for conformational analysis *via* molecular dynamics calculations which are mentioned in chapter above. In some cases, the interpretation of NMR spectra of MBP peptides was impossible due to overlapping the signals. In this context, it was decided that the structures with the shortest peptide chains, particularly MBP(99-106) (**6**) and MBP(81-92) (**5**), were analysed and applied in further studies.

The values of chemical shifts of analysed peptides **5** and **6** are presented in Supplementary material as **Table S25-S32**.

According to chemical shift values, it was suggested that peptides MBP(81-92) (**5**) and MBP(99-106) (**6**) present unordered conformation in both solvents. It is in accordance with the CD experiments demonstrated above in this doctoral dissertation.

5.3.3.4 NMR structure calculations of MBP peptides

The distance constraints contained in Supplementary material as **Table S33** were applied in molecular dynamics calculations of MBP(99-106) (**6**) in a mixture of TFE-d$_3$:D$_2$O:H$_2$O (50:10:90, v:v:v).

Based on experimental data with peptide **6**, one thousand structures were optimised each time starting with a stretched compound. For the selected central structure, the structure was refined using the refinement protocol. The obtained one thousand structures were divided into clusters considering the positions of the main chain of atoms. Unfortunately, an attempt at clustering based on the entire amino acid sequence, taking into account the RMSD value at the level of 1.0 Å, led to many clusters with a small number. Clustering based on the first five amino acids of the sequence with an acceptable RMSD value allowed the definition of a cluster containing 58.1% of the structures. For the obtained cluster, torsion angles were analysed (**Table S34**). In **Figure 35**, there are graphical representations of the obtained structures.
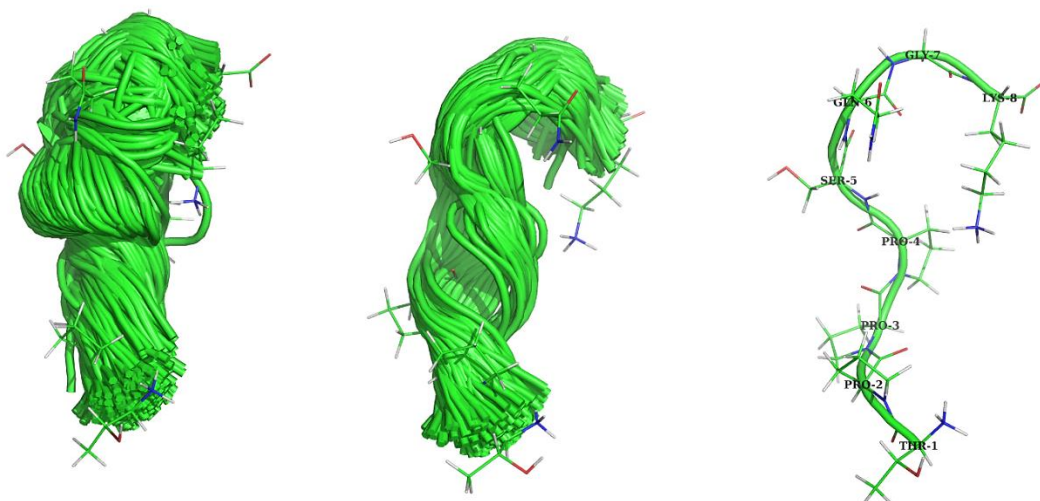
Figure 35 Graphical representation of the structures of cluster 1 obtained after refining the structure of the MBP(99-106) (**6**) based on the NOESY spectrum prepared in a mixture of TFE-d$_3$:D$_2$O:H$_2$O (50:10:90, v:v:v); left: frontal view, middle: side view, right: central structure.

According to experimental data on MBP(99-106) (**6**) in a mixture of $H_2O:D_2O$ (90:10, v:v), one thousand independent structures were optimised, each time starting with a stretched structure (**Table S35**). The compound was refined using the refinement protocol for the selected central structure. The obtained one thousand systems were divided into clusters studying the positions of the main chain. Awkwardly, an attempt at clustering based on the entire amino acid sequence, considering the RMSD value at the level of 1.0 Å, led to many clusters with a small number. Clustering based on the first six amino acid residues with an acceptable RMSD value of 0.75 Å allowed the definition of a cluster containing 16.4% of the structures. The values of torsion angles for the obtained cluster are presented in **Table S36**. In **Figure 36**, there are graphical representations of the found structures.
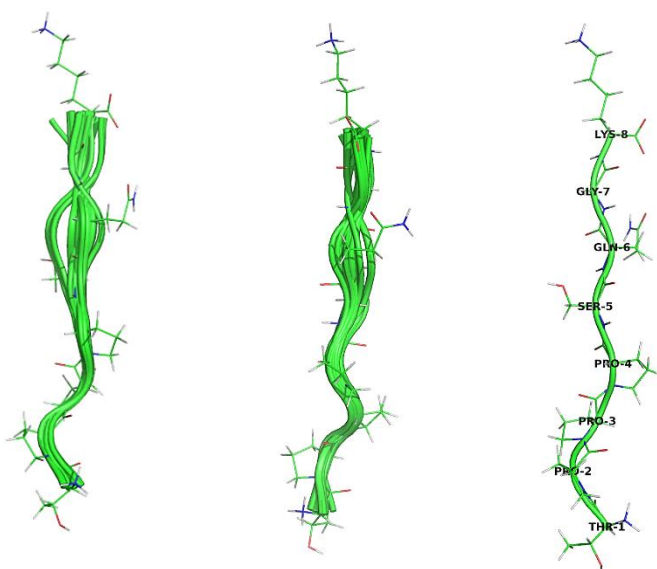
Figure 36 Graphical representation of the structures of cluster 1 obtained after refining the structure of the MBP(99-106) (**6**) based on the NOESY spectrum prepared in a mixture of $H_2O:D_2O$ (90:10, v:v); left: frontal view, middle: side view, right: central structure.

On the other hand, analysis of results obtained for peptide MBP(81-92) (**5**) in the mixture of TFE-d_3:D_2O:H_2O (50:10:90, v:v:v) suggests that the structures obtained after refinement indicate a relatively high lability of the C-terminal fragment of the amino acid sequence. **Table S37** demonstrates the distance constraints applied in molecular dynamics calculations.

Clustering the obtained structures based on the first eleven amino acid residues allows two dominant structural clusters containing 23.6% and 25.9% of the structures, respectively. The comparison of the values of torsion angles shows their magnificent similarities in the N-terminal part of the peptide chain (**Table S38-S39**). Therefore, reclustering based on the first nine amino acid residues defines one dominant structural cluster with 54.3% of the structures (**Table S40**). Oppositely, the analysis of torsion angles suggests helical conformations, including the Gln[82]-Asn[85] and Val[87]-Val[88] fragments. The visualisation of the obtained structures is shown in **Figure 37**.
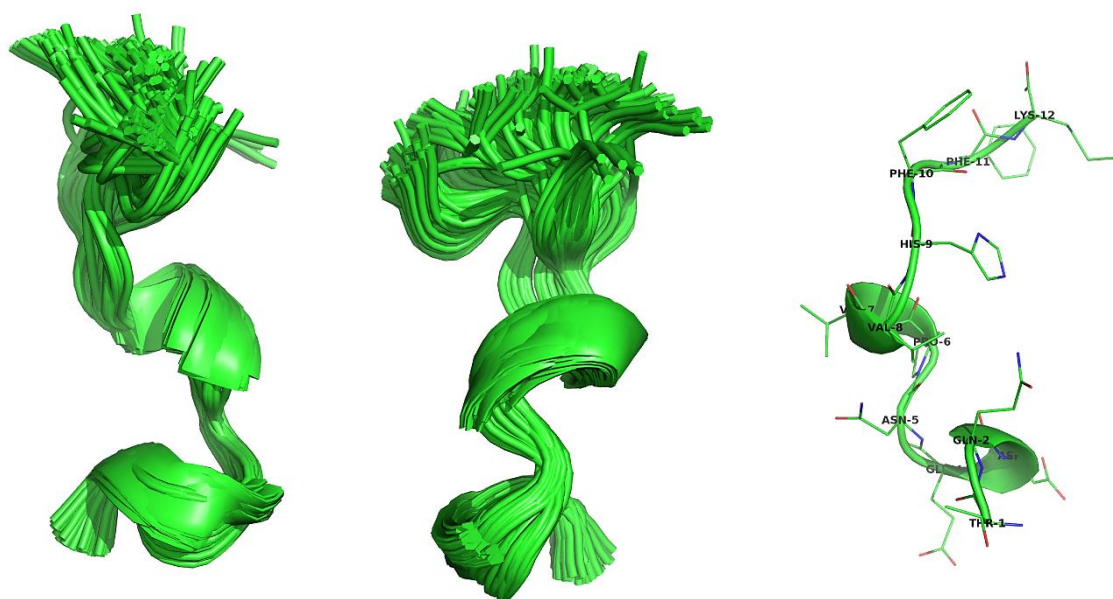
Figure 37 Graphical representation of the structures of cluster 1 obtained after refining MBP(81-92) (**5**) structure based on the NOESY spectrum prepared in a mixture of TFE-d_3:D_2O:H_2O (50:10:90, v:v:v); left: frontal view, middle: side view, right: central structure.

Furthermore, molecular dynamics calculations were performed for peptide MBP(81-92) (**5**) in the mixture of H_2O:D_2O (90:10, v:v) (**Table S41**). Based on the first eleven and the first nine residues, structural analysis of the obtained conformations allows the identification of two dominant structural clusters, containing 23.7% and 13% (**Table S42-S43**), 37.3% and 22.5% (**Table S44-S45**) of the obtained corresponding structures. Nevertheless, the analysis of torsion angles in each of the found structural clusters did not allow for identifying the dominant secondary structure, indicating the dominant presence of unorganised structures in aqueous

solutions. In **Figure 38**, there is a graphical representation of clusters 1 and 2 of peptide MBP(81-92) (**5**).
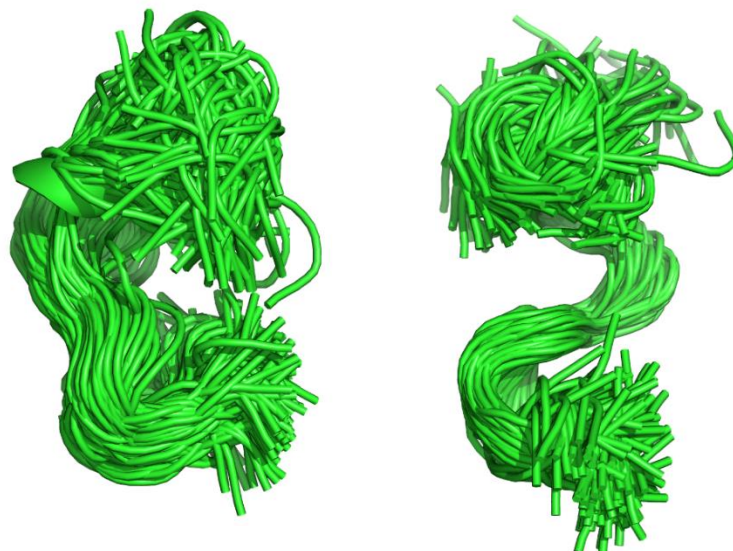
Figure 38 Graphical representation of the structures of clusters 1 and 2 obtained after refining MBP(81-92) (**5**) based on the NOESY spectrum prepared in a mixture of $H_2O:D_2O$ (90:10, v:v); clustering based on 1-9 residues; left: cluster 1, right: cluster 2.

5.4   The pharmaceutical activity of analogues of oxytocin

For pharmacological characterisation of the 1*H*-[1,2,3]triazolyl-containing OT analogues, **I-VII** and **IR-VIIR**, their affinity was analysed *via* radioligand binding assays in cell membranes stably expressing OTR. Functional receptor G_q activation was measured utilising the homogeneous time-resolved fluorescence (HTRF) inositol-1-phosphate (IP-1) protocol with human OTR in stable HEK293 cell lines [262,281].

All peptidomimetics **I-VII** and **IR-VIIR** were screened in a one-point radioligand displacement assay on OTR to identify lead compounds for in-depth pharmacological characterisation. Analogues **II**, **IIR**, **III**, **IIIR**, **VI**, **VIR**, and **VIIR** (each at 10 μM) did not displace the radioligand from any of the four receptors with more than 30% efficacy and were considered as inactive.

On the other hand, peptidomimetics **IV**, **IVR**, **V**, and **VII** displaced tritiated OT from the OTR with greater than 50% effectiveness (**Figure 39A**). The most promising compounds from the pre-screening, *i.e.*, **IV** and **IVR** as lead pair and **I**, **VI**, **VR**, **VII**, and **VII** for comparison, were measured in competitive radioligand binding experiments to determine their affinity (**Table 10**). Analogues **IV** and **IVR** displaced tritiated oxytocin with a K_i of ~2.80 µM and 0.68 µM, respectively (**Figure 39B**, **Table 10**) [264].

Table 10 Pharmacological properties of clicked oxytocin analogues at OTR.

Ligand	Affinity binding	Potency/efficacy IP-1	
	$K_i \pm SEM$ (M)	$EC_{50} \pm SEM$ (M)	$E_{max} \pm SEM$ (%)
OT	$1.7 \pm 0.1 \times 10^{-10}$	$3.2 \pm 1.7 \times 10^{-8}$	97.4 ± 0.8
I	$9.8 \pm 1.1 \times 10^{-6}$	n.d.	n.d.
IV	$2.8 \pm 1.6 \times 10^{-6}$	$6.5 \pm 2.2 \times 10^{-7}$	32.6 ± 2.1
IVR	$6.8 \pm 0.5 \times 10^{-7}$	$1.7 \pm 0.7 \times 10^{-5}$	19.8 ± 5.3
V	$4.0 \pm 0.7 \times 10^{-6}$	n.d.	n.d.
VR	$1.2 \pm 0.1 \times 10^{-5}$	n.d.	n.d.
VII	$2.5 \pm 1.4 \times 10^{-6}$	$2.5 \pm 0.3 \times 10^{-6}$	80.4 ± 2.0
VIIR	$3.1 \pm 0.7 \times 10^{-5}$	n.d.	n.d.

Presented data are from at least two independent experiments (n≥2); n.d. no data.

The two lead analogues were further explored in second messenger functional assays for potency and efficacy to activate the OTR. OTR-dependent activation of the G_q-pathway was measured by detecting the accumulation of IP-1, a downstream metabolite of D-*myo*-inositol 1,4,5-trisphosphate (IP-3). Peptidomimetic **IV** activated the OTR with an EC_{50} of 0.65 µM E_{max} of 32.6%, suggesting partial agonism. In contrast, a deficient level of receptor activation by structure **IVR** was observed for concentrations up to 10 µM (**Figure 39C**), indicating that it may be an inhibitor.

To investigate the mechanism of the antagonism (competitive *vs.* non-competitive), a Schild regression analysis of peptidomimetic **IVR** was performed on the OTR. In this context, concentration-dependent receptor activation was measured by its endogenous ligand oxytocin alone or in several concentrations of analogue **IVR** (100 nM, 300 nM, 1 µM, and 3 µM).

As expected for a competitive antagonist, it was observed a dextral shift of the oxytocin potency without affecting the efficacy (**Figure 39D**,

Table 11), resulting in a linear regression slope of 1.0 ± 0.12 and a pA2 value of 7.1 (~79 nM functional inhibitory affinity) (**Figure 39E**) [264].

Table 11 Antagonist properties of clicked oxytocin analogue **IVR** at OTR comparable with OT.

Ligand	Potency/efficacy IP-1	
	$EC_{50} \pm SEM$ (M)	$E_{max} \pm SEM$ (%)
OT	$2.1 \pm 0.4 \times 10^{-8}$	99.5 ± 7.7
IVR (100 nM)	$2.9 \pm 0.7 \times 10^{-8}$	96.8 ± 9.0
IVR (300 nM)	$4.2 \pm 0.1 \times 10^{-8}$	114.5 ± 2.9
IVR (1 μM)	$1.6 \pm 0.3 \times 10^{-7}$	103.7 ± 7.9
IVR (3 μM)	$2.6 \pm 0.9 \times 10^{-7}$	106.6 ± 8.2

The presented data are from four independent experiments (n=4).
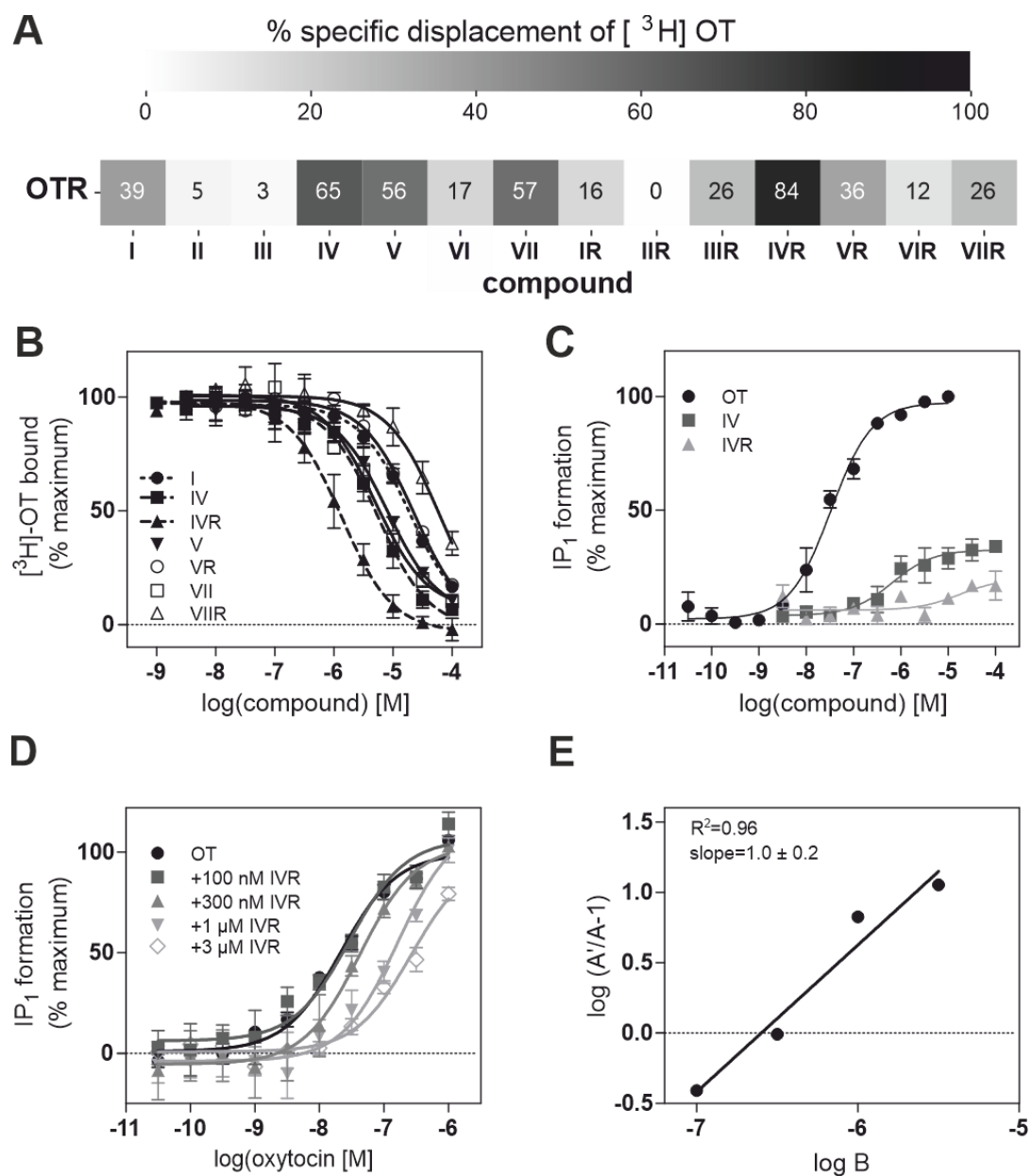
Figure 39 Pharmacology of oxytocin analogues: (**A**) One-point radioligand displacement experiments; (**B**) Concentration-dependent displacement of [^{3}H]-OT from the OTR by analogues **I** (n=2), **IV** (n=2), **IVR** (n=3), **V** (n=4), **VR** (n=2), **VII** (n=4), **VIIR** (n=2); (**C**) Ligand-induced activation of the G_q-pathway. Concentration-dependent formation of IP-1 by analogues **IV** (n=3) and **IVR** (n=3); (**D**) Accumulation of IP-1 by stimulation of OTR with OT in the absence or presence of 100 nM, 300 nM, 1 µM or 3 µM of **IVR**; (**E**) Schild regression analysis of **IVR** at the OTR: A = EC$_{50}$ of OT alone, A' = EC$_{50}$ of OT in the presence of **IVR**, B = logarithm of **IVR** concentration [264].

5.4.1 Stability of analogues of oxytocin in the serum of pregnant women

The stability of the serum of the partial agonist **IV** and competitive antagonist **IVR** was evaluated to confirm the increased enzymatic stability of the studied peptidomimetics. The serum of women was selected at the 40th week of pregnancy, containing a high concentration of oxytocinase, a specific aminopeptidase reported to be the leading player of OT plasma degradation [303–305]. Peptidomimetics **IV**, **IVR**, and OT, as control, were incubated at 37°C in a phosphate buffer at pH 7.2 and in selected serum. Their stability was evaluated at different points (1, 3, 5, 20, 24, and 48 h) by RP-HPLC-MS (**Figure 40**).
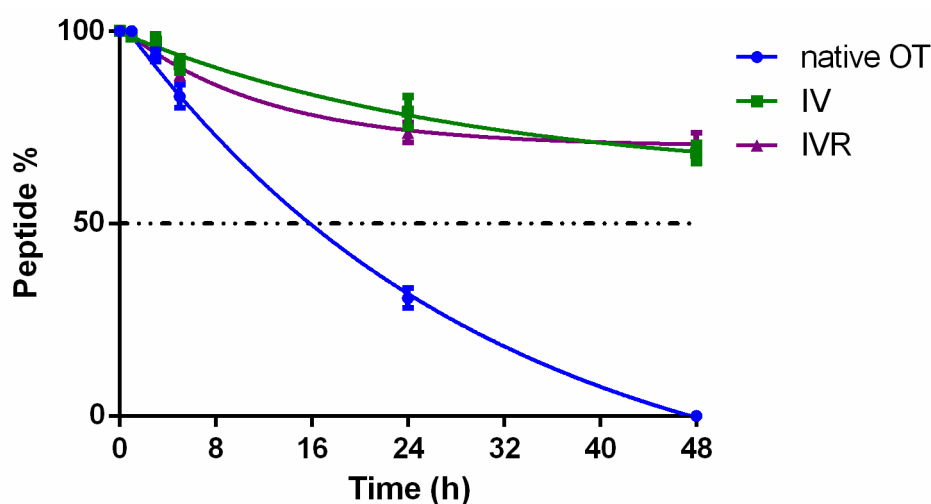
Figure 40 Stability of OT, analogues **IV**, and **IVR** in woman serum at the 40th week of pregnancy (n=2) [264].

The native OT exhibited a half-time of 24 h in the phosphate buffer. In the same conditions and after 72 h no traces of OT were observed in RP-HPLC. In women serum at the 40th week of pregnancy, native OT displayed a shorter half-life of 16 h, and after 48 h, it was not detectable by analytical RP-HPLC.

Interestingly, both analogues **IV** and **IVR** exhibited more substantial stability than native oxytocin. After incubation at 37°C in selected serum, the half-time of analogues **IV** and **IVR** was more incredible than 48 h, demonstrating more excellent stability than the native OT. Worth to mention that after ten days of incubation in serum both peptidomimetics **IV** and **IVR** were not detectable by analytical RP-HPLC [264].

6 CONCLUSIONS

Due to the possibility of mimicking natural peptides and proteins, peptidomimetics are considered a fascinating group of macromolecules. Structures of peptidomimetics can preserve the capability for interactions with the biological targets and display identical *in vivo* effects of the corresponding unmodified peptides.

On the other hand, peptides are compounds with reduced immunogenic activity and can penetrate tissues and organs due to their small size. Moreover, their synthesis is relatively easy and inexpensive.

6.1 Oxytocin and its analogues

In this doctoral dissertation, it was described structure optimisation, methods of synthesis, conformational analysis, and pharmaceutical assays of oxytocin and its analogues. The main object of the presented studies is to understand how the replacement of the native -CH_2-S-S-CH_2- bridge (presented in oxytocin) by -$(CH_2)_m$-1,4-/4,1-1*H*-([1,2,3]triazol-1-yl)-$(CH_2)_n$- (presented in analogues of oxytocin) will affect receptor selectivity, binding affinity, the potency of signalling, metabolic and conformation stability.

In this context, fourteen cyclopeptides **I-VII** and **IR-VIIR** were synthesised, presenting a systematic permutation of the triazolyl moieties ring size, location, and orientation. The clicked oxytocin analogues were obtained by replacing Cys^1 and Cys^6 at positions *i* and *i*+5 with N^α-Fmoc-ω-azido-α-amino acids and N^α-Fmoc-ω-ynoic-α-amino acids with $(CH_2)_{n/m}$ (n/m = 1-4 or 2-3 or 1-1). The intramolecular cyclisation of the linear precursors was carried out by solution-phase and on-resin microwave strategy.

The [1,2,3]-triazolyl-bridging approach was applied to stabilise the β-turn conformation of oxytocin analogues. Within this framework, circular spectroscopy measurements were performed. According to the CD spectra performed in water, almost all analysed peptidomimetics displayed characteristic signals for random coil structures, especially analogues **I**, **II**, **III**, **VI**, **IIR**, **IIIR**, and **VIR**. Peptidomimetics **IV**, **V**, **IVR**, and **VR** presented a tendency to form β-turn conformation, which was also observed in native oxytocin. One of the studied structures, analogue **IR**, demonstrated a tendency to form helix conformation. Additionally, analogues **VII** and **VIIR** displayed unordered structures in water.

Worth to note that all analysed peptidomimetics **I-IV** *vs.* **IR-IVR** and **V-VII** *vs.* **VR-VIIR** were able to form related structures with the same amount of -CH$_2$ groups in the surrounding of the triazolyl bridge though the different orientation of the triazole. It was also confirmed in the molecular modelling studies because the calculated values in each pair of compounds, for example, **I-IR** or **II-IIR**, were comparable.

The NMR studies of oxytocin and its analogues confirmed that oxytocin preferentially adopts a type I β-turn conformation in water centred on Ile^3-Gln^4 residues. As in oxytocin, a type I β-turn conformation centred on Ile^3-Gln^4 is noted in the structures of ten analogues among the fourteen studied, in particular **IR**, **II**, **IIR**, **IVR**, **V-VII**, and **VR-VIIR**. While analogue **IVR** shows all diagnostic ROEs of a type I β-turn cantered on Ile^3-Gln^4, similar to OT, compound **IV** lacks characteristic Ile^3 HN/Gln^4 HN and Tyr^2 Hδ/Gln^4 HN ROE correlations. Likewise, analogues **III**, **IIIR**, and **VIR** also populate inverse γ-turn conformations on Asn^5 or a type I β-turn shift on Gln^4-Asn^5 in peptidomimetic **VII**. Additionally, the analogue **IR** possesses a 3$_{10}$ helical folding with a double turn conformation, which is in agreement with the characteristic signals observed in the CD spectrum.

Among all examined oxytocin analogues, peptidomimetics **IV** and **IVR** possess the most interesting pharmacological properties. Analogue **IV** presents characteristic features of a weak partial agonist. On the other hand, peptidomimetic **IVR** is a weak competitive antagonist. In both mentioned analogues, the disulphide bridge is replaced by a longer 1*H*-[1,2,3]triazol-1-yl-containing bridge, where m=1, n=4, and m+n=5, as compared with the -CH$_2$-S-S-CH$_2$- in OT and the location of the 1*H*-[1,2,3]triazol-1-yl moiety in the bridge is removed by only one methylene from the N-proximal bridgehead. The only structural difference between analogues **IV** and **IVR** is the reversed orientation of the 1*H*-[1,2,3]triazol-1-yl moieties in the bridges (1,4- and 4,1-, respectively). The competitive weak antagonistic activity of structure **IVR** compared to peptidomimetic **IV** can be clarified with its significant conformational properties similar to native OT. This interesting issue was established to analyse these analogues in the serum of 40-week pregnant women. Both studied analogues, **IV** and **IVR**, demonstrate a meaningful increase in metabolic stability relative to OT when incubated in serum taken from pregnant women at the 40th week.

Likewise, analogues **II**, **IIR**, **III**, **IIIR**, **VI**, and **VIR** were inactive because they did not displace the radioligand from OTR with more than 30% efficacy.

It was observed that analogues **IV** and **IVR**, featuring the longest bridges (m+n=5), are the best binders to the OTR, while the analogues with shorter bridges (m+n=2 and 3),

such as **VI**, **VIR**, **VII**, and **VIIR**, are poor binders to oxytocin receptor. As discussed in this PhD thesis, the length of the bridge is not always associated with the best binding to the OTR.

6.2 Synthetic MBP peptides

It is well-known that the structure of a peptide or a protein is the essential element of its biological activity, which was presented above. In this sense, a synthesised series of MBP peptides **1-6** also possess a significant role in efficient IgM antibody recognition in Multiple Sclerosis. In the serum of patients suffering from MuSc, the myelin sheath is damaged by the autoimmune response involving autoreactive antibodies. Therefore, the characterisation of antigens, particularly those expressed by proteins in the central nervous system, is highly related.

To this aim, the series of synthetic MBP peptides **1-6** was evaluated in SP-ELISA. However, my attention was focused on IgM antibodies, noted in one representative serum using the peptides MBP(81-106) (**1**) and MBP(76-116) (**2**). The reactivity of peptides **1** and **2** is especially relevant since the frequency of serum anti-MBP IgMs is lower in patients with long-term disease duration. Furthermore, competitive ELISA experiments established the specificity of the interaction and possibly high antibody affinity to these peptide sequences.

Additionally, NMR conformational analysis in DPC micelles indicates that the peptides MBP(81-106) (**1**) and MBP(76-116) (**2**) demonstrate a stable helical conformation along residues 87-96, while the remaining regions display unordered conformation.

The CD experiments were performed to clarify the secondary structures of a series of MBP peptides **1-6**. The CD spectra registered in water showed that most synthetic MBP peptides form unordered structures. What is more, peptide MBP(76-96) (**3**) shows characteristic signals for helical conformation in a mixture of H_2O:TFE (50:50, v:v). The maximum at around 195 nm and the minimums corresponding to 210 nm and 220 nm present that peptides MBP(81-106) (**1**) and MBP(76-116) (**2**) form α-helix structures, although MBP(81-106) (**1**) displays a slightly higher tendency than MBP(76-116) (**2**) in a mixture of H_2O:TFE (50:50, v:v), which may be considered the bioactive conformation of the epitope recognised by IgMs, since the competitive ELISA experiments show a 4-fold greater affinity of IgMs for peptide **1**, as compared to peptide **2**. Nevertheless, the peptide MBP(76-116) (**2**) seems to be much more

suitable to be efficiently coated on the ELISA plate, correctly showing the helical epitope to capture IgMs in SP-ELISA. At variance, the correct epitope exposition is hampered by the flanking flexible N- and C-terminal regions when the peptide MBP(76-116) (**2**) was tested in solution. Moreover, peptides **4-6** can create random coil structures in a mixture of 50% TFE.

All obtained results from CD experiments were in agreement with predictions of secondary structures based on *DichroWeb* and calculated helix content.

Moreover, it was performed the determination of the structural preferences of the analysed peptides MBP(81-92) (**5**) and MBP(99-106) (**6**) based on molecular modelling methods using linear simulated annealing molecular dynamics and molecular mechanics. The results suggest that compounds **5** and **6** present unordered conformation in a mixture of $H_2O:D_2O$ (90:10, v:v). Interestingly, the conformational analysis of peptide MBP(81-92) (**5**) in a mixture of TFE-d_3:D_2O:H_2O (50:10:90, v:v:v) indicates a relatively high lability of the C-terminal fragment of the amino acid sequence. Moreover, comparing the values of torsion angles demonstrates the similarities in the N-terminal fragment of the peptide chain. On the other hand, the studies of torsion angles in peptide MBP(81-92) (**5**) suggest that the helical conformation is presented, including the Gln^{82}-Asn^{85} and Val^{87}-Val^{88} residues.

In conclusion, it was highlighted that the role of secondary structures in developing peptides, mainly synthetic MBP peptides, and peptidomimetics, such as oxytocin analogues, contain biological activities.

Worth to note that a better understanding of the structural modification of peptides and peptidomimetics can improve knowledge of designing the compounds, especially peptides, tailored biological and pharmacological profiles in the future.

7   REFERENCES

[1]   C. Testa, A.M. Papini, M. Chorev, P. Rovero, Copper-Catalyzed Azide-Alkyne Cycloaddition (CuAAC)-Mediated Macrocyclization of Peptides: Impact on Conformation and Biological Activity, Curr. Top. Med. Chem. 18 (2018) 591–610. https://doi.org/10.2174/1568026618666180518095755.

[2]   C. Testa, M. Scrima, M. Grimaldi, A.M. D'Ursi, M.L. Dirain, N. Lubin-Germain, A. Singh, C. Haskell-Luevano, M. Chorev, P. Rovero, A.M. Papini, 1,4-Disubstituted-[1,2,3]triazolyl-Containing Analogues of MT-II: Design, Synthesis, Conformational Analysis, and Biological Activity, J. Med. Chem. 57 (2014) 9424–9434. https://doi.org/10.1021/jm501027w.

[3]   N.-B. Sun, J.-Z. Jin, F.-Y. He, Microwave Assisted Synthesis, Antifungal Activity, and DFT Study of Some Novel Triazolinone Derivatives, BioMed Res. Int. 2015 (2015) 1–7. https://doi.org/10.1155/2015/916059.

[4]   L. Mabonga, A.P. Kappo, Peptidomimetics: A Synthetic Tool for Inhibiting Protein–Protein Interactions in Cancer, Int. J. Pept. Res. Ther. 26 (2020) 225–241. https://doi.org/10.1007/s10989-019-09831-5.

[5]   A. Staśkiewicz, P. Ledwoń, P. Rovero, A.M. Papini, R. Latajka, Triazole-Modified Peptidomimetics: An Opportunity for Drug Discovery and Development, Front. Chem. 9 (2021) 674705. https://doi.org/10.3389/fchem.2021.674705.

[6]   M. Scrima, A. Le Chevalier-Isaad, P. Rovero, A.M. Papini, M. Chorev, A.M. D'Ursi, Cu^I-Catalyzed Azide–Alkyne Intramolecular *i*-to-(*i*+4) Side-Chain-to-Side-Chain Cyclization Promotes the Formation of Helix-Like Secondary Structures, Eur. J. Org. Chem. 2010 (2010) 446–457. https://doi.org/10.1002/ejoc.200901157.

[7]   A. Le Chevalier Isaad, A.M. Papini, M. Chorev, P. Rovero, Side chain-to-side chain cyclization by click reaction, J. Peptide Sci. 15 (2009) 451–454. https://doi.org/10.1002/psc.1141.

[8]   K. Holland-Nell, M. Meldal, Maintaining Biological Activity by Using Triazoles as Disulfide Bond Mimetics, Angew. Chem. Int. Ed. 50 (2011) 5204–5206. https://doi.org/10.1002/anie.201005846.

[9]   A. Argiolas, G.L. Gessa, Central functions of oxytocin, Neurosci. Biobehav. Rev. 15 (1991) 217–231. https://doi.org/10.1016/S0149-7634(05)80002-8.

[10] G. Gimpl, F. Fahrenholz, The Oxytocin Receptor System: Structure, Function, and Regulation, Physiol. Rev. 81 (2001) 629–683. https://doi.org/10.1152/physrev.2001.81.2.629.

[11] V. Magafa, L. Borovičková, J. Slaninová, P. Cordopatis, Synthesis and biological activity of oxytocin analogues containing unnatural amino acids in position 9: structure activity study, Amino Acids. 38 (2010) 1549–1559. https://doi.org/10.1007/s00726-009-0372-2.

[12] J.L. Stymiest, B.F. Mitchell, S. Wong, J.C. Vederas, Synthesis of Oxytocin Analogues with Replacement of Sulfur by Carbon Gives Potent Antagonists with Increased Stability, J. Org. Chem. 70 (2005) 7799–7809. https://doi.org/10.1021/jo050539l.

[13] T. Koshimizu, K. Nakamura, N. Egashira, M. Hiroyama, H. Nonoguchi, A. Tanoue, Vasopressin V1a and V1b Receptors: From Molecules to Physiological Systems, Physiol. Rev. 92 (2012) 1813–1864. https://doi.org/10.1152/physrev.00035.2011.

[14] H.-J. Lee, A.H. Macbeth, J. Pagani, W.S. Young, Oxytocin: The Great Facilitator of Life, Prog. Neurobiol. (2009) S030100820900046X. https://doi.org/10.1016/j.pneurobio.2009.04.001.

[15] I. Poláček, I. Krejčí, H. Nesvadba, J. Rudinger, Action of [1,6-Di-alanine]-oxytocin and [1,6-Di-serine]-oxytocin on the rat uterus and mammary gland in vitro, Eur. J. Pharmacol. 9 (1970) 239–245. https://doi.org/10.1016/0014-2999(70)90306-7.

[16] A.I.R. Brewster, V.J. Hruby, A.F. Spatola, F.A. Bovey, Carbon-13 nuclear magnetic resonance spectroscopy of oxytocin, related oligopeptides, and selected analogs, Biochemistry. 12 (1973) 1643–1649. https://doi.org/10.1021/bi00732a028.

[17] A.I.R. Brewster, V.J. Hruby, 300-MHz Nuclear Magnetic Resonance Study of Oxytocin in Aqueous Solution: Conformational Implications, Proc. Natl. Acad. Sci. U.S.A. 70 (1973) 3806–3809. https://doi.org/10.1073/pnas.70.12.3806.

[18] S.P. Wood, I.J. Tickle, A.M. Treharne, J.E. Pitts, Y. Mascarenhas, J.Y. Li, J. Husain, S. Cooper, T.L. Blundell, V.J. Hruby, A. Buku, A.J. Fischman, H.R. Wyssbrod, Crystal Structure Analysis of Deamino-Oxytocin: Conformational Flexibility and Receptor Binding, Science. 232 (1986) 633–636. https://doi.org/10.1126/science.3008332.

[19] C.W. Gruber, J. Koehbach, M. Muttenthaler, Exploring bioactive peptides from natural sources for oxytocin and vasopressin drug discovery, Future Med. Chem. 4 (2012) 1791–1798. https://doi.org/10.4155/fmc.12.108.

[20] T. Kato, S. Endo, T. Fujiwara, K. Nagayama, Oxytocin solution structure changes upon protonation of the N-terminus in dimethyl sulfoxide, J. Biomol. NMR. 3 (1993) 653–673. https://doi.org/10.1007/BF00198370.

[21] E.C. McKay, S.E. Counts, Oxytocin Receptor Signaling in Vascular Function and Stroke, Front. Neurosci. 14 (2020) 574499. https://doi.org/10.3389/fnins.2020.574499.

[22] T.R. Insel, L.J. Young, The neurobiology of attachment, Nat. Rev. Neurosci. 2 (2001) 129–136. https://doi.org/10.1038/35053579.

[23] O.J. Bosch, Brain Oxytocin Correlates with Maternal Aggression: Link to Anxiety, J. Neurosci. 25 (2005) 6807–6815. https://doi.org/10.1523/JNEUROSCI.1342-05.2005.

[24] D. Huber, P. Veinante, R. Stoop, Vasopressin and Oxytocin Excite Distinct Neuronal Populations in the Central Amygdala, Science. 308 (2005) 245–248. https://doi.org/10.1126/science.1105636.

[25] S. Ma, M.J. Shipston, D. Morilak, J.A. Russell, Reduced Hypothalamic Vasopressin Secretion Underlies Attenuated Adrenocorticotropin Stress Responses in Pregnant Rats, Endocrinology. 146 (2005) 1626–1637. https://doi.org/10.1210/en.2004-1368.

[26] K.J. Parker, C.L. Buckmaster, A.F. Schatzberg, D.M. Lyons, Intranasal oxytocin administration attenuates the ACTH stress response in monkeys, Psychoneuroendocrinology. 30 (2005) 924–929. https://doi.org/10.1016/j.psyneuen.2005.04.002.

[27] P. Kirsch, Oxytocin Modulates Neural Circuitry for Social Cognition and Fear in Humans, J. Neurosci. 25 (2005) 11489–11493. https://doi.org/10.1523/JNEUROSCI.3984-05.2005.

[28] E. Hollander, J. Bartz, W. Chaplin, A. Phillips, J. Sumner, L. Soorya, E. Anagnostou, S. Wasserman, Oxytocin Increases Retention of Social Cognition in Autism, Biol. Psychiatry. 61 (2007) 498–503. https://doi.org/10.1016/j.biopsych.2006.05.030.

[29] E. Hollander, S. Novotny, M. Hanratty, R. Yaffe, C.M. DeCaria, B.R. Aronowitz, S. Mosovich, Oxytocin Infusion Reduces Repetitive Behaviors in Adults with Autistic and Asperger's Disorders, Neuropsychopharmacol. 28 (2003) 193–198. https://doi.org/10.1038/sj.npp.1300021.

[30] H. Harony, S. Wagner, The Contribution of Oxytocin and Vasopressin to Mammalian Social Behavior: Potential Role in Autism Spectrum Disorder, Neurosignals. 18 (2010) 82–97. https://doi.org/10.1159/000321035.

[31] A. Meyer-Lindenberg, G. Domes, P. Kirsch, M. Heinrichs, Oxytocin and vasopressin in the human brain: social neuropeptides for translational medicine, Nat. Rev. Neurosci. 12 (2011) 524–538. https://doi.org/10.1038/nrn3044.

[32] N. Striepens, K.M. Kendrick, W. Maier, R. Hurlemann, Prosocial effects of oxytocin and clinical evidence for its therapeutic potential, Front. Neuroendocrinol. 32 (2011) 426–450. https://doi.org/10.1016/j.yfrne.2011.07.001.

[33] M.A. Ellenbogen, A. Linnen, R. Grumet, C. Cardoso, R. Joober, The acute effects of intranasal oxytocin on automatic and effortful attentional shifting to emotional faces, Psychophysiology. 49 (2012) 128–137. https://doi.org/10.1111/j.1469-8986.2011.01278.x.

[34] M. Manning, A. Misicka, A. Olma, K. Bankowski, S. Stoev, B. Chini, T. Durroux, B. Mouillac, M. Corbani, G. Guillon, Oxytocin and Vasopressin Agonists and Antagonists as Research Tools and Potential Therapeutics, J. Neuroendocrinol. 24 (2012) 609–628. https://doi.org/10.1111/j.1365-2826.2012.02303.x.

[35] R. Postina, E. Kojro, F. Fahrenholz, Separate Agonist and Peptide Antagonist Binding Sites of the Oxytocin Receptor Defined by Their Transfer into the V_2 Vasopressin Receptor, J. Biol. Chem. 271 (1996) 31593–31601. https://doi.org/10.1074/jbc.271.49.31593.

[36] N. Vrachnis, F.M. Malamas, S. Sifakis, E. Deligeoroglou, Z. Iliodromiti, The Oxytocin-Oxytocin Receptor System and Its Antagonists as Tocolytic Agents, Int. J. Endocrinol. 2011 (2011) 1–8. https://doi.org/10.1155/2011/350546.

[37] J. Bockaert, Molecular tinkering of G protein-coupled receptors: an evolutionary success, EMBO J. 18 (1999) 1723–1729. https://doi.org/10.1093/emboj/18.7.1723.

[38] F. Fanelli, P. Barbier, D. Zanchetta, P.G. de Benedetti, B. Chini, Activation Mechanism of Human Oxytocin Receptor: A Combined Study of Experimental and Computer-Simulated Mutagenesis, Mol. Pharmacol. 56 (1999) 214–225. https://doi.org/10.1124/mol.56.1.214.

[39] M. Wheatley, S.R. Hawtin, N.J. Yarwood, Structure/Function Studies on Receptors for Vasopressin and Oxytocin, in: H.H. Zingg, C.W. Bourque, D.G. Bichet (Eds.),

Vasopressin and Oxytocin, Springer US, Boston, MA, 1998: pp. 363–365. https://doi.org/10.1007/978-1-4615-4871-3_46.

[40] S.H. Kim, L. Riaposova, H. Ahmed, O. Pohl, A. Chollet, J.-P. Gotteland, A. Hanyaloglu, P.R. Bennett, V. Terzidou, Oxytocin Receptor Antagonists, Atosiban and Nolasiban, Inhibit Prostaglandin F2α-induced Contractions and Inflammatory Responses in Human Myometrium, Sci. Rep. 9 (2019) 5792. https://doi.org/10.1038/s41598-019-42181-2.

[41] M. Manning, S. Stoev, B. Chini, T. Durroux, B. Mouillac, G. Guillon, Peptide and non-peptide agonists and antagonists for the vasopressin and oxytocin V_{1a}, V_{1b}, V_2 and OT receptors: research tools and potential therapeutic agents, in: Progress in Brain Research, Elsevier, 2008: pp. 473–512. https://doi.org/10.1016/S0079-6123(08)00437-8.

[42] G. Pitt, A. Batt, R. Haigh, A. Penson, P. Robson, D. Rooker, A. Tartar, J. Trim, C. Yea, M. Roe, Non-peptide oxytocin agonists, Bioorg. Med. Chem. Lett. 14 (2004) 4585–4589. https://doi.org/10.1016/j.bmcl.2004.04.107.

[43] A.D. Borthwick, Oxytocin Antagonists and Agonists, in: Annual Reports in Medicinal Chemistry, Elsevier, 2006: pp. 409–421. https://doi.org/10.1016/S0065-7743(06)41028-9.

[44] C. Hicks, W. Jorgensen, C. Brown, J. Fardell, J. Koehbach, C.W. Gruber, M. Kassiou, G.E. Hunt, I.S. McGregor, The Nonpeptide Oxytocin Receptor Agonist WAY 267,464: Receptor-Binding Profile, Prosocial Effects and Distribution of c-Fos Expression in Adolescent Rats: WAY 267,464 versus oxytocin, J. Neuroendocrinol. 24 (2012) 1012–1029. https://doi.org/10.1111/j.1365-2826.2012.02311.x.

[45] J.G. Westergaard, A.P. Lange, G.T. Pedersen, N.J. Secher, Use of Oral Oxytocics for Stimulation of Labor in Cases of Premature Rupture of the Membranes at Term: A randomized comparative study of prostaglandin E_2 tablets and demoxytocin resoriblets, Acta Obstet. Gynecol. Scand. 62 (1983) 111–116. https://doi.org/10.3109/00016348309155773.

[46] W. Rath, Prevention of postpartum haemorrhage with the oxytocin analogue carbetocin, Eur. J. Obstet. Gynecol. 147 (2009) 15–20. https://doi.org/10.1016/j.ejogrb.2009.06.018.

[47] H.M. Georgiou, M.K.W. Di Quinzio, M. Permezel, S.P. Brennecke, Predicting Preterm Labour: Current Status and Future Prospects, Dis. Markers. 2015 (2015) 1–9. https://doi.org/10.1155/2015/435014.

[48] V. Tsatsaris, B. Carbonne, D. Cabrol, Atosiban for Preterm Labour:, Drugs. 64 (2004) 375–382. https://doi.org/10.2165/00003495-200464040-00003.

[49] R.F. Lamont, The development and introduction of anti-oxytocic tocolytics, Int. J. Gynecol. Obstet. 110 (2003) 108–112. https://doi.org/10.1046/j.1471-0528.2003.00055.x.

[50] B. Chini, M. Manning, G. Guillon, Affinity and efficacy of selective agonists and antagonists for vasopressin and oxytocin receptors: an "easy guide" to receptor pharmacology, in: Progress in Brain Research, Elsevier, 2008: pp. 513–517. https://doi.org/10.1016/S0079-6123(08)00438-X.

[51] P. Pierzynski, A. Lemancewicz, T. Reinheimer, M. Akerlund, T. Laudanski, Inhibitory Effect of Barusiban and Atosiban on Oxytocin-Induced Contractions of Myometrium

From Preterm and Term Pregnant Women, J. Soc. Gynecol. Investig. 11 (2004) 384–387. https://doi.org/10.1016/j.jsgi.2004.02.008.

[52] A.D. Borthwick, J. Liddle, The design of orally bioavailable 2, 5-diketopiperazine oxytocin antagonists: from concept to clinical candidate for premature labor, Med. Res. Rev. 31 (2011) 576–604. https://doi.org/10.1002/med.20193.

[53] S.H. Kim, O. Pohl, A. Chollet, J.-P. Gotteland, A.D.J. Fairhurst, P.R. Bennett, V. Terzidou, Differential Effects of Oxytocin Receptor Antagonists, Atosiban and Nolasiban, on Oxytocin Receptor–Mediated Signaling in Human Amnion and Myometrium, Mol. Pharmacol. 91 (2017) 403–415. https://doi.org/10.1124/mol.116.106013.

[54] V. Jai Kartik, T. Lavanya, K. Guruprasad, Analysis of disulphide bond connectivity patterns in protein tertiary structure, Int. J. Biol. Macromol. 38 (2006) 174–179. https://doi.org/10.1016/j.ijbiomac.2006.02.004.

[55] C. Testa, D. D'Addona, M. Scrima, A.M. Tedeschi, A.M. D'Ursi, C. Bernhard, F. Denat, C. Bello, P. Rovero, M. Chorev, A.M. Papini, Design, synthesis, and conformational studies of [DOTA]-Octreotide analogs containing [1,2,3]triazolyl as a disulfide mimetic, J. Pept. Sci. 110 (2018) e24071. https://doi.org/10.1002/pep2.24071.

[56] A.D. de Araujo, M. Mobli, J. Castro, A.M. Harrington, I. Vetter, Z. Dekan, M. Muttenthaler, J. Wan, R.J. Lewis, G.F. King, S.M. Brierley, P.F. Alewood, Selenoether oxytocin analogues have analgesic properties in a mouse model of chronic abdominal pain, Nat. Commun. 5 (2014) 3165. https://doi.org/10.1038/ncomms4165.

[57] H.-K. Cui, Y. Guo, Y. He, F.-L. Wang, H.-N. Chang, Y.-J. Wang, F.-M. Wu, C.-L. Tian, L. Liu, Diaminodiacid-Based Solid-Phase Synthesis of Peptide Disulfide Bond Mimics, Angew. Chem. Int. Ed. 52 (2013) 9558–9562. https://doi.org/10.1002/anie.201302197.

[58] C.W. Smith, R. Walter, S. Moore, R.C. Makofske, J. Meienhofer, Replacement of the disulfide bond in oxytocin by an amide group. Synthesis and some biological properties of [cyclo-(1-L-aspartic acid, 6-L-.alpha.,.beta.-diaminopropionic acid)]oxytocin, J. Med. Chem. 21 (1978) 117–120. https://doi.org/10.1021/jm00199a023.

[59] J.L. Stymiest, B.F. Mitchell, S. Wong, J.C. Vederas, Synthesis of Biologically Active Dicarba Analogues of the Peptide Hormone Oxytocin Using Ring-Closing Metathesis, Org. Lett. 5 (2003) 47–49. https://doi.org/10.1021/ol027160v.

[60] C.D. Hein, X.-M. Liu, D. Wang, Click Chemistry, A Powerful Tool for Pharmaceutical Sciences, Pharm. Res. 25 (2008) 2216–2230. https://doi.org/10.1007/s11095-008-9616-1.

[61] M. Meldal, C.W. Tornøe, Cu-Catalyzed Azide−Alkyne Cycloaddition, Chem. Rev. 108 (2008) 2952–3015. https://doi.org/10.1021/cr0783479.

[62] S.R. Tala, A. Singh, C.J. Lensing, S.M. Schnell, K.T. Freeman, J.R. Rocca, C. Haskell-Luevano, 1,2,3-Triazole Rings as a Disulfide Bond Mimetic in Chimeric AGRP-Melanocortin Peptides: Design, Synthesis, and Functional Characterization, ACS Chem. Neurosci. 9 (2018) 1001–1013. https://doi.org/10.1021/acschemneuro.7b00422.

[63] A.V. Costa, M.V.L. de Oliveira, R.T. Pinto, L.C. Moreira, E.M.C. Gomes, T. de A. Alves, P.F. Pinheiro, V.T. de Queiroz, L.F.A. Vieira, R.R. Teixeira, W.C. de J. Júnior, Synthesis of Novel Glycerol-Derived 1,2,3-Triazoles and Evaluation of Their Fungicide,

Phytotoxic and Cytotoxic Activities, Molecules. 22 (2017) 1666. https://doi.org/10.3390/molecules22101666.

[64] R.O.M.A.D. Souza, L.S.D.M.E. Miranda, Strategies Towards the Synthesis of N^2-Substituted 1,2,3-Triazoles, An. Acad. Bras. Ciênc. 91 (2019) e20180751. https://doi.org/10.1590/0001-3765201820180751.

[65] H. Li, R. Aneja, I. Chaiken, Click Chemistry in Peptide-Based Drug Design, Molecules. 18 (2013) 9797–9817. https://doi.org/10.3390/molecules18089797.

[66] H. Xu, S. Ma, Y. Xu, L. Bian, T. Ding, X. Fang, W. Zhang, Y. Ren, Copper-Catalyzed One-Pot Synthesis of 1,2,4-Triazoles from Nitriles and Hydroxylamine, J. Org. Chem. 80 (2015) 1789–1794. https://doi.org/10.1021/jo502709t.

[67] A.K. Jordão, V.F. Ferreira, T.M.L. Souza, G.G. de Souza Faria, V. Machado, J.L. Abrantes, M.C.B.V. de Souza, A.C. Cunha, Synthesis and anti-HSV-1 activity of new 1,2,3-triazole derivatives, Bioorg. Med. Chem. 19 (2011) 1860–1865. https://doi.org/10.1016/j.bmc.2011.02.007.

[68] S. Ueda, H. Nagasawa, Facile Synthesis of 1,2,4-Triazoles via a Copper-Catalyzed Tandem Addition−Oxidative Cyclization, J. Am. Chem. Soc. 131 (2009) 15080–15081. https://doi.org/10.1021/ja905056z.

[69] K. Sudheendran, D. Schmidt, W. Frey, J. Conrad, U. Beifuss, Facile synthesis of 3,5-diaryl-1,2,4-triazoles via copper-catalyzed domino nucleophilic substitution/oxidative cyclization using amidines or imidates as substrates, Tetrahedron. 70 (2014) 1635–1645. https://doi.org/10.1016/j.tet.2014.01.019.

[70] X. Creary, A.F. Sky, Reaction of arylbromodiazirines with azide ion. Evidence for N-azidodiazirine intermediates, J. Am. Chem. Soc. 112 (1990) 368–374. https://doi.org/10.1021/ja00157a056.

[71] L. Zhang, X. Chen, P. Xue, H.H.Y. Sun, I.D. Williams, K.B. Sharpless, V.V. Fokin, G. Jia, Ruthenium-Catalyzed Cycloaddition of Alkynes and Organic Azides, J. Am. Chem. Soc. 127 (2005) 15998–15999. https://doi.org/10.1021/ja054114s.

[72] V. Ganesh, V.S. Sudhir, T. Kundu, S. Chandrasekaran, 10 Years of Click Chemistry: Synthesis and Applications of Ferrocene-Derived Triazoles, Chem. Asian J. 6 (2011) 2670–2694. https://doi.org/10.1002/asia.201100408.

[73] R. Huisgen, Kinetics and Mechanism of 1,3-Dipolr Cycloadditions, Angew. Chem. Int. Ed. Engl. 2 (1963) 633–645. https://doi.org/10.1002/anie.196306331.

[74] H.K. Akula, M.K. Lakshman, Synthesis of Deuterated 1,2,3-Triazoles, J. Org. Chem. 77 (2012) 8896–8904. https://doi.org/10.1021/jo301146j.

[75] V.V. Rostovtsev, L.G. Green, V.V. Fokin, K.B. Sharpless, A Stepwise Huisgen Cycloaddition Process: Copper(I)-Catalyzed Regioselective "Ligation" of Azides and Terminal Alkynes, Angew. Chem. Int. Ed. Engl. 41 (2002) 2596–2599. https://doi.org/10.1002/1521-3773(20020715)41:14<2596::AID-ANIE2596>3.0.CO;2-4.

[76] C.W. Tornøe, C. Christensen, M. Meldal, Peptidotriazoles on Solid Phase: [1,2,3]-Triazoles by Regiospecific Copper(I)-Catalyzed 1,3-Dipolar Cycloadditions of Terminal Alkynes to Azides, J. Org. Chem. 67 (2002) 3057–3064. https://doi.org/10.1021/jo011148j.

[77] H. Struthers, T.L. Mindt, R. Schibli, Metal chelating systems synthesized using the copper(I) catalyzed azide-alkynecycloaddition, Dalton Trans. 39 (2010) 675–696. https://doi.org/10.1039/B912608B.

[78] J. Totobenazara, A.J. Burke, New click-chemistry methods for 1,2,3-triazoles synthesis: recent advances and applications, Tetrahedron Lett. 56 (2015) 2853–2859. https://doi.org/10.1016/j.tetlet.2015.03.136.

[79] C.P. Kaushik, K. Kumar, D. Singh, S.K. Singh, D.K. Jindal, R. Luxmi, Synthesis, Characterization, and Antimicrobial Potential of Some 1,4-Disubstituted 1,2,3-Bistriazoles, Synth. Commun. 45 (2015) 1977–1985. https://doi.org/10.1080/00397911.2015.1056796.

[80] I.E. Valverde, F. Lecaille, G. Lalmanach, V. Aucagne, A.F. Delmas, Synthesis of a Biologically Active Triazole-Containing Analogue of Cystatin A Through Successive Peptidomimetic Alkyne-Azide Ligations, Angew. Chem. Int. Ed. 51 (2012) 718–722. https://doi.org/10.1002/anie.201107222.

[81] G.-C. Kuang, H.A. Michaels, J.T. Simmons, R.J. Clark, L. Zhu, Chelation-Assisted, Copper(II)-Acetate-Accelerated Azide−Alkyne Cycloaddition, J. Org. Chem. 75 (2010) 6540–6548. https://doi.org/10.1021/jo101305m.

[82] J. McNulty, K. Keskar, Discovery of a Robust and Efficient Homogeneous Silver(I) Catalyst for the Cycloaddition of Azides onto Terminal Alkynes, Eur. J. Org. Chem. 2012 (2012) 5462–5470. https://doi.org/10.1002/ejoc.201200930.

[83] C.D. Smith, M.F. Greaney, Zinc Mediated Azide–Alkyne Ligation to 1,5- and 1,4,5-Substituted 1,2,3-Triazoles, Org. Lett. 15 (2013) 4826–4829. https://doi.org/10.1021/ol402225d.

[84] S.W. Kwok, J.R. Fotsing, R.J. Fraser, V.O. Rodionov, V.V. Fokin, Transition-Metal-Free Catalytic Synthesis of 1,5-Diaryl-1,2,3-triazoles, Org. Lett. 12 (2010) 4217–4219. https://doi.org/10.1021/ol101568d.

[85] P. Cintas, A. Barge, S. Tagliapietra, L. Boffa, G. Cravotto, Alkyne–azide click reaction catalyzed by metallic copper under ultrasound, Nat. Protoc. 5 (2010) 607–616. https://doi.org/10.1038/nprot.2010.1.

[86] I.E. Valverde, T.L. Mindt, 1,2,3-Triazoles as Amide-bond Surrogates in Peptidomimetics, Chimia. 67 (2013) 262. https://doi.org/10.2533/chimia.2013.262.

[87] A. Le Chevalier Isaad, F. Barbetti, P. Rovero, A.M. D'Ursi, M. Chelli, M. Chorev, A.M. Papini, N^{α}-Fmoc-Protected ω-Azido- and ω-Alkynyl-L-amino Acids as Building Blocks for the Synthesis of "Clickable" Peptides, Eur. J. Org. Chem. 2008 (2008) 5308–5314. https://doi.org/10.1002/ejoc.200800717.

[88] A. D'Ercole, G. Sabatino, L. Pacini, E. Impresari, I. Capecchi, A.M. Papini, P. Rovero, On-resin microwave-assisted copper-catalyzed azide-alkyne cycloaddition of H1-relaxin B single chain 'stapled' analogues, J. Pept. Sci. 112 (2020) e24159. https://doi.org/10.1002/pep2.24159.

[89] E. Nasli-Esfahani, M. Mohammadi-Khanaposhtani, S. Rezaei, Y. Sarrafi, Z. Sharafi, N. Samadi, M.A. Faramarzi, F. Bandarian, H. Hamedifar, B. Larijani, M. Hajimiri, M. Mahdavi, A new series of Schiff base derivatives bearing 1,2,3-triazole: Design,

synthesis, molecular docking, and α-glucosidase inhibition, Arch. Pharm. Chem. Life Sci. 352 (2019) 1900034. https://doi.org/10.1002/ardp.201900034.

[90] B. Liu, W. Zhang, S. Gou, H. Huang, J. Yao, Z. Yang, H. Liu, C. Zhong, B. Liu, J. Ni, R. Wang, Intramolecular cyclization of the antimicrobial peptide Polybia-MPI with triazole stapling: influence on stability and bioactivity, J. Pept. Sci. 23 (2017) 824–832. https://doi.org/10.1002/psc.3031.

[91] S. Yu, K. Xu, L. Huang, Z. Xu, Y. Wang, G. Bai, Q. Wu, X. Wang, Y. Jiang, Design, synthesis, and antifungal activities of novel triazole derivatives containing the benzyl group, DDDT. (2015) 1459–1467. https://doi.org/10.2147/DDDT.S74989.

[92] Y. Wang, K. Xu, G. Bai, L. Huang, Q. Wu, W. Pan, S. Yu, Synthesis and Antifungal Activity of Novel Triazole Compounds Containing Piperazine Moiety, Molecules. 19 (2014) 11333–11340. https://doi.org/10.3390/molecules190811333.

[93] E.F.C. Junior, Glycotriazole-peptides derived from the peptide HSP1: synergistic effect of triazole and saccharide rings on the antifungal activity, Amino Acids. 49 (2017) 1389–1400. https://doi.org/10.1007/s00726-017-2441-2.

[94] A. Rosemary Bastian, A. Nangarlia, L.D. Bailey, A. Holmes, R.V. Kalyana Sundaram, C. Ang, D.R.M. Moreira, K. Freedman, C. Duffy, M. Contarino, C. Abrams, M. Root, I. Chaiken, Mechanism of Multivalent Nanoparticle Encounter with HIV-1 for Potency Enhancement of Peptide Triazole Virus Inactivation, J. Biol. Chem. 290 (2015) 529–543. https://doi.org/10.1074/jbc.M114.608315.

[95] K. McFadden, P. Fletcher, F. Rossi, Kantharaju, M. Umashankara, V. Pirrone, S. Rajagopal, H. Gopi, F.C. Krebs, J. Martin-Garcia, R.J. Shattock, I. Chaiken, Antiviral Breadth and Combination Potential of Peptide Triazole HIV-1 Entry Inhibitors, Antimicrob. Agents Chemother. 56 (2012) 1073–1080. https://doi.org/10.1128/AAC.05555-11.

[96] A.A. Rashad, R.V.K. Sundaram, R. Aneja, C. Du, I. Chaiken, Macrocyclic Envelope Glycoprotein Antagonists that Irreversibly Inactivate HIV-1 before Host Cell Encounter, J. Med. Chem. 58 (2015) 7603–7606. https://doi.org/10.1021/acs.jmedchem.5b00935.

[97] H. Sun, L. Liu, J. Lu, S. Qiu, C.-Y. Yang, H. Yi, S. Wang, Cyclopeptide Smac mimetics as antagonists of IAP proteins, Bioorg. Med. Chem. Lett. 20 (2010) 3043–3046. https://doi.org/10.1016/j.bmcl.2010.03.114.

[98] N.Y.M. Abdo, M.M. Kamel, Synthesis and Anticancer Evaluation of 1,3,4-Oxadiazoles, 1,3,4-Thiadiazoles, 1,2,4-Triazoles and Mannich Bases, Chem. Pharm. Bull. 63 (2015) 369–376. https://doi.org/10.1248/cpb.c15-00059.

[99] M. Baharloui, S.A. Mirshokraee, A. Monfared, M.H. Houshdar Tehrani, Design and Synthesis of Novel Triazole-based Peptide Analogues as Anticancer Agents, Iran. J. Pharm. Sci. 18 (2019) 1299–1308. https://doi.org/10.22037/ijpr.2019.111722.13320.

[100] F. Tahoori, S. Balalaie, R. Sheikhnejad, M. Sadjadi, P. Boloori, Design and synthesis of anti-cancer cyclopeptides containing triazole skeleton, Amino Acids. 46 (2014) 1033–1046. https://doi.org/10.1007/s00726-013-1663-1.

[101] F. Errante, P. Ledwoń, R. Latajka, P. Rovero, A.M. Papini, Cosmeceutical Peptides in the Framework of Sustainable Wellness Economy, Front. Chem. 8 (2020) 572923. https://doi.org/10.3389/fchem.2020.572923.

[102] P. Ledwoń, F. Errante, A.M. Papini, P. Rovero, R. Latajka, Peptides as Active Ingredients: A Challenge for Cosmeceutical Industry, Chem. Biodiversity. 18 (2021) e2000833. https://doi.org/10.1002/cbdv.202000833.

[103] P. Fabbrizzi, G. Menchi, A. Guarna, A. Trabocchi, Use of Click-Chemistry in the Development of Peptidomimetic Enzyme Inhibitors, Curr. Med. Chem. 21 (2014) 1467–1477. https://doi.org/10.2174/09298673216661131218093611.

[104] A. Staśkiewicz, M. Quagliata, F. Real-Fernandez, F. Nuti, R. Lanzillo, V. Brescia-Morra, H. Rusche, M. Jewginski, A. Carotenuto, D. Brancaccio, R. Aharoni, R. Arnon, P. Rovero, R. Latajka, A.M. Papini, Role of Helical Structure in MBP Immunodominant Peptides for Efficient IgM Antibody Recognition in Multiple Sclerosis, Front. Chem. 10 (2022) 885180. https://doi.org/10.3389/fchem.2022.885180.

[105] A. Trabocchi, N. Pala, I. Krimmelbein, G. Menchi, A. Guarna, M. Sechi, T. Dreker, A. Scozzafava, C.T. Supuran, F. Carta, Peptidomimetics as protein arginine deiminase 4 (PAD4) inhibitors, J. Enzyme Inhib. Med. Chem. 30 (2015) 466–471. https://doi.org/10.3109/14756366.2014.947976.

[106] F. Zhao, J.E. Darling, R.A. Gibbs, J.L. Hougland, A new class of ghrelin O-acyltransferase inhibitors incorporating triazole-linked lipid mimetic groups, Bioorg. Med. Chem. Lett. 25 (2015) 2800–2803. https://doi.org/10.1016/j.bmcl.2015.05.009.

[107] Z. Guo, Z. Yan, X. Zhou, Q. Wang, M. Lu, W. Liu, H. Zhou, C. Yang, E.J. McClain, Synthesis and biological evaluation of novel 1,2-benzisothiazol-3-one-derived 1,2,3-triazoles as caspase-3 inhibitors, Med. Chem. Res. 24 (2015) 1814–1829. https://doi.org/10.1007/s00044-014-1259-7.

[108] M.J. Leyva, F. DeGiacomo, L.S. Kaltenbach, J. Holcomb, N. Zhang, J. Gafni, H. Park, D.C. Lo, G.S. Salvesen, L.M. Ellerby, J.A. Ellman, Identification and Evaluation of Small Molecule Pan-Caspase Inhibitors in Huntington's Disease Models, Chem. Biol. 17 (2010) 1189–1200. https://doi.org/10.1016/j.chembiol.2010.08.014.

[109] M. Galibert, M. Wartenberg, F. Lecaille, A. Saidi, S. Mavel, A. Joulin-Giet, B. Korkmaz, D. Brömme, V. Aucagne, A.F. Delmas, G. Lalmanach, Substrate-derived triazolo- and azapeptides as inhibitors of cathepsins K and S, Eur. J. Med. Chem. 144 (2018) 201–210. https://doi.org/10.1016/j.ejmech.2017.12.012.

[110] H. Fittler, O. Avrutina, B. Glotzbach, M. Empting, H. Kolmar, Combinatorial tuning of peptidic drug candidates: high-affinity matriptase inhibitors through incremental structure-guided optimization, Org. Biomol. Chem. 11 (2013) 1848–1857. https://doi.org/10.1039/c3ob27469a.

[111] M. Empting, O. Avrutina, R. Meusinger, S. Fabritz, M. Reinwarth, M. Biesalski, S. Voigt, G. Buntkowsky, H. Kolmar, "Triazole Bridge": Disulfide-Bond Replacement by Ruthenium-Catalyzed Formation of 1,5-Disubstituted 1,2,3-Triazoles, Angew. Chem. Int. Ed. 50 (2011) 5207–5211. https://doi.org/10.1002/anie.201008142.

[112] H.M. Werner, W.S. Horne, Folding and function in α/β-peptides: targets and therapeutic applications, Curr. Opin. Chem. Biol. 28 (2015) 75–82. https://doi.org/10.1016/j.cbpa.2015.06.013.

[113] N. Trier, P. Hansen, G. Houen, Peptides, Antibodies, Peptide Antibodies and More, Int. J. Mol. Sci. 20 (2019) 6289. https://doi.org/10.3390/ijms20246289.

[114] A. Compston, A. Coles, Multiple sclerosis, The Lancet. 372 (2008) 1502–1517. https://doi.org/10.1016/S0140-6736(08)61620-7.

[115] I. Loma, R. Heyman, Multiple Sclerosis: Pathogenesis and Treatment, Curr. Neuropharmacol. 9 (2011) 409–416. https://doi.org/10.2174/157015911796557911.

[116] R. Dobson, G. Giovannoni, Multiple sclerosis – a review, Eur. J. Neurol. 26 (2019) 27–40. https://doi.org/10.1111/ene.13819.

[117] H.L. Weiner, A shift from adaptive to innate immunity: a potential mechanism of disease progression in multiple sclerosis, J. Neurol. 255 (2008) 3–11. https://doi.org/10.1007/s00415-008-1002-8.

[118] S.-M. Orton, B.M. Herrera, I.M. Yee, W. Valdar, S.V. Ramagopalan, A.D. Sadovnick, G.C. Ebers, Sex ratio of multiple sclerosis in Canada: a longitudinal study, Lancet Neurol. 5 (2006) 932–936. https://doi.org/10.1016/S1474-4422(06)70581-6.

[119] P. Browne, D. Chandraratna, C. Angood, H. Tremlett, C. Baker, B.V. Taylor, A.J. Thompson, Atlas of Multiple Sclerosis 2013: A growing global problem with widespread inequity, Neurology. 83 (2014) 1022–1024. https://doi.org/10.1212/WNL.0000000000000768.

[120] M.N. Hatch, C.S. Schaumburg, T.E. Lane, H.S. Keirstead, Endogenous remyelination is induced by transplant rejection in a viral model of multiple sclerosis, J. Neuroimmunol. 212 (2009) 74–81. https://doi.org/10.1016/j.jneuroim.2009.05.002.

[121] R. Gandhi, A. Laroni, H.L. Weiner, Role of the innate immune system in the pathogenesis of multiple sclerosis, J. Neuroimmunol. 221 (2010) 7–14. https://doi.org/10.1016/j.jneuroim.2009.10.015.

[122] L.H. Kasper, J. Shoemaker, Multiple sclerosis immunology: The healthy immune system vs the MS immune system, Neurology. 74 (2010) S2–S8. https://doi.org/10.1212/WNL.0b013e3181c97c8f.

[123] M. Duddy, M. Niino, F. Adatia, S. Hebert, M. Freedman, H. Atkins, H.J. Kim, A. Bar-Or, Distinct Effector Cytokine Profiles of Memory and Naive Human B Cell Subsets and Implication in Multiple Sclerosis, J. Immunol. 178 (2007) 6092–6099. https://doi.org/10.4049/jimmunol.178.10.6092.

[124] E. Kouchaki, M. Salehi, M.R. Sharif, H. Nikoueinejad, H. Akbari, Numerical status of $CD4^+CD25^+FoxP3^+$ and $CD8^+CD28^-$ regulatory T cells in multiple sclerosis, Iran J. Basic Med. Sci. 17 (2014) 250–255. https://doi.org/10.22038/IJBMS.2014.2582.

[125] R.S. Fujinami, M.G. von Herrath, U. Christen, J.L. Whitton, Molecular Mimicry, Bystander Activation, or Viral Persistence: Infections and Autoimmune Disease, Clin. Microbiol. Rev. 19 (2006) 80–94. https://doi.org/10.1128/CMR.19.1.80-94.2006.

[126] M.T.C. Walvoort, C. Testa, R. Eilam, R. Aharoni, F. Nuti, G. Rossi, F. Real-Fernandez, R. Lanzillo, V. Brescia Morra, F. Lolli, P. Rovero, B. Imperiali, A.M. Papini, Antibodies from multiple sclerosis patients preferentially recognize hyperglucosylated adhesin of non-typeable Haemophilus influenzae, Sci. Rep. 6 (2016) 39430. https://doi.org/10.1038/srep39430.

[127] C. O'Gorman, W. Bukhari, A. Todd, S. Freeman, S.A. Broadley, Smoking increases the risk of multiple sclerosis in Queensland, Australia, J. Clin. Neurosci. 21 (2014) 1730–1733. https://doi.org/10.1016/j.jocn.2014.01.009.

[128] N. Ghasemi, Multiple Sclerosis: Pathogenesis, Symptoms, Diagnoses and Cell-Based Therapy, Cell J. 19 (2017) 1–10. https://doi.org/10.22074/cellj.2016.4867.

[129] S.M. Zhang, W.C. Willett, M.A. Hernán, M.J. Olek, A. Ascherio, Dietary Fat in Relation to Risk of Multiple Sclerosis among Two Large Cohorts of Women, Am. J. Epidemiol. 152 (2000) 1056–1064. https://doi.org/10.1093/aje/152.11.1056.

[130] M. Bäärnhielm, T. Olsson, L. Alfredsson, Fatty fish intake is associated with decreased occurrence of multiple sclerosis, Mult. Scler. 20 (2014) 726–732. https://doi.org/10.1177/1352458513509508.

[131] S. Sloka, C. Silva, W. Pryse-Phillips, S. Patten, L. Metz, V.W. Yong, A Quantitative Analysis of Suspected Environmental Causes of MS, Can. J. Neurol. Sci. 38 (2011) 98–105. https://doi.org/10.1017/S0317167100011124.

[132] J.A. Hollenbach, J.R. Oksenberg, The immunogenetics of multiple sclerosis: A comprehensive review, J. Autoimmun. 64 (2015) 13–25. https://doi.org/10.1016/j.jaut.2015.06.010.

[133] The International Multiple Sclerosis Genetics Consortium, Class II HLA interactions modulate genetic risk for multiple sclerosis, Nat. Genet. 47 (2015) 1107–1113. https://doi.org/10.1038/ng.3395.

[134] E. Røsjø, K.-M. Myhr, K.I. Løken-Amsrud, S.J. Bakke, A.G. Beiske, K.S. Bjerve, H. Hovdal, F. Lilleås, R. Midgard, T. Pedersen, J. Šaltytė Benth, Ø. Torkildsen, S. Wergeland, A.E. Michelsen, P. Aukrust, T. Ueland, T. Holmøy, Increasing serum levels of vitamin A, D and E are associated with alterations of different inflammation markers in patients with multiple sclerosis, J. Neuroimmunol. 271 (2014) 60–65. https://doi.org/10.1016/j.jneuroim.2014.03.014.

[135] D.N. Greene, R.L. Schmidt, A.R. Wilson, M.S. Freedman, D.G. Grenache, Cerebrospinal Fluid Myelin Basic Protein Is Frequently Ordered but Has Little Value, Am. J. Clin. Pathol. 138 (2012) 262–272. https://doi.org/10.1309/AJCPCYCH96QYPHJM.

[136] I. Shah, R. James, J. Barker, A. Petroczi, D.P. Naughton, Misleading measures in Vitamin D analysis: A novel LC-MS/MS assay to account for epimers and isobars, Nutr. J. 10 (2011) 46. https://doi.org/10.1186/1475-2891-10-46.

[137] V. Martinsen, P. Kursula, Multiple sclerosis and myelin basic protein: insights into protein disorder and disease, Amino Acids. 54 (2022) 99–109. https://doi.org/10.1007/s00726-021-03111-7.

[138] J.M. Boggs, Myelin basic protein: a multifunctional protein, Cell. Mol. Life Sci. 63 (2006) 1945–1961. https://doi.org/10.1007/s00018-006-6094-7.

[139] V.N. Uversky, Natively unfolded proteins: A point where biology waits for physics, Protein Sci. 11 (2002) 739–756. https://doi.org/10.1110/ps.4210102.

[140] H.J. Dyson, P.E. Wright, Coupling of folding and binding for unstructured proteins, Curr. Opin. Struct. Biol. 12 (2002) 54–60. https://doi.org/10.1016/S0959-440X(02)00289-0.

[141] C. Readhead, N. Takasashi, H.D. Shine, R. Saavedra, R. Sidman, L. Hood, Role of Myelin Basic Protein in the Formation of Central Nervous System Myelin, Ann. N. Y. Acad. Sci. 605 (1990) 280–285. https://doi.org/10.1111/j.1749-6632.1990.tb42401.x.

[142] F.X. Omlin, Immunocytochemical localization of basic protein in major dense line regions of central and peripheral myelin, J. Cell Biol. 95 (1982) 242–248. https://doi.org/10.1083/jcb.95.1.242.

[143] C.A. Dyer, T.M. Philibotte, S. Billings-Gagliardi, M.K. Wolf, Cytoskeleton in Myelin-Basic Protein-Deficient Shiverer Oligodendrocytes, Dev. Neurosci. 17 (1995) 53–62. https://doi.org/10.1159/000111273.

[144] C.A. Dyer, The Structure and Function of Myelin: From Inert Membrane to Perfusion Pump, Neurochem. Res. 27 (2002) 1279–1292. https://doi.org/10.1023/A:1021611430052.

[145] S.M. Staugaitis, D.R. Colman, L. Pedraza, Membrane adhesion and other functions for the myelin basic proteins, Bioessays. 18 (1996) 13–18. https://doi.org/10.1002/bies.950180106.

[146] J.-L. Carré, B.D. Goetz, L.T. O'Connor, Q. Bremer, I.D. Duncan, Mutations in the rat myelin basic protein gene are associated with specific alterations in other myelin gene expression, Neurosci. Lett. 330 (2002) 17–20. https://doi.org/10.1016/S0304-3940(02)00709-7.

[147] R.J. Hardy, R.A. Lazzarini, D.R. Colman, V.L. Friedrich, Cytoplasmic and nuclear localization of myelin basic proteins reveals heterogeneity among oligodendrocytes, J. Neurosci. Res. 46 (1996) 246–257. https://doi.org/10.1002/(SICI)1097-4547(19961015)46:2<246::AID-JNR13>3.0.CO;2-0.

[148] J.M. Boggs, G. Rangaraj, Interaction of Lipid-Bound Myelin Basic Protein with Actin Filaments and Calmodulin, Biochemistry. 39 (2000) 7799–7806. https://doi.org/10.1021/bi0002129.

[149] D.S. Libich, C.M.D. Hill, I.R. Bates, F.R. Hallett, S. Armstrong, A. Siemiarczuk, G. Harauz, Interaction of the 18.5-kD isoform of myelin basic protein with Ca^{2+}-calmodulin: Effects of deimination assessed by intrinsic Trp fluorescence spectroscopy, dynamic light scattering, and circular dichroism, Protein Sci. 12 (2003) 1507–1521. https://doi.org/10.1110/ps.0303603.

[150] J.M. Boggs, G. Rangaraj, C.M.D. Hill, I.R. Bates, Y.-M. Heng, G. Harauz, Effect of Arginine Loss in Myelin Basic Protein, as Occurs in Its Deiminated Charge Isoform, on Mediation of Actin Polymerization and Actin Binding to a Lipid Membrane in Vitro, Biochemistry. 44 (2005) 3524–3534. https://doi.org/10.1021/bi0473760.

[151] J.M. Boggs, G. Rangaraj, W. Gao, Y.-M. Heng, Effect of Phosphorylation of Myelin Basic Protein By MAPK on its Interactions with Actin and Actin Binding to a Lipid Membrane in Vitro, Biochemistry. 45 (2006) 391–401. https://doi.org/10.1021/bi0519194.

[152] R. Smith, Non-covalent cross-linking of lipid bilayers by myelin basic protein. A possible role in myelin formation, Biochim. Biophys. Acta - Biomembr. 470 (1977) 170–184. https://doi.org/10.1016/0005-2736(77)90098-0.

[153] R. Smith, The Basic Protein of CNS Myelin: Its Structure and Ligand Binding, J. Neurochem. 59 (1992) 1589–1608. https://doi.org/10.1111/j.1471-4159.1992.tb10989.x.

[154] S. Cheifetz, M.A. Moscarello, Effect of bovine basic protein charge microheterogeneity on protein-induced aggregation of unilamellar vesicles containing a mixture of acidic and

neutral phospholipids, Biochemistry. 24 (1985) 1909–1914. https://doi.org/10.1021/bi00329a016.

[155] M.B.A. Beest, D. Hoekstra, Interaction of myelin basic protein with artificial membranes. Parameters governing binding, aggregation and dissociation, Eur. J. Biochem. 211 (1993) 689–696. https://doi.org/10.1111/j.1432-1033.1993.tb17597.x.

[156] E. Jo, J.M. Boggs, Aggregation of Acidic Lipid Vesicles by Myelin Basic Protein: Dependence on Potassium Concentration, Biochemistry. 34 (1995) 13705–13716. https://doi.org/10.1021/bi00041a053.

[157] Y. Hu, I. Doudevski, D. Wood, M. Moscarello, C. Husted, C. Genain, J.A. Zasadzinski, J. Israelachvili, Synergistic interactions of lipids and myelin basic protein, Proc. Natl. Acad. Sci. U.S.A. 101 (2004) 13466–13471. https://doi.org/10.1073/pnas.0405665101.

[158] L. Mateu, V. Luzzati, Y. London, R.M. Gould, F.G.A. Vosseberg, J. Olive, X-ray diffraction and electron microscope study of the interactions of myelin components. The structure of a lamellar phase with a 150 to 180 Å repeat distance containing basic proteins and acidic lipids, J. Mol. Biol. 75 (1973) 697–709. https://doi.org/10.1016/0022-2836(73)90302-1.

[159] G.W. Brady, N.S. Murthy, D.B. Fein, D.D. Wood, M.A. Moscarello, The effect of basic myelin protein on multilayer membrane formation, Biophys. J. 34 (1981) 345–350. https://doi.org/10.1016/S0006-3495(81)84853-9.

[160] J. Sędzik, A.E. Blaurock, M. Höchli, Lipid/myelin basic protein multilayers, J. Mol. Biol. 174 (1984) 385–409. https://doi.org/10.1016/0022-2836(84)90344-9.

[161] N.M. Modesti, H.S. Barra, The interaction of myelin basic protein with tubulin and the inhibition of tubulin carboxypeptidase activity, Biochem. Biophys. Res. Commun. 136 (1986) 482–489. https://doi.org/10.1016/0006-291X(86)90466-3.

[162] C.M.D. Hill, D.S. Libich, G. Harauz, Assembly of Tubulin by Classic Myelin Basic Protein Isoforms and Regulation by Post-Translational Modification, Biochemistry. 44 (2005) 16672–16683. https://doi.org/10.1021/bi050646+.

[163] G. Roth, M. Gonzalez, C. Monferran, M. Desantis, F. Cumar, Myelin basic protein domains involved in the interaction with actin, Neurochem. Int. 23 (1993) 459–465. https://doi.org/10.1016/0197-0186(93)90130-W.

[164] C.M.D. Hill, G. Harauz, Charge effects modulate actin assembly by classic myelin basic protein isoforms, Biochem. Biophys. Res. Commun. 329 (2005) 362–369. https://doi.org/10.1016/j.bbrc.2005.01.151.

[165] K. Prasad, W. Barouch, B.M. Martin, L.E. Greene, E. Eisenberg, Purification of a New Clathrin Assembly Protein from Bovine Brain Coated Vesicles and Its Identification as Myelin Basic Protein, J. Biol. Chem. 270 (1995) 30551–30556. https://doi.org/10.1074/jbc.270.51.30551.

[166] R.J. Grand, S.V. Perry, The binding of calmodulin to myelin basic protein and histone H2B, Biochem. J. 189 (1980) 227–240. https://doi.org/10.1042/bj1890227.

[167] K.-F.J. Chan, N.D. Robb, W.H. Chen, Myelin basic protein: Interaction with calmodulin and gangliosides, J. Neurosci. Res. 25 (1990) 535–544. https://doi.org/10.1002/jnr.490250410.

[168] E. Polverini, J.M. Boggs, I.R. Bates, G. Harauz, P. Cavatorta, Electron paramagnetic resonance spectroscopy and molecular modelling of the interaction of myelin basic protein (MBP) with calmodulin (CaM)—diversity and conformational adaptability of MBP CaM-targets, J. Struct. Biol. 148 (2004) 353–369. https://doi.org/10.1016/j.jsb.2004.08.004.

[169] D.S. Libich, C.M.D. Hill, J.D. Haines, G. Harauz, Myelin basic protein has multiple calmodulin-binding sites, Biochem. Biophys. Res. Commun. 308 (2003) 313–319. https://doi.org/10.1016/S0006-291X(03)01380-9.

[170] G. Harauz, N. Ishiyama, C.M.D. Hill, I.R. Bates, D.S. Libich, C. Farès, Myelin basic protein—diverse conformational states of an intrinsically unstructured protein and its roles in myelin assembly and multiple sclerosis, Micron. 35 (2004) 503–542. https://doi.org/10.1016/j.micron.2004.04.005.

[171] R.A. Saavedra, L. Fors, R.H. Aebersold, B. Arden, S. Horvath, J. Sanders, L. Hood, The myelin proteins of the shark brain are similar to the myelin proteins of the mammalian peripheral nervous system, J. Mol. Evol. 29 (1989) 149–156. https://doi.org/10.1007/BF02100113.

[172] T.J. Milne, A.R. Atkins, J.A. Warren, W.P. Auton, R. Smith, Shark Myelin Basic Protein: Amino Acid Sequence, Secondary Structure, and Self-Association, J. Neurochem. 55 (1990) 950–955. https://doi.org/10.1111/j.1471-4159.1990.tb04583.x.

[173] M.I. Givogri, E.R. Bongarzone, V. Schonmann, A.T. Campagnoni, Expression and regulation of golli products of myelin basic protein gene during in vitro development of oligodendrocytes, J. Neurosci. Res. 66 (2001) 679–690. https://doi.org/10.1002/jnr.10031.

[174] C. Brösamle, M.E. Halpern, Characterization of myelination in the developing zebrafish: Myelination in Zebrafish, Glia. 39 (2002) 47–57. https://doi.org/10.1002/glia.10088.

[175] E. Barbarese, J.H. Carson, P.E. Braun, Accumulation of the four myelin basic proteins in mouse brain during development, J. Neurochem. 31 (1978) 779–782. https://doi.org/10.1111/j.1471-4159.1978.tb00110.x.

[176] L. Pedraza, Nuclear transport of myelin basic protein, J. Neurosci. Res. 50 (1997) 258–264. https://doi.org/10.1002/(SICI)1097-4547(19971015)50:2<258::AID-JNR14>3.0.CO;2-4.

[177] H. de Vries, J.C. de Jonge, C. Schrage, M.E. van der Haar, D. Hoekstra, Differential and cell development-dependent localization of myelin mRNAs in oligodendrocytes, J. Neurosci. Res. 47 (1997) 479–488. https://doi.org/10.1002/(SICI)1097-4547(19970301)47:5<479::AID-JNR3>3.0.CO;2-E.

[178] J. Kamholz, J. Toffenetti, R.A. Lazzarini, Organization and expression of the human myelin basic protein gene, J. Neurosci. Res. 21 (1988) 62–70. https://doi.org/10.1002/jnr.490210110.

[179] F.C. Chou, C.H. Chou, R. Shapira, R.F. Kibler, Basis of microheterogeneity of myelin basic protein., J. Biol. Chem. 251 (1976) 2671–2679. https://doi.org/10.1016/S0021-9258(17)33540-8.

[180] R. Zand, M.X. Li, X. Jin, D. Lubman, Determination of the Sites of Posttranslational Modifications in the Charge Isomers of Bovine Myelin Basic Protein by Capillary

Electrophoresis-Mass Spectroscopy, Biochemistry. 37 (1998) 2441–2449. https://doi.org/10.1021/bi972347t.

[181] D.D. Wood, M.A. Moscarello, The Isolation, Characterization, and Lipid-aggregating Properties of a Citrulline Containing Myelin Basic Protein, J. Biol. Chem. 264 (1989) 5121–5127. https://doi.org/10.1016/S0021-9258(18)83707-3.

[182] J.K. Kim, F.G. Mastronardi, D.D. Wood, D.M. Lubman, R. Zand, M.A. Moscarello, Multiple Sclerosis. An Important Role for Post-Translational Modifications of Myelin Basic Protein in Pathogenesis, Mol. Cell. Proteom. 2 (2003) 453–462. https://doi.org/10.1074/mcp.M200050-MCP200.

[183] D. Jantz, J.M. Berg, Expanding the DNA-Recognition Repertoire for Zinc Finger Proteins beyond 20 Amino Acids, J. Am. Chem. Soc. 125 (2003) 4960–4961. https://doi.org/10.1021/ja029671i.

[184] J.B. Ulmer, P.E. Braun, In vivo phosphorylation of myelin basic proteins: Single and double isotope incorporation in developmentally related myelin fractions, Dev. Biol. 117 (1986) 502–510. https://doi.org/10.1016/0012-1606(86)90317-9.

[185] K.C. DesJardins, P. Morell, Phosphate groups modifying myelin basic proteins are metabolically labile; methyl groups are stable., J. Cell Biol. 97 (1983) 438–446. https://doi.org/10.1083/jcb.97.2.438.

[186] N. Murray, A.J. Steck, Impulse Conduction Regulates Myelin Basic Protein Phosphorylation in Rat Optic Nerve, J. Neurochem. 43 (1984) 243–248. https://doi.org/10.1111/j.1471-4159.1984.tb06702.x.

[187] C.M. Atkins, S.-J. Chen, E. Klann, J.D. Sweatt, Increased Phosphorylation of Myelin Basic Protein During Hippocampal Long-Term Potentiation, J. Neurochem. 68 (2002) 1960–1967. https://doi.org/10.1046/j.1471-4159.1997.68051960.x.

[188] C.M. Atkins, M. Yon, N.P. Groome, J.D. Sweatt, Regulation of Myelin Basic Protein Phosphorylation by Mitogen-Activated Protein Kinase During Increased Action Potential Firing in the Hippocampus, J. Neurochem. 73 (2001) 1090–1097. https://doi.org/10.1046/j.1471-4159.1999.0731090.x.

[189] C.A. Dyer, T.M. Philibotte, M.K. Wolf, S. Billings-Gagliardi, Myelin basic protein mediates extracellular signals that regulate microtubule stability in oligodendrocyte membrane sheets, J. Neurosci. Res. 39 (1994) 97–107. https://doi.org/10.1002/jnr.490390112.

[190] T. Vartanian, S. Szuchet, G. Dawson, A.T. Campagnoni, Oligodendrocyte Adhesion Activates Protein Kinase C-Mediated Phosphorylation of Myelin Basic Protein, Science. 234 (1986) 1395–1398. https://doi.org/10.1126/science.2431483.

[191] T. Vartanian, S. Szuchet, G. Dawson, Oligodendrocyte-substratum adhesion activates the synthesis of specific lipid species involved in cell signaling, J. Neurosci. Res. 32 (1992) 69–78. https://doi.org/10.1002/jnr.490320109.

[192] B. Soliven, M. Takeda, S. Szuchet, Depolarizing agents and tumor necrosis factor-α modulate protein phosphorylation in oligodendrocytes, J. Neurosci. Res. 38 (1994) 91–100. https://doi.org/10.1002/jnr.490380112.

[193] A.K. Erickson, D.M. Payne, P.A. Martino, A.J. Rossomando, J. Shabanowitz, M.J. Weber, D.F. Hunt, T.W. Sturgill, Identification by mass spectrometry of threonine 97 in

bovine myelin basic protein as a specific phosphorylation site for mitogen-activated protein kinase., J. Biol. Chem. 265 (1990) 19728–19735. https://doi.org/10.1016/S0021-9258(17)45433-0.

[194] J.-S. Yu, S.-D. Yang, Protein Kinase F_A/Glycogen Synthase Kinase-3 Predominantly Phosphorylates the In Vivo Site Thr[97]-Pro in Brain Myelin Basic Protein: Evidence for Thr-Pro and Ser-Arg-X-X-Ser as Consensus Sequence Motifs, J. Neurochem. 62 (2008) 1596–1603. https://doi.org/10.1046/j.1471-4159.1994.62041596.x.

[195] A. Kishimoto, K. Nishiyama, H. Nakanishi, Y. Uratsuji, H. Nomura, Y. Takeyama, Y. Nishizuka, Studies on the phosphorylation of myelin basic protein by protein kinase C and adenosine 3':5'-monophosphate-dependent protein kinase., J. Biol. Chem. 260 (1985) 12492–12499. https://doi.org/10.1016/S0021-9258(17)38898-1.

[196] R.E. Martenson, M.J. Law, G.E. Deibler, Identification of multiple in vivo phosphorylation sites in rabbit myelin basic protein, J. Biol. Chem. 258 (1983) 930–937. https://doi.org/10.1016/S0021-9258(18)33140-5.

[197] D. Hirschberg, O. Rådmark, H. Jörnvall, T. Bergman, Thr94 in Bovine Myelin Basic Protein Is a Second Phosphorylation Site for 42-kDa Mitogen-Activated Protein Kinase (ERK2), J. Protein Chem. 22 (2003) 177–181. https://doi.org/10.1023/A:1023479131488.

[198] M.A. Moscarello, D.D. Wood, C. Ackerley, C. Boulias, Myelin in multiple sclerosis is developmentally immature., J. Clin. Invest. 94 (1994) 146–154. https://doi.org/10.1172/JCI117300.

[199] F.G. Mastronardi, M.A. Moscarello, Molecules affecting myelin stability: A novel hypothesis regarding the pathogenesis of multiple sclerosis, J. Neurosci. Res. 80 (2005) 301–308. https://doi.org/10.1002/jnr.20420.

[200] C.M. Hill, I.R. Bates, G.F. White, F. Ross Hallett, G. Harauz, Effects of the osmolyte trimethylamine-N-oxide on conformation, self-association, and two-dimensional crystallization of myelin basic protein, J. Struct. Biol. 139 (2002) 13–26. https://doi.org/10.1016/S1047-8477(02)00513-0.

[201] C.M.D. Hill, J.D. Haines, C.E. Antler, I.R. Bates, D.S. Libich, G. Harauz, Terminal deletion mutants of myelin basic protein: new insights into self-association and phospholipid interactions, Micron. 34 (2003) 25–37. https://doi.org/10.1016/S0968-4328(02)00058-6.

[202] G.L. Stoner, Predicted Folding of β-Structure in Myelin Basic Protein, J. Neurochem. 43 (1984) 433–447. https://doi.org/10.1111/j.1471-4159.1984.tb00919.x.

[203] G.L. Mendz, L.R. Brown, R.E. Martenson, Interactions of myelin basic protein with mixed dodecylphosphocholine/palmitoyllysophosphatidic acid micelles, Biochemistry. 29 (1990) 2304–2311. https://doi.org/10.1021/bi00461a014.

[204] C.S. Randall, R. Zand, Spectroscopic assessment of secondary and tertiary structure in myelin basic protein, Biochemistry. 24 (1985) 1998–2004. https://doi.org/10.1021/bi00329a030.

[205] E. Polverini, A. Fasano, F. Zito, P. Riccio, P. Cavatorta, Conformation of bovine myelin basic protein purified with bound lipids, Eur. Biophys. J. 28 (1999) 351–355. https://doi.org/10.1007/s002490050218.

[206] M.A. Keniry, R. Smith, Circular dichroic analysis of the secondary structure of myelin basic protein and derived peptides bound to detergents and to lipid vesicles, Biochim. Biophys. Acta. 578 (1979) 381–391. https://doi.org/10.1016/0005-2795(79)90169-7.

[207] J.S. Anthony, M.A. Moscarello, A conformation change induced in the basic encephalitogen by lipids, Biochim. Biophys. Acta. 243 (1971) 429–433. https://doi.org/10.1016/0005-2795(71)90011-0.

[208] I.R. Bates, J.B. Feix, J.M. Boggs, G. Harauz, An Immunodominant Epitope of Myelin Basic Protein Is an Amphipathic α-Helix, J. Biol. Chem. 279 (2004) 5757–5764. https://doi.org/10.1074/jbc.M311504200.

[209] K.G. Warren, I. Catz, Kinetic profiles of cerebrospinal fluid anti-MBP in response to intravenous MBP synthetic peptide DENP85VVHFFKNIVTP96RT in multiple sclerosis patients, Mult. Scler. 6 (2000) 300–311. https://doi.org/10.1177/135245850000600502.

[210] D.S. Libich, V.J. Robertson, M.M. Monette, G. Harauz, Backbone resonance assignments of the 18.5 kDa isoform of murine myelin basic protein (MBP), J. Biomol. NMR. 29 (2004) 545–546. https://doi.org/10.1023/B:JNMR.0000034348.99658.d7.

[211] C. Fares, D.S. Libich, G. Harauz, Solution NMR structure of an immunodominant epitope of myelin basic protein. Conformational dependence on environment of an intrinsically unstructured protein, FEBS J. 273 (2006) 601–614. https://doi.org/10.1111/j.1742-4658.2005.05093.x.

[212] C.S. Constantinescu, N. Farooqi, K. O'Brien, B. Gran, Experimental autoimmune encephalomyelitis (EAE) as a model for multiple sclerosis (MS): EAE as model for MS, Br. J. Pharmacol. 164 (2011) 1079–1106. https://doi.org/10.1111/j.1476-5381.2011.01302.x.

[213] I.M. Stromnes, J.M. Goverman, Active induction of experimental allergic encephalomyelitis, Nat. Protoc. 1 (2006) 1810–1819. https://doi.org/10.1038/nprot.2006.285.

[214] M.V. Tejada-Simon, Y.C.Q. Zang, J. Hong, V.M. Rivera, J.Z. Zhang, Cross-reactivity with myelin basic protein and human herpesvirus-6 in multiple sclerosis, Ann. Neurol. 53 (2003) 189–197. https://doi.org/10.1002/ana.10425.

[215] Y. Guan, D. Jakimovski, M. Ramanathan, B. Weinstock-Guttman, R. Zivadinov, The role of Epstein-Barr virus in multiple sclerosis: from molecular pathophysiology to in vivo imaging, Neural. Regen. Res. 14 (2019) 373. https://doi.org/10.4103/1673-5374.245462.

[216] G.T. Rozenblum, T. Kaufman, A.D. Vitullo, Myelin Basic Protein and a Multiple Sclerosis-related MBP-peptide Bind to Oligonucleotides, Mol. Ther. Nucleic Acids. 3 (2014) e192. https://doi.org/10.1038/mtna.2014.43.

[217] D.D. Wood, M.A. Moscarello, J.M. Bilbao, P. O'Connors, Acute multiple sclerosis (marburg type) is associated with developmentally immature myelin basic protein, Ann. Neurol. 40 (1996) 18–24. https://doi.org/10.1002/ana.410400106.

[218] D.R. Beniac, D.D. Wood, N. Palaniyar, F.P. Ottensmeyer, M.A. Moscarello, G. Harauz, Marburg's Variant of Multiple Sclerosis Correlates with a Less Compact Structure of Myelin Basic Protein, Mol. Biol. Res. Commun. 1 (1999) 48–51. https://doi.org/10.1006/mcbr.1999.0111.

[219] J.M. Boggs, G. Rangaraj, K.M. Koshy, C. Ackerley, D.D. Wood, M.A. Moscarello, Highly deiminated isoform of myelin basic protein from multiple sclerosis brain causes fragmentation of lipid vesicles, J. Neurosci. Res. 57 (1999) 529–535. https://doi.org/10.1002/(SICI)1097-4547(19990815)57:4<529::AID-JNR12>3.0.CO;2-0.

[220] M. Ohta, K. Ohta, M. Nishimura, T. Saida, Detection of Myelin Basic Protein in Cerebrospinal Fluid and Serum from Patients with HTLV-1-Associated Myelopathy/Tropical Spastic Paraparesis, Ann. Clin. Biochem. 39 (2002) 603–605. https://doi.org/10.1177/000456320203900610.

[221] M. Cruz, T. Olsson, J. Ernerudh, B. Hojeberg, H. Link, Immunoblot detection of oligoclonal anti-myelin basic protein IgG antibodies in cerebrospinal fluid in multiple sclerosis, Neurology. 37 (1987) 1515–1515. https://doi.org/10.1212/WNL.37.9.1515.

[222] F. Lolli, B. Mulinacci, A. Carotenuto, B. Bonetti, G. Sabatino, B. Mazzanti, A.M. D'Ursi, E. Novellino, M. Pazzagli, L. Lovato, M.C. Alcaro, E. Peroni, M.C. Pozo-Carrero, F. Nuti, L. Battistini, G. Borsellino, M. Chelli, P. Rovero, A.M. Papini, An N-glucosylated peptide detecting disease-specific autoantibodies, biomarkers of multiple sclerosis, Proc. Natl. Acad. Sci. U.S.A. 102 (2005) 10273–10278. https://doi.org/10.1073/pnas.0503178102.

[223] K.G. Warren, I. Catz, L. Steinman, Fine specificity of the antibody response to myelin basic protein in the central nervous system in multiple sclerosis: the minimal B-cell epitope and a model of its features., Proc. Natl. Acad. Sci. U.S.A. 92 (1995) 11061–11065. https://doi.org/10.1073/pnas.92.24.11061.

[224] F. Sellebjerg, C.V. Jensen, M. Christiansen, Intrathecal IgG synthesis and autoantibody-secreting cells in multiple sclerosis, J. Neuroimmunol. 108 (2000) 207–215. https://doi.org/10.1016/S0165-5728(00)00292-7.

[225] F. Sellebjerg, H.O. Madsen, J.L. Frederiksen, L.P. Ryder, A. Svejgaard, Acute optic neuritis: Myelin basic protein and proteolipid protein antibodies, affinity, and the HLA system, Ann. Neurol. 38 (1995) 943–950. https://doi.org/10.1002/ana.410380616.

[226] K.C. O'Connor, T. Chitnis, D.E. Griffin, S. Piyasirisilp, A. Bar-Or, S. Khoury, K.W. Wucherpfennig, D.A. Hafler, Myelin basic protein-reactive autoantibodies in the serum and cerebrospinal fluid of multiple sclerosis patients are characterized by low-affinity interactions, J. Neuroimmunol. 136 (2003) 140–148. https://doi.org/10.1016/S0165-5728(03)00002-X.

[227] T. Berger, P. Rubner, F. Schautzer, R. Egg, H. Ulmer, I. Mayringer, E. Dilitz, F. Deisenhammer, M. Reindl, Antimyelin Antibodies as a Predictor of Clinically Definite Multiple Sclerosis after a First Demyelinating Event, N. Engl. J. Med. 349 (2003) 139–145. https://doi.org/10.1056/NEJMoa022328.

[228] N. Sewald, H.-D. Jakubke, Peptides: chemistry and biology, Wiley-VCH, Weinheim, 2002.

[229] R.J. Ouellette, J.D. Rawn, Amino Acids, Peptides, and Proteins, in: Principles of Organic Chemistry, Elsevier, 2015: pp. 371–396. https://doi.org/10.1016/B978-0-12-802444-7.00014-8.

[230] L.-G. Milroy, T.N. Grossmann, S. Hennig, L. Brunsveld, C. Ottmann, Modulators of Protein–Protein Interactions, Chem. Rev. 114 (2014) 4695–4748. https://doi.org/10.1021/cr400698c.

[231] M. Pelay-Gimeno, A. Glas, O. Koch, T.N. Grossmann, Structure-Based Design of Inhibitors of Protein-Protein Interactions: Mimicking Peptide Binding Epitopes, Angew. Chem. Int. Ed. 54 (2015) 8896–8927. https://doi.org/10.1002/anie.201412070.

[232] L. Wang, N. Wang, W. Zhang, X. Cheng, Z. Yan, G. Shao, X. Wang, R. Wang, C. Fu, Therapeutic peptides: current applications and future directions, Sig. Transduct. Target. Ther. 7 (2022) 48. https://doi.org/10.1038/s41392-022-00904-4.

[233] C.J. White, A.K. Yudin, Contemporary strategies for peptide macrocyclization, Nature Chem. 3 (2011) 509–524. https://doi.org/10.1038/nchem.1062.

[234] M. Pelay-Gimeno, J. Tulla-Puche, F. Albericio, "Head-to-Side-Chain" Cyclodepsipeptides of Marine Origin, Mar. Drugs. 11 (2013) 1693–1717. https://doi.org/10.3390/md11051693.

[235] C.B.F. Mourão, G.D. Brand, J.P.C. Fernandes, M.V. Prates, C. Bloch, J.A.R.G. Barbosa, S.M. Freitas, R. Restano-Cassulini, L.D. Possani, E.F. Schwartz, Head-to-Tail Cyclization after Interaction with Trypsin: A Scorpion Venom Peptide that Resembles Plant Cyclotides, J. Med. Chem. 63 (2020) 9500–9511. https://doi.org/10.1021/acs.jmedchem.0c00686.

[236] P.G. Dougherty, J. Wen, X. Pan, A. Koley, J.-G. Ren, A. Sahni, R. Basu, H. Salim, G. Appiah Kubi, Z. Qian, D. Pei, Enhancing the Cell Permeability of Stapled Peptides with a Cyclic Cell-Penetrating Peptide, J. Med. Chem. 62 (2019) 10098–10107. https://doi.org/10.1021/acs.jmedchem.9b00456.

[237] S.R. Perry, T.A. Hill, A.D. de Araujo, H.N. Hoang, D.P. Fairlie, Contiguous hydrophobic and charged surface patches in short helix-constrained peptides drive cell permeability, Org. Biomol. Chem. 16 (2018) 367–371. https://doi.org/10.1039/C7OB02952G.

[238] Y. Tian, Y. Jiang, J. Li, D. Wang, H. Zhao, Z. Li, Effect of Stapling Architecture on Physiochemical Properties and Cell Permeability of Stapled α-Helical Peptides: A Comparative Study, ChemBioChem. 18 (2017) 2087–2093. https://doi.org/10.1002/cbic.201700352.

[239] P.-Y. Yang, H. Zou, C. Lee, A. Muppidi, E. Chao, Q. Fu, X. Luo, D. Wang, P.G. Schultz, W. Shen, Stapled, Long-Acting Glucagon-like Peptide 2 Analog with Efficacy in Dextran Sodium Sulfate Induced Mouse Colitis Models, J. Med. Chem. 61 (2018) 3218–3223. https://doi.org/10.1021/acs.jmedchem.7b00768.

[240] M.G. Ricardo, A.M. Ali, J. Plewka, E. Surmiak, B. Labuzek, C.G. Neochoritis, J. Atmaj, L. Skalniak, R. Zhang, T.A. Holak, M. Groves, D.G. Rivera, A. Dömling, Multicomponent Peptide Stapling as a Diversity-Driven Tool for the Development of Inhibitors of Protein–Protein Interactions, Angew. Chem. Int. Ed. 59 (2020) 5235–5241. https://doi.org/10.1002/anie.201916257.

[241] C.Y. Li, K. Yap, J.E. Swedberg, D.J. Craik, S.J. de Veer, Binding Loop Substitutions in the Cyclic Peptide SFTI-1 Generate Potent and Selective Chymase Inhibitors, J. Med. Chem. 63 (2020) 816–826. https://doi.org/10.1021/acs.jmedchem.9b01811.

[242] S. Rubin, N. Qvit, Cyclic Peptides for Protein-Protein Interaction Targets: Applications to Human Disease, Crit. Rev. Eukaryot. Gene Expr. 26 (2016) 199–221. https://doi.org/10.1615/CritRevEukaryotGeneExpr.2016016525.

[243] M.G. Ricardo, A.V. Vasco, D.G. Rivera, L.A. Wessjohann, Stabilization of Cyclic β-Hairpins by Ugi-Reaction-Derived *N*-Alkylated Peptides: The Quest for Functionalized β-Turns, Org. Lett. 21 (2019) 7307–7310. https://doi.org/10.1021/acs.orglett.9b02592.

[244] M. van der Knaap, J.M. Otero, A. Llamas-Saiz, M.J. van Raaij, L.I. Lageveen, H.J. Busscher, G.M. Grotenbreg, G.A. van der Marel, H.S. Overkleeft, M. Overhand, Design, synthesis and structural analysis of mixed α/β-peptides that adopt stable cyclic hairpin-like conformations, Tetrahedron. 68 (2012) 2391–2400. https://doi.org/10.1016/j.tet.2012.01.015.

[245] O. Koch, J. Cole, P. Block, G. Klebe, Secbase: Database Module To Retrieve Secondary Structure Elements with Ligand Binding Motifs, J. Chem. Inf. Model. 49 (2009) 2388–2402. https://doi.org/10.1021/ci900202d.

[246] B.N. Bullock, A.L. Jochim, P.S. Arora, Assessing Helical Protein Interfaces for Inhibitor Design, J. Am. Chem. Soc. 133 (2011) 14220–14223. https://doi.org/10.1021/ja206074j.

[247] A.L. Jochim, P.S. Arora, Systematic Analysis of Helical Protein Interfaces Reveals Targets for Synthetic Inhibitors, ACS Chem. Biol. 5 (2010) 919–923. https://doi.org/10.1021/cb1001747.

[248] C.M. Bergey, A.M. Watkins, P.S. Arora, HippDB: a database of readily targeted helical protein-protein interactions, Bioinformatics. 29 (2013) 2806–2807. https://doi.org/10.1093/bioinformatics/btt483.

[249] N. Sawyer, A.M. Watkins, P.S. Arora, Protein Domain Mimics as Modulators of Protein–Protein Interactions, Acc. Chem. Res. 50 (2017) 1313–1322. https://doi.org/10.1021/acs.accounts.7b00130.

[250] A.K. Galande, K.S. Bramlett, T.P. Burris, J.L. Wittliff, A.F. Spatola, Thioether side chain cyclization for helical peptide formation: inhibitors of estrogen receptor-coactivator interactions, J. Pept. Res. 63 (2004) 297–302. https://doi.org/10.1111/j.1399-3011.2004.00152.x.

[251] K.K. Khoo, M.J. Wilson, B.J. Smith, M.-M. Zhang, J. Gulyas, D. Yoshikami, J.E. Rivier, G. Bulaj, R.S. Norton, Lactam-Stabilized Helical Analogues of the Analgesic μ-Conotoxin KIIIA, J. Med. Chem. 54 (2011) 7558–7566. https://doi.org/10.1021/jm200839a.

[252] A. Muppidi, K. Doi, S. Edwardraja, E.J. Drake, A.M. Gulick, H.-G. Wang, Q. Lin, Rational Design of Proteolytically Stable, Cell-Permeable Peptide-Based Selective Mcl-1 Inhibitors, J. Am. Chem. Soc. 134 (2012) 14734–14737. https://doi.org/10.1021/ja306864v.

[253] A. Muppidi, H. Zhang, F. Curreli, N. Li, A.K. Debnath, Q. Lin, Design of antiviral stapled peptides containing a biphenyl cross-linker, Bioorganic Med. Chem. Lett. 24 (2014) 1748–1751. https://doi.org/10.1016/j.bmcl.2014.02.038.

[254] K. Sakagami, T. Masuda, K. Kawano, S. Futaki, Importance of Net Hydrophobicity in the Cellular Uptake of All-Hydrocarbon Stapled Peptides, Mol. Pharmaceutics. 15 (2018) 1332–1340. https://doi.org/10.1021/acs.molpharmaceut.7b01130.

[255] L. Reguera, D.G. Rivera, Multicomponent Reaction Toolbox for Peptide Macrocyclization and Stapling, Chem. Rev. 119 (2019) 9836–9860. https://doi.org/10.1021/acs.chemrev.8b00744.

[256] Z. Athanassiou, R.L.A. Dias, K. Moehle, N. Dobson, G. Varani, J.A. Robinson, Structural Mimicry of Retroviral Tat Proteins by Constrained β-Hairpin Peptidomimetics: Ligands with High Affinity and Selectivity for Viral TAR RNA Regulatory Elements, J. Am. Chem. Soc. 126 (2004) 6906–6913. https://doi.org/10.1021/ja0497680.

[257] R. Fasan, R.L.A. Dias, K. Moehle, O. Zerbe, J.W. Vrijbloed, D. Obrecht, J.A. Robinson, Using a β-Hairpin To Mimic anα-Helix: Cyclic Peptidomimetic Inhibitors of the p53–HDM2 Protein–Protein Interaction, Angew. Chem. Int. Ed. 43 (2004) 2109–2112. https://doi.org/10.1002/anie.200353242.

[258] P.-N. Cheng, C. Liu, M. Zhao, D. Eisenberg, J.S. Nowick, Amyloid β-sheet mimics that antagonize protein aggregation and reduce amyloid toxicity, Nature Chem. 4 (2012) 927–933. https://doi.org/10.1038/nchem.1433.

[259] C. Liu, M.R. Sawaya, P.-N. Cheng, J. Zheng, J.S. Nowick, D. Eisenberg, Characteristics of Amyloid-Related Oligomers Revealed by Crystal Structures of Macrocyclic β-Sheet Mimics, J. Am. Chem. Soc. 133 (2011) 6736–6744. https://doi.org/10.1021/ja200222n.

[260] H.M. König, A.F.M. Kilbinger, Learning from Nature: β-Sheet-Mimicking Copolymers Get Organized, Angew. Chem. Int. Ed. 46 (2007) 8334–8340. https://doi.org/10.1002/anie.200701167.

[261] O. Khakshoor, B. Demeler, J.S. Nowick, Macrocyclic β-Sheet Peptides That Mimic Protein Quaternary Structure through Intermolecular β-Sheet Interactions, J. Am. Chem. Soc. 129 (2007) 5558–5569. https://doi.org/10.1021/ja068511u.

[262] J. Koehbach, M. O'Brien, M. Muttenthaler, M. Miazzo, M. Akcan, A.G. Elliott, N.L. Daly, P.J. Harvey, S. Arrowsmith, S. Gunasekera, T.J. Smith, S. Wray, U. Goransson, P.E. Dawson, D.J. Craik, M. Freissmuth, C.W. Gruber, Oxytocic plant cyclotides as templates for peptide G protein-coupled receptor ligand design, PNAS. 110 (2013) 21183–21188. https://doi.org/10.1073/pnas.1311183110.

[263] E. Kaiser, R.L. Colescott, C.D. Bossinger, P.I. Cook, Color test for detection of free terminal amino groups in the solid-phase synthesis of peptides, Anal. Biochem. 34 (1970) 595–598. https://doi.org/10.1016/0003-2697(70)90146-6.

[264] F. Nuti, M. Larregola, A. Staśkiewicz, B. Retzl, N. Tomašević, L. Macchia, M.E. Street, M. Jewgiński, O. Lequin, R. Latajka, P. Rovero, C.W. Gruber, M. Chorev, A.M. Papini, Design, synthesis, conformational analysis, and biological activity of Cα^1-to-Cα^6 1,4- and 4,1-disubstituted 1 *H* -[1,2,3]triazol-1-yl-bridged oxytocin analogues, J. Enzyme Inhib. Med. Chem. 38 (2023) 2254019. https://doi.org/10.1080/14756366.2023.2254019.

[265] F. Rizzolo, C. Testa, D. Lambardi, M. Chorev, M. Chelli, P. Rovero, A.M. Papini, Conventional and microwave-assisted SPPS approach: a comparative synthesis of PTHrP(1-34)NH$_2$, J. Peptide Sci. 17 (2011) 708–714. https://doi.org/10.1002/psc.1395.

[266] S. Pandey, M.C. Alcaro, M. Scrima, E. Peroni, I. Paolini, S. Di Marino, F. Barbetti, A. Carotenuto, E. Novellino, A.M. Papini, A.M. D'Ursi, P. Rovero, Designed

Glucopeptides Mimetics of Myelin Protein Epitopes As Synthetic Probes for the Detection of Autoantibodies, Biomarkers of Multiple Sclerosis, J. Med. Chem. 55 (2012) 10437–10447. https://doi.org/10.1021/jm301031r.

[267] F. Nuti, F.R. Fernandez, G. Sabatino, E. Peroni, B. Mulinacci, I. Paolini, M.D. Pisa, C. Tiberi, F. Lolli, M. Petruzzo, R. Lanzillo, V.B. Morra, P. Rovero, A.M. Papini, A Multiple N-Glucosylated Peptide Epitope Efficiently Detecting Antibodies in Multiple Sclerosis, Brain Sci. 10 (2020) 453. https://doi.org/10.3390/brainsci10070453.

[268] C.H. Polman, S.C. Reingold, B. Banwell, M. Clanet, J.A. Cohen, M. Filippi, K. Fujihara, E. Havrdova, M. Hutchinson, L. Kappos, F.D. Lublin, X. Montalban, P. O'Connor, M. Sandberg-Wollheim, A.J. Thompson, E. Waubant, B. Weinshenker, J.S. Wolinsky, Diagnostic criteria for multiple sclerosis: 2010 Revisions to the McDonald criteria, Ann. Neurol. 69 (2011) 292–302. https://doi.org/10.1002/ana.22366.

[269] A.J. Thompson, B.L. Banwell, F. Barkhof, W.M. Carroll, T. Coetzee, G. Comi, J. Correale, F. Fazekas, M. Filippi, M.S. Freedman, K. Fujihara, S.L. Galetta, H.P. Hartung, L. Kappos, F.D. Lublin, R.A. Marrie, A.E. Miller, D.H. Miller, X. Montalban, E.M. Mowry, P.S. Sorensen, M. Tintoré, A.L. Traboulsee, M. Trojano, B.M.J. Uitdehaag, S. Vukusic, E. Waubant, B.G. Weinshenker, S.C. Reingold, J.A. Cohen, Diagnosis of multiple sclerosis: 2017 revisions of the McDonald criteria, Lancet Neurol. 17 (2018) 162–173. https://doi.org/10.1016/S1474-4422(17)30470-2.

[270] F. Real Fernández, M. Di Pisa, G. Rossi, N. Auberger, O. Lequin, M. Larregola, A. Benchohra, C. Mansuy, G. Chassaing, F. Lolli, J. Hayek, S. Lavielle, P. Rovero, J.-M. Mallet, A.M. Papini, Antibody Recognition in multiple sclerosis and rett syndrome using a collection of linear and cyclic *N*-glucosylated antigenic probes: Antibody Recognition in Multiple Sclerosis and Rett Syndrome, Biopolymers. 104 (2015) 560–576. https://doi.org/10.1002/bip.22677.

[271] R.F. Sommese, S. Sivaramakrishnan, R.L. Baldwin, J.A. Spudich, Helicity of short E-R/K peptides: Helicity of Short E-R/K Peptides, Protein Sci. 19 (2010) 2001–2005. https://doi.org/10.1002/pro.469.

[272] W. Lee, M. Tonelli, J.L. Markley, NMRFAM-SPARKY: enhanced software for biomolecular NMR spectroscopy, Bioinformatics. 31 (2015) 1325–1327. https://doi.org/10.1093/bioinformatics/btu830.

[273] D.S. Wishart, C.G. Bigam, A. Holm, R.S. Hodges, B.D. Sykes, ^{1}H, ^{13}C and ^{15}N random coil NMR chemical shifts of the common amino acids. Investigations of nearest-neighbor effects, J. Biomol. NMR. 5 (1995) 67–81. https://doi.org/10.1007/BF00227471.

[274] T.L. Hwang, A.J. Shaka, Water Suppression That Works. Excitation Sculpting Using Arbitrary Wave-Forms and Pulsed-Field Gradients, J. Magn. Reson., Ser. A. 112 (1995) 275–279. https://doi.org/10.1006/jmra.1995.1047.

[275] U. Piantini, O.W. Sorensen, R.R. Ernst, Multiple quantum filters for elucidating NMR coupling networks, J. Am. Chem. Soc. 104 (1982) 6800–6801. https://doi.org/10.1021/ja00388a062.

[276] D. Marion, K. Wüthrich, Application of phase sensitive two-dimensional correlated spectroscopy (COSY) for measurements of ^{1}H-^{1}H spin-spin coupling constants in

proteins, Biochem. Biophys. Res. Commun. 113 (1983) 967–974. https://doi.org/10.1016/0006-291X(83)91093-8.

[277] L. Braunschweiler, R.R. Ernst, Coherence transfer by isotropic mixing: Application to proton correlation spectroscopy, J. Magn. Reson. 53 (1983) 521–528. https://doi.org/10.1016/0022-2364(83)90226-3.

[278] J. Jeener, B.H. Meier, P. Bachmann, R.R. Ernst, Investigation of exchange processes by two-dimensional NMR spectroscopy, Chem. Phys. 71 (1979) 4546–4553. https://doi.org/10.1063/1.438208.

[279] E. Ämmälahti, M. Bardet, D. Molko, J. Cadet, Evaluation of Distances from ROESY Experiments with the Intensity-Ratio Method, J. Magn. Reson., Ser. A. 122 (1996) 230–232. https://doi.org/10.1006/jmra.1996.0199.

[280] M. Waskom, Seaborn: statistical data visualization, JOSS. 6 (2021) 3021. https://doi.org/10.21105/joss.03021.

[281] M.G. Di Giglio, M. Muttenthaler, K. Harpsøe, Z. Liutkeviciute, P. Keov, T. Eder, T. Rattei, S. Arrowsmith, S. Wray, A. Marek, T. Elbert, P.F. Alewood, D.E. Gloriam, C.W. Gruber, Development of a human vasopressin V_{1a}-receptor antagonist from an evolutionary-related insect neuropeptide, Sci. Rep. 7 (2017) 41002. https://doi.org/10.1038/srep41002.

[282] L. Duerrauer, E. Muratspahić, J. Gattringer, P. Keov, H.C. Mendel, K.D.G. Pfleger, M. Muttenthaler, C.W. Gruber, I8-arachnotocin–an arthropod-derived G protein-biased ligand of the human vasopressin V_2 receptor, Sci. Rep. 9 (2019) 19295. https://doi.org/10.1038/s41598-019-55675-w.

[283] S. Cantel, A. Le Chevalier Isaad, M. Scrima, J.J. Levy, R.D. DiMarchi, P. Rovero, J.A. Halperin, A.M. D'Ursi, A.M. Papini, M. Chorev, Synthesis and Conformational Analysis of a Cyclic Peptide Obtained via *i* to *i*+4 Intramolecular Side-Chain to Side-Chain Azide−Alkyne 1,3-Dipolar Cycloaddition, J. Org. Chem. 73 (2008) 5663–5674. https://doi.org/10.1021/jo800142s.

[284] K. Ota, M. Matsui, E.L. Milford, G.A. Mackin, H.L. Weiner, D.A. Hafler, T-cell recognition of an immuno-dominant myelin basic protein epitope in multiple sclerosis, Nature. 346 (1990) 183–187. https://doi.org/10.1038/346183a0.

[285] A. Kim, I.Z. Hartman, B. Poore, T. Boronina, R.N. Cole, N. Song, M.T. Ciudad, R.R. Caspi, D. Jaraquemada, S. Sadegh-Nasseri, Divergent paths for the selection of immunodominant epitopes from distinct antigenic sources, Nat. Commun. 5 (2014) 5369. https://doi.org/10.1038/ncomms6369.

[286] R. Martin, D. Jaraquemada, M. Flerlage, J. Richert, J. Whitaker, E.O. Long, D.E. McFarlin, H.F. McFarland, Fine specificity and HLA restriction of myelin basic protein-specific cytotoxic T cell lines from multiple sclerosis patients and healthy individuals., J. Immunol. 145 (1990) 540–548. https://doi.org/10.4049/jimmunol.145.2.540.

[287] B.E. Hansen, A.H. Rasmussen, B.K. Jakobsen, L.P. Ryder, A. Svejgaard, Extraordinary cross-reactivity of an autoimmune T-cell receptor recognizing specific peptides both on autologous and on allogeneic HLA class II molecules, Tissue Antigens. 70 (2007) 42–52. https://doi.org/10.1111/j.1399-0039.2007.00849.x.

[288] M.H.V. Van Regenmortel, Antigenicity and Immunogenicity of Synthetic Peptides, Biologicals. 29 (2001) 209–213. https://doi.org/10.1006/biol.2001.0308.

[289] R. Egg, M. Reindl, F. Deisenhammer, C. Linington, T. Berger, Anti-MOG and anti-MBP antibody subclasses in multiple sclerosis, Mult. Scler. 7 (2001) 285–289. https://doi.org/10.1177/135245850100700503.

[290] Y. Wei, A.A. Thyparambil, R.A. Latour, Protein helical structure determination using CD spectroscopy for solutions with strong background absorbance from 190 to 230 nm, Biochim. Biophys. Acta - Proteins Proteom. 1844 (2014) 2331–2337. https://doi.org/10.1016/j.bbapap.2014.10.001.

[291] S. Campagna, B. Vitoux, G. Humbert, J.M. Girardet, G. Linden, T. Haertle, J.L. Gaillard, Conformational Studies of a Synthetic Peptide from the Putative Lipid-binding Domain of Bovine Milk Component PP3, J. Dairy Sci. 81 (1998) 3139–3148. https://doi.org/10.3168/jds.S0022-0302(98)75879-5.

[292] P. Khandelwal, S. Seth, R. V. Hosur, CD and NMR investigations on trifluoroethanol-induced step-wise folding of helical segment from scorpion neurotoxin, Eur. J. Biochem. 264 (1999) 468–478. https://doi.org/10.1046/j.1432-1327.1999.00641.x.

[293] E.K. Bradley, J.F. Thomason, F.E. Cohen, P.A. Kosen, I.D. Kuntz, Studies of synthetic helical peptides using circular dichroism and nuclear magnetic resonance, J. Mol. Biol. 215 (1990) 607–622. https://doi.org/10.1016/S0022-2836(05)80172-X.

[294] M.A.M. Ahmed, M. De Avila, E. Polverini, K. Bessonov, V.V. Bamm, G. Harauz, Solution Nuclear Magnetic Resonance Structure and Molecular Dynamics Simulations of a Murine 18.5 kDa Myelin Basic Protein Segment (S72–S107) in Association with Dodecylphosphocholine Micelles, Biochemistry. 51 (2012) 7475–7487. https://doi.org/10.1021/bi300998x.

[295] A.J. Miles, S.G. Ramalli, B.A. Wallace, DICHROWEB , a website for calculating protein secondary structure from circular dichroism spectroscopic data, Protein Sci. 31 (2022) 37–46. https://doi.org/10.1002/pro.4153.

[296] J. Yang, E.J. Spek, Y. Gong, H. Zhou, N.R. Kallenbach, The role of context on α-helix stabilization: Host-guest analysis in a mixed background peptide model: α-helix stability, Protein Sci. 6 (1997) 1264–1272. https://doi.org/10.1002/pro.5560060614.

[297] B. Forood, E.J. Feliciano, K.P. Nambiar, Stabilization of alpha-helical structures in short peptides via end capping., Proc. Natl. Acad. Sci. U.S.A. 90 (1993) 838–842. https://doi.org/10.1073/pnas.90.3.838.

[298] D. Sitkoff, D.J. Lockhart, K.A. Sharp, B. Honig, Calculation of electrostatic effects at the amino terminus of an alpha helix, Biophys. J. 67 (1994) 2251–2260. https://doi.org/10.1016/S0006-3495(94)80709-X.

[299] G. Muruganandam, J. Bürck, A.S. Ulrich, I. Kursula, P. Kursula, Lipid Membrane Association of Myelin Proteins and Peptide Segments Studied by Oriented and Synchrotron Radiation Circular Dichroism Spectroscopy, J. Phys. Chem. B. 117 (2013) 14983–14993. https://doi.org/10.1021/jp4098588.

[300] D.K. Lanthier, K.A. Vassall, G. Harauz, Biophysical characterization of 21.5-kDa myelin basic protein (MBP) and the effects of zinc on its structure, SURG. 7 (2014) 30–41. https://doi.org/10.21083/surg.v7i3.2958.

[301] Y. Waltenspühl, J. Ehrenmann, S. Vacca, C. Thom, O. Medalia, A. Plückthun, Structural basis for the activation and ligand recognition of the human oxytocin receptor, Nat. Commun. 13 (2022) 4153. https://doi.org/10.1038/s41467-022-31325-0.

[302] J.G. Meyerowitz, M.J. Robertson, X. Barros-Álvarez, O. Panova, R.M. Nwokonko, Y. Gao, G. Skiniotis, The oxytocin signaling complex reveals a molecular switch for cation dependence, Nat. Struct. Mol. Biol. 29 (2022) 274–281. https://doi.org/10.1038/s41594-022-00728-4.

[303] T. Rogi, M. Tsujimoto, H. Nakazato, S. Mizutani, Y. Tomoda, Human Placental Leucine Aminopeptidase/Oxytocinase, J. Biol. Chem. 271 (1996) 56–61. https://doi.org/10.1074/jbc.271.1.56.

[304] N. Yamahara, S. Nomura, T. Suzuki, A. Itakura, M. Ito, T. Okamoto, M. Tsujimoto, H. Nakazato, S. Mizutani, Placental leucine aminopeptidase/oxytocinase in maternal serum and placenta during normal pregnancy, Life Sci. 66 (2000) 1401–1410. https://doi.org/10.1016/S0024-3205(00)00451-3.

[305] H. Kobayashi, S. Nomura, T. Mitsui, T. Ito, N. Kuno, Y. Ohno, K. Kadomatsu, T. Muramatsu, T. Nagasaka, S. Mizutani, Tissue Distribution of Placental Leucine Aminopeptidase/Oxytocinase During Mouse Pregnancy, J. Histochem. Cytochem. 52 (2004) 113–121. https://doi.org/10.1177/002215540405200111.

8   SUPPLEMENTARY MATERIAL

Supplementary material prepared as additional fragments of this doctoral dissertation, including, for instance, spectra, tables or figures. This material is an essential fragment of this PhD thesis. It was performed as a PDF file and saved on a CD, which can be found inside the cover of the printed version of the doctoral dissertation.

List of Figures

List of Tables

SCIENTIFIC ACHIEVEMENTS

- **Total publications: 7**
- **Total IF: 21.617**
- **Total citations obtained until 12.09.2024: 33**
- *h*-**index: 2**

Publications

I.   Publications related to the PhD thesis

1. F. Nuti, M. Larregola, **A. Staśkiewicz**, B. Retzl, N. Tomašević, L. Macchia, M.E. Street, M. Jewgiński, O. Lequin, R. Latajka, P. Rovero, C.W. Gruber, M. Chorev, A.M. Papini, Design, synthesis, conformational analysis, and biological activity of $C\alpha^1$-to-$C\alpha^6$ 1,4- and 4,1-disubstituted 1*H*-[1,2,3]triazol-1-yl-bridged oxytocin analogues, *J. Enzyme Inhib. Med. Chem.*, **2023**, 1, 38, 1-15, DOI: 10.1080/14756366.2023.2254019, IF: 5.6

2. **A. Staśkiewicz**, M. Quagliata, F. Real-Fernandez, F. Nuti, R. Lanzillo, V. Brescia-Morra, H. Rusche, M. Jewginski, A. Carotenuto, D. Brancaccio, R. Aharoni, R. Arnon, P. Rovero, R. Latajka, A.M. Papini, Role of Helical Structure in MBP Immunodominant Peptides for Efficient IgM Antibody Recognition in Multiple Sclerosis, *Front. Chem.*, **2022**, 10, 885180, 1-11, DOI: 10.3389/fchem.2022.885180, IF: 5.545

3. **A. Staśkiewicz**, P. Ledwoń, P. Rovero, A.M. Papini, R. Latajka, Triazole-modified peptidomimetics: an opportunity for drug discovery and development, *Front. Chem.*, **2021**, 9, 674705, 1-16, DOI: 10.3389/fchem.2021.674705, IF: 5.545
Citations obtained until 12.09.2024: 23

II. Publications not related to the PhD thesis

4. P. Ledwoń, **A. Staśkiewicz**, M. Jewgiński, R. Latajka, Peptidomimetics and aromatic foldamers in biological chemistry, *Wiadomości Chemiczne*, **2022**, 76, 5-6, 349-363, DOI: 10.53584/wiadchem.2022.5.6

5. J.I. Krzciuk-Gula, P. Ledwoń, **A. Staśkiewicz**, R. Latajka, The influence of different β-amino acid residues on coordinating abilities of peptides toward transition metal ions, *Wiadomości Chemiczne*, **2020**, 74, 285-310

6. P. Ledwoń, **A. Staśkiewicz**, M. Jewgiński, R. Latajka, Influence of ΔPhe residues on conformation of peptide chain, *Wiadomości Chemiczne*, **2020**, 74, 9-32

7. M. Kijewska, F. Nuti, M. Wierzbicka, M. Waliczek, P. Ledwoń, **A. Staśkiewicz**, F. Real-Fernandez, G. Sabatino, P. Rovero, P. Stefanowicz, Z. Szewczuk, A.M. Papini, An Optimised Di Boronate ChemMatrix Affnity Chromatography to Trap Deoxyfructosylated Peptides as Biomarkers of Glycation, *Molecules*, **2020**, 25, 1-15, DOI: 10.3390/molecules25030755, IF: 4.927
Citations obtained until 12.09.2024: 10

Conferences

Oral presentations

1. **A. Staśkiewicz**, M. Quagliata, F. Nuti, F. Real-Fernandez, R. Lanzillo, V. Brescia-Morra, H. Rusche, M. Jewgiński, A. Carotenuto, D. Brancaccio, R. Aharoni, R. Arnon, P. Rovero, R. Latajka, A.M. Papini, The role of helical structure in a series of Myelin Basic Protein peptides for antibody recognition in Multiple Sclerosis, Symposium "PhD in Chemical Sciences at UniFi - PiCSU2023", 25-27.01.2023, Florence, Italy (*as presenting author, in English*),

2. **A. Staśkiewicz**, F. Nuti, M. Jewgiński, M. Larregola, O. Lequin, C.W. Gruber, M. Chorev, P. Rovero, A.M. Papini, R. Latajka, Design, synthesis, conformational studies, and biological activity of clicked oxytocin analogues, II International Multidisciplinary Doctoral Conference at University of Szczecin "MKDUS 2.0", 22-24.06.2022, Szczecin, Poland (*as presenting author, in English*),

3. **A. Staśkiewicz**, M. Quagliata, F. Nuti, F. Real-Fernandez, M. Jewgiński, R. Aharoni, R. Arnon, P. Rovero, A.M. Papini, R. Latajka, The role of secondary structure in series of MBP peptides for antibody recognition in Multiple Sclerosis, XVIII Ogólnopolskie Seminarium dla Doktorantów i Studentów. Na pograniczu chemii i biologii, 12-15.06.2022, Smardzewice, Poland (*as presenting author, in English*),

4. **A. Staśkiewicz**, F. Nuti, M. Jewgiński, M. Larregola, O. Lequin, C.W. Gruber, M. Chorev, P. Rovero, R. Latajka, A.M. Papini, Design, synthesis, conformational studies, and biological activity of clicked oxytocin analogues, Symposium "PhD in Chemical Sciences at UniFi - PiCSU2022", 19-21.02.2022, Florence, Italy (*as presenting author, in English*),

5. **A. Staśkiewicz**, L. Macchia, F, Nuti, M. Jewgiński, M. Chorev, P. Rovero, A.M. Papini, R. Latajka, Projektowanie i synteza cyklicznych analogów oksytocyny, Od teorii do eksperymentu - czyli wpływ reorganizacji wewnątrz- i międzycząsteczkowej na właściwości cząsteczek w mikro- i makroskali, 18.02.2021, Wrocław, Poland (*as presenting author, in Polish*),

6. **A. Staśkiewicz**, L. Macchia, F. Nuti, M. Jewgiński, M. Chorev, P. Rovero, A.M. Papini, R. Latajka, Design and synthesis of clicked oxytocin analogs, IV Doctoral Forum Jan Kochanowski University, 17-19.11.2020, Kielce, Poland (*as presenting author, in English*),

7. M. Kijewska, F. Nuti, M. Wierzbicka, M. Waliczek, P. Ledwoń, **A. Staśkiewicz**, T. Koch, F. Real-Fernandez, G. Sabatino, P. Rovero, P. Stefanowicz, Z. Szewczuk, A.M. Papini, The novel Boronic-ChemMatrix Resin to selectively fish

out deoxyfructosylated peptides, 25th Polish Peptide Symposium, 08-12.09.2019, Wojanów, Poland (*as co-author, in English*),

8. **A. Staśkiewicz**, M. Jewgiński, A.M. Papini, R. Latajka, Design and synthesis of [1,2,3]-triazolyl containing cyclo-nonapeptides, analogs of oxytocin, XVII Ogólnopolskie Seminarium dla Doktorantów i Studentów. Na pograniczu chemii i biologii, 12-15.05.2019, Jastrzębia Góra, Poland (*as presenting author, in English*).

Posters

1. **A. Staśkiewicz**, M. Jewgiński, A.M. Papini, P. Rovero, R. Latajka, The influence of the amino acid sequence length on the helical nature of the epitope fragment of the MBP protein tyrosinase, 26th Polish Peptide Symposium, 03-07.09.2023, Stare Jabłonki, Poland (*as co-author, in English*),

2. **A. Staśkiewicz**, M. Quagliata, F. Nuti, F. Real-Fernandez, M. Jewgiński, R. Aharoni, R. Arnon, P. Rovero, R. Latajka, A.M. Papini, The role of α-helix motif in MBP peptides for antibody recognition in Multiple Sclerosis, 36th European Peptide Symposium and 12th International Peptide Symposium, 28.08-02.09.2022, Sitges, Barcelona, Spain (*as presenting author, in English*),

3. F. Nuti, **A. Staśkiewicz**, M. Larregola, B. Reztl, N. Tomasevic, M. Jewgiński, O. Lequin, C.W. Gruber, M. Chorev, P. Rovero, R. Latajka, A.M. Papini, Design, synthesis, conformational studies, and biological activity of clicked oxytocin analogues, 36th European Peptide Symposium and 12th International Peptide Symposium, 28.08-02.09.2022, Sitges, Barcelona, Spain (*as co-author, in English*),

4. **A. Staśkiewicz**, F. Nuti, M. Jewgiński, M. Larregola, O. Lequin, C.W. Gruber, M. Chorev, P. Rovero, A.M. Papini, R. Latajka, Projektowanie, synteza, preferencje konformacyjne oraz aktywność biologiczna analogów oksytocyny, IX Łódzkie Sympozjum Doktorantów Chemii, 19-20.05.2022, Łódź, Poland (*as presenting author, in Polish*),

5. **A. Staśkiewicz**, F. Nuti, M. Jewgiński, M. Larregola, O. Lequin, C.W. Gruber, M. Chorev, P. Rovero, A.M. Papini, R. Latajka, Projektowanie, synteza, badania konformacyjne oraz aktywność biologiczna triazolowych analogów oksytocyny, X Kongres Technologii Chemicznej, 11-14.05.2022, Wrocław, Poland (*as co-author, in Polish*),

6. **A. Staśkiewicz**, L. Macchia, F. Nuti, M. Jewgiński, M. Chorev, P. Rovero, A.M. Papini, R. Latajka, Design, synthesis and conformational studies of clicked oxytocin analogs, 63. Annual Congress of Polish Chemical Society, 13-17.09.2021, Łódź, Poland (*as presenting author, in English*),

7. **A. Staśkiewicz**, L. Macchia, F. Nuti, M. Jewgiński, M. Chorev, P. Rovero, A.M. Papini, R. Latajka, Design and synthesis of clicked oxytocin analogs, 25th Polish Peptide Symposium, 08-12.09.2019, Wojanów, Poland (*as presenting author, in English*).

Scientific traineeships

1. **10.2021 – 02.2022** – *Erasmus+ Traineeship* programme, Interdepartmental Research Unit of Peptide and Protein Chemistry and Biology, Department of Chemistry "Ugo Schiff", University of Florence, Italy. Project title: *Advanced techniques of synthesis and purification of peptides and proteins*. Supervisor: Prof. Dr. Anna Maria Papini,

2. **04.2021 – 08.2021** – *Erasmus+ Traineeship* programme, Interdepartmental Research Unit of Peptide and Protein Chemistry and Biology, Department of Chemistry "Ugo Schiff", University of Florence, Italy. Project title: *Development in peptide chemistry*. Supervisor: Prof. Dr. Anna Maria Papini,

3. **07.2020 – 08.2020** – *BioTechNan* project (PhD thesis development), Interdepartmental Research Unit of Peptide and Protein Chemistry and Biology, Department of Chemistry "Ugo Schiff", University of Florence, Italy. Supervisor: Prof. Dr. Anna Maria Papini,

4. **03.2020 – 07.2020** – *Erasmus+ Traineeship* programme, Interdepartmental Research Unit of Peptide and Protein Chemistry and Biology, Department of "Ugo Schiff", University of Florence, Italy. Project title: *Professional development in the field of bioorganic chemistry*. Supervisor: Prof. Dr. Anna Maria Papini,

5. **06.2019 – 07.2019** – *BioTechNan* project (PhD thesis development), Interdepartmental Research Unit of Peptide and Protein Chemistry and Biology, Department of Chemistry "Ugo Schiff", University of Florence, Italy. Supervisor: Prof. Dr. Anna Maria Papini,

6. **07.2018 – 09.2018** – *Erasmus+ Traineeship* programme, Interdepartmental Research Unit of Peptide and Protein Chemistry and Biology, Department of Chemistry "Ugo Schiff", University of Florence, Italy. Project title: *Development of a diagnostic technology based on mass spectrometry to fish out biologically relevant glycopeptides by phenylboronic-modified resin*. Supervisors: Prof. Dr. Anna Maria Papini and Prof. Dr. Paolo Rovero.

Scholarships and grants

1. Pro-quality scholarship for PhD students at the Wrocław University of Science and Technology (10.2022-09.2023),

2. Conference grant for participation in 36th European Peptide Symposium and 12th International Peptide Symposium (28.08-02.09.2022, Sitges, Barcelona, Spain),

3. Grants as part of the *Erasmus+ Traineeship* programme (07.2018-09.2018, 03.2020-07.2020, 04.2021-08.2021, 10.2021-02.2022),

4. Motivational scholarship as part of the *BioTechNan* project (01.10.2018-31.03.2019, 01.04.2019-30.09.2019, 01.10.2019-31.03.2020, 01.04.2020-30.09.2020, 01.10.2020-31.03.2021, 01.04.2021-30.09.2021, 01.10.2021-31.03.2022, 01.04.2022-30.09.2022),

5. Travel scholarship for an internship at the University of Florence in Italy as part of the *BioTechNan* project (06.2019-07.2019).

FUNDING AND ACKNOWLEDGEMENTS